The Pennsylvania State University

The Graduate School

Department of Engineering Science and Mechanics

MULTI-ENERGY OPTIMIZED PROCESSING: THE USE OF HIGH INTENSITY ULTRASONIC AND ELECTROMAGNETIC RADIATION FOR BIOFUEL PRODUCTION PROCESSES

A Dissertation in

Engineering Science and Mechanics
by

Matthew Mason Kropf

Submitted in Partial Fulfillment
of the Requirements
for the Degree of

Doctor of Philosophy

May 2008

The thesis of Matthew Mason Kropf was reviewed and approved* by the following:

Bernhard R. Tittmann
Schell Professor of Engineering Science and Mechanics
Thesis Advisor
Chair of Committee

Dinsesh K. Agrawal
Professor of Materials and Engineering Science and Mechanics

Michael T. Lanagan
Associate Professor of Engineering Science and Mechanics

André Boehman
Professor of Fuel Science and Materials Science and Engineering

Judith A. Todd
P.B. Breneman Department Head
Head of the Department of Engineering Science and Mechanics

*Signatures are on file in the Graduate School

ABSRACT

This work aimed to improve the understanding of the use of microwaves and ultrasound for chemical processes. Using biodiesel production as the case for study, the non-linear effects of high intensity ultrasonics, electromagnetic loss, and microwave heating were explored. Cavitation and atomization phenomena were used to describe the process of ultrasonic emulsification. The dielectric loss mechanisms pertinent to the biodiesel production materials were described as the connection to between the effects of ultrasonic emulsification and microwave heating. Superheating and anisothermal heating phenomena were identified as the specific advantages afforded by microwave heating.

High intensity ultrasonics was found to be capable of creating emulsions of biodiesel reactants with uniform dispersed phase droplets. Through optical microscopy, the ability to control the dispersed phase droplet size by altering the frequency and intensity of ultrasound was confirmed. This ultrasonic technique was investigated by measuring complex permittivity of the emulsions from 500 MHz and 5 GHz. The dielectric loss of emulsions consisting of methanol and soybean oil indicated that ultrasonic treatments could be used to alter the microwave absorption. Microwave heating tests of ultrasonically formed emulsions confirmed the permittivity results practically. The superheated boiling point of methanol and heating rate of methanol was extended to higher temperatures and rates in ultrasonically formed emulsions. Microwave heating of ultrasonically mixed emulsions was shown to result in faster transesterification relations than microwave heating of conventionally mixed emulsions. Finally, utilizing ultrasonics to optimize microwave absorption was shown capable of transesterification without catalyst.

TABLE OF CONTENTS

LIST OF FIGURES

Chapter 1 – Introduction

1.1 Historical Preface

Fuel: material consumed to produce energy and humanity's focus. The word *fuel* stems from the 14th century word *feuaile,* Old French for a bundle of firewood. This word came from the pronunciation of the 2nd century Medieval Latin legal term *focalia*, or, the right of all people to demand material for making fire. This legal term is the neutral plural of the word *focus,* ancient Latin for a home-hearth or a fireplace. The ability to harness fire is mankind's first innovation and enabled the very spread of civilization as it allowed people to inhabit cooler climates and sterilize food. In this way, fuel is the substance used to compensate for the energy deficit created by the growth of human civilization beyond its natural abilities.

For some time this energy deficit was readily met with the renewable resources afforded by nature. Despite the knowledge of coal, mankind would satisfy its energy needs using firewood for as long as it is feasible. However, soon civilizations became connected through trade and giant cities formed with populations much larger than the area of land would naturally support. In 1600 London, the human density far exceeded even the surrounding land's ability to make up the energy deficit. Accordingly, mass excavations of fossilized deposits in the form of coal had become the most feasible fuel source to compensate for this growth.

The availability of this new fuel created a lasting shift in the paradigm of energy and growth. Once only used to augment man's ability to maintain temperature and sanitize food, fuel began to replace the energy of human labor through machinery. As labor is replaced and life expectancies increase, human energies are redirected and so through the industrial revolution, mankind first established fuel as a *mechanism* for growth, as opposed to the substance of response. As industry

flourished, fuel began to be used not only to replace animal or human labor, but to achieve labors unmatched by anything in the natural world.

In recent times, the magnitude of global industrial growth is beginning to rival the planet's natural resources and its capacity for industrial waste - in no greater means than that of fuels for manufacture and transport of goods. Industrial growth's link to navigable waterways and coastal trade routes is long surpassed by modern transportation, almost entirely through the use of fossil fuels. Indeed the infeasibility of moving goods across long stretches of land, once covered by the horses and massive carriages necessary, has been disguised in more severe, albeit delayed, consequences. This progression is nowhere better realized than in the United States, where the industrial growth of a young nation has left a civil infrastructure where neither the delivery of goods nor regular and necessary personal travel can be achieved outside any major metropolitan area with out the use of transport fuels. In this way, those nations with modern civil infrastructures have made union with national security and the availability of transport fuels, which, in current times, are predominantly fossil fuels.

This necessity for industry has tied developing nations' economic growth to ever increasing demand in the fossil fuels market. As the growth and survival of nations mutually depend on an inevitably limited and geographically concentrated supply of crude oil, political and military turmoil will continue to escalate. Sociopolitical considerations aside, the use of fossil fuels to date demonstrates the ability of mankind to adversely and directly effect global weather patterns. Today, nearly a third of the world's population exists in two developing nations, India and China, whose momentum towards industrialization is inevitable and alarming. Truly, mankind's propensity for self preservation is pitted against its depth of wit and scope of reason.

1.2 Justification for research

As the world's increasing energy needs constrained by the supply and environmental impact of fossil fuels, alternative fuels are sought towards a sustainable fuel economy. Fuels derived from biological sources, called biofuels, present an opportunity to replace petroleum fuels within current infrastructure with a renewable alternative. However, it is often overlooked that for biofuels to become a sustainable and environmentally favorable fuel, efficiencies of all related manufacturing processes involved must also be considered and optimized.

A prime case for such a life cycle assessment is biodiesel production. With well established industrial sectors already in existence in Europe and many new US government initiatives, biodiesel is a rapidly growing alternative fuel. Despite its increasing prevalence in world markets, biodiesel manufacturing practices often involve toxic reagents and variable feedstock, resulting in inefficient use of resources, complicated downstream separations, and inconsistent fuel quality. These production aspects are do not include the energy expended to harvest, extract, process, and transport oil used as feedstock. In fact, modern research initiatives are likely to shift towards genetic optimization of oil yielding plants and extraction processes. [**1**]

The volume of renewable fuel that would be necessary to offset the petroleum usage makes biodiesel the most pertinent chemical industry with which to apply the tenants of Green Chemistry. While researchers show that less then a tenth of total petroleum diesel fuel consumption could be offset by current feedstock supplies [**1**], it can be argued that the current availability of feedstock is based on the previous demand in a food based market. As new feedstock choices, such as jatropha seed oil or algal oil, are developed specifically for the biofuel production, biodiesel may begin to replace a more significant percentage of petroleum diesel fuel. Following the Pollution Prevention Act of 1990, the Environmental Protection Agency defined Green Chemistry as "the design of chemical products and processes that reduce or eliminate the use and generation of hazardous substance." Twelve principles of green chemistry were set forth in an introductory textbook highlighting the

achievements of this emerging field [**2**]. A cornerstone of these principles is the concept of atom economy first set forth by Trost [**3**]. This concept strives towards the maximization of the number of atoms from raw materials in the resulting product. In the early stages of Green Chemistry, it was suggested that homogenous catalysis was a superior method as compared to stoichiometric reagents. This is true, as small amounts of catalyst can reduce reagent requirements and the energy necessary maintain the reaction environment. However, the ideals of Green Chemistry suggest reactions at molar ratios with renewable raw materials resulting in useful and benign co-products. Today, this aim has brought about renewed research interest in several reaction enhancement mechanisms previously established as mere laboratory curiosities.

The chemical reactions in biodiesel production, transesterification and esterification, involve the combining of fatty acids with alkyl- group alcohols. Transesterification is used to replace the alkoxy group of the saturated ester compounds with the desired alkyl group (usually methanol or ethanol). Industrial biodiesel production is most commonly achieved using a homogeneous base catalyzed reaction. The dissolved catalyst (commonly sodium hydroxide) removes a proton from the alcohol increasing its reactivity allowing for lower concentrations, enhances reaction rates, and enables better yields. However, the toxic catalyst also facilitates saponification of fatty acids, which vary in concentration in different feedstock and are present in large amounts in low value feedstock such as used fryer oil. This undesirable formation of soap lowers yields, complicates byproduct purification, and increases the amount of hazardous waste. [**4**] In addition, common industrial practice still utilizes concentrations of alcohol several factors greater then the stoichiometric ratio (3:1 molar). [**5**]

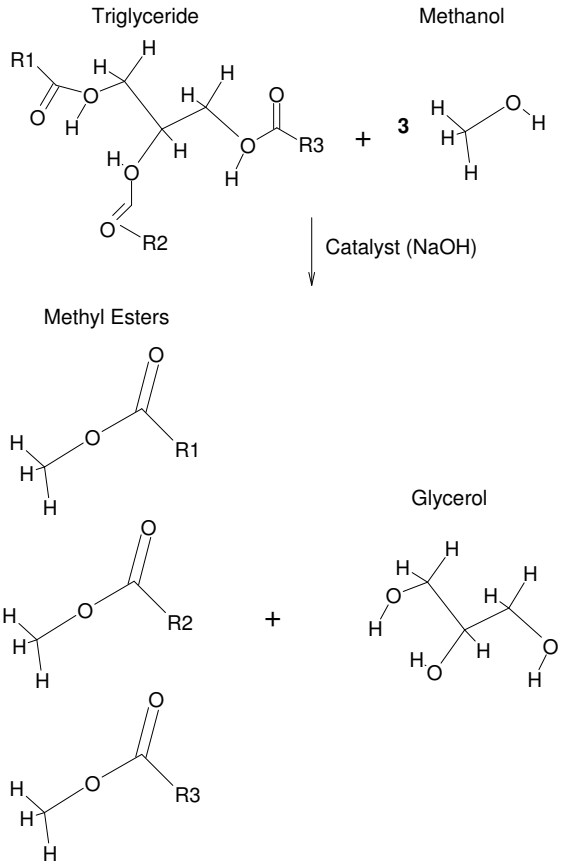

Figure **1**: The typical reaction scheme for the production of biodiesel from transesterification of triglycerides with methanol and base catalyst.

A simplistic view of the reaction and overall product composition involved in biodiesel production indicates the dilemma posed by atom economy between energy and chemical efficiency. Figure **1** The products do not contain the atoms of the catalyst chemical and only require a 3:1 molar ratio of methanol to triglycerides. Ideally, the catalyst would be collected and reused, however in industrial biodiesel production it is discarded after its use. [**4**] Furthermore it has been shown that given enough time and at the right temperatures and pressures, transesterification can proceed using only oil and alcohol. [**6**], [**7**], [**8**] The only process technique capable of achieving reasonable conversion rates involve the use of supercritical methanol. However, an industrial scale process utilizing this fact is mired by large excesses of alcohol, long reaction times, and the energy needed to

sustain the reaction environment. Recently, several research issues regarding the mechanism behind supercritical transesterification have been suggested. Of most interest is the question regarding the solubility of methanol in oil; citing that high temperatures and pressures, a large excess of methanol, and sometimes co-solvents are used to increase miscibility, the question arises regarding the effect of mixing. [**9**]

In an attempt to address the problems associated with homogenous catalysis in biodiesel production, recent research has demonstrated heterogeneous catalysts, ultrasonic cavitation, microwave radiation, and supercritical fluids as reaction intensification mechanisms capable of alleviating problems associated with current practices. However, scalability, energy consumption, and chemical requirements prevent these techniques from increasing atom economy in the industrial biodiesel process. In an attempt to achieve ideal reaction kinetics on the molecular scale in an industrial biodiesel process, an innovative multi-energy process, utilizing both ultrasound (US) and microwave (MW) energy is proposed in this work. [**10**]

Though MW and US have been documented in Green Chemistry, pioneering attempts to utilize them together have only demonstrated the potential advantages as a green technology in more exotic reactions; for example in [**11**] and [**12**]. Using an Edisonian approach, investigations in the literature have combined the two process technologies for independent purposes, without addressing the use for a combined purpose.[**13**] As the recent and lone review on the subject admits, "Nowadays many scientists are familiarized with MW (microwave) irradiation, some with US (ultrasound), but few with both." [**14**]

1.3 Types of interactions of waves and matter

The interaction of matter and energy refers to the exchanges of energy within a physical substance that has been perturbed from some stable state. Most mathematical representations generally involve equilibrium conditions about which the material perturbs and limits within which the material retains the ability to restore the energy from the imparting wave. However, in some cases, the imparted wave is of sufficient potency to exceed the materials ability to restore the particular energy. In such cases, the excess energy performs work on the material. Such waves are considered high intensity, while those that oscillate within the restoring energies of a material are considered low intensity waves. The propagation aspects of low intensity waves are determined by the materials affinity to restore the particular imparted energy, thus are used as a means to investigate material properties. Conversely, high intensity waves are used to alter or improve material properties

For purposes herein, waves are considered to be intentionally imparted into a material from either a mechanical or electromagnetic source. In most cases, the electromagnetic waves are in the Microwave (MW) frequency regime and the mechanical waves are in Ultrasonic (US) frequency regime.

1.4 Thesis Impact and Scope

The goal of this thesis is to formally identify specific synergistic effects of combined MW and US in chemical processing applications. The research will focus specifically on the production of biodiesel through the transesterification reaction. With reactants comprised of immiscible fluids, the effect of ultrasonic parameters on emulsification is investigated in terms of emulsion microstructure. Reaction mixtures consisting of a polar and a dielectric liquid allow for new investigations of microwave superheating and anisothermal heating. The mixture parameters necessary to maximize desired microwave effects are related to the ultrasonic parameters affecting emulsion properties. The

microwave absorption of ultrasonically formed emulsions is determined through microwave heating rates and complex permittivity measurements. The ultrasonic parameters', frequency and intensity, effect on emulsification is measured by microscopic imaging and correlated to complex permittivity measurements. The effects of US and MW are studied on biodiesel reaction mixtures varying molar ratios of methanol to oil and catalyst concentrations from typical industry values to ideal values specified by atom economy. The results are used as a basis for the design of a catalyst free biodiesel process with potentially lower energy and reactant requirements then supercritical approaches. The scope of the research is limited to establishing the procedure and measurements of US and MW energy interactions with reactant mixtures towards the identification of optimization parameters.

The specific contributions of this thesis include:

- Measure the effect of high intensity ultrasonics on dispersed phase droplet size of emulsions consisting of biodiesel reagents
- Complex permittivity analysis of biodiesel reagents at microwave heating frequencies
- Measurement of complex permittivity of ultrasonically formed emulsions of biodiesel reagent mixtures over microwave frequencies
- Measurement of microwave heating profiles of ultrasonically formed emulsions with dispersed polar phase
- Enhanced microwave superheating through use of ultrasonic emulsification
- Combined use of microwaves and ultrasound for catalyst free transesterification at sub-critical temperatures.

1.5 Thesis Organization

The following chapters comprise the body of this thesis.

Chapter 2: Biodiesel production

- Biodiesel materials
- Transesterification reactions
    - Catalyzed reactions
    - Catalyst free reactions
- Supercritical Fluids
- Emulsion Science

Chapter 3: Electromagnetic Energy

- Electromagnetic wave propagation
- Microwave heating applications
    - Superheating
    - Anisothermal heating
    - Microwaves in biodiesel production

Chapter 4: Mechanical Energy

- Mechanical wave propagation in fluids
- High intensity applications
    - Cavitation
    - Emulsification
    - Ultrasonics in biodiesel production

Chapter 5: Methodology

- Emulsion preparations
- Optical microscopy of emulsions
- Complex permittivity measurements
- Microwave heating measurements

- Biodiesel chemical measurments

Chapter 6: Results

- Effect of ultrasonic parameters on emulsification
- Complex permittivity of reactants and emulsions
- Effect of microwave heating on emulsions
- MW-US effect on biodiesel conversion

Chapter 7: Conclusions

- Overview of thesis contributions
- Optimization strategy for combined MW-US biodiesel production
- Practical design of catalyst free MW-US reactor
- Future Work

Chapter 2

Biodiesel Production and Materials

2.1 Introduction:

With the goal of describing the effects of high intensity microwaves and ultrasonics for use in biodiesel production, the nature of the materials involved and common processes are discussed. With an understanding of the reaction mechanisms and kinetics of existing biodiesel production methods, a qualitative strategy towards the optimization of combined microwave and ultrasound is obtained. Finally, the physical properties of the reactants and their mixtures are discussed as a means to anticipate the interaction with electrical and mechanical energy.

Three dimensional molecular models in this section were obtained from the chemical data table (in the molfile format) available in the NIST standard reference data base number 69 which can be found at found in [**15**]. The colors red, grey, and white represent oxygen, carbon, and hydrogen respectively. A single connection between the model atoms represents the single bond and double bonds are represented by two connections. The chemical equations were rendered from the same molecular data file as the images.

2.2 Biodiesel Production:

2.2.1 Materials:

Biodiesel is defined as being comprised of mono-alkyl esters of long chain fatty acids obtained from vegetable oils and animal fats, or lipids, which meet the fuel specification requirements of ASTM D 6751. [**16**] To begin, the structure biodiesel is considered in terms of its components' properties. While discussions of the reaction mechanism and material properties will emerge, the detailed analysis is left to the subsequent section and chapters.

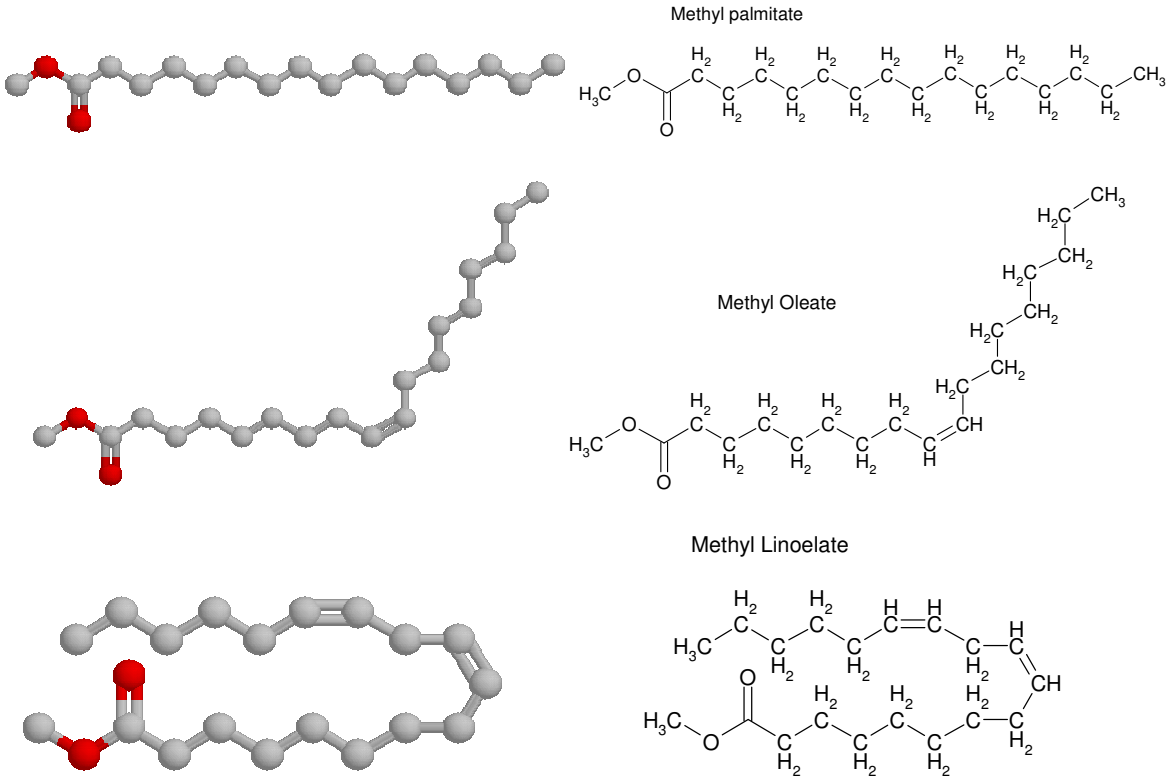

Figure **2**: Three mono-alkyl esters representative of typical molecules found in biodiesel fuel in three-dimensional illustrations (left) and chemical diagrams (right). [**15**]

In Figure **2** , methyl esters of three different fatty acids, each found in soybean oil, represent chemicals typically found in a biodiesel fuel product. The oxygen atom bonded to the shorter carbon chain represents the hydroxyl group of the short chain alcohol, or alkyl group, used in the production. For example, the above molecules are methyl esters which are identified by methanol as the single carbon chain connected to the hydroxyl group. The type of alcohol used is not limited to methanol, as might be inferred from the above illustrations; in fact, studies discussed later investigated ethanol and butanol among others for biodiesel production. The longer chain represents the fatty acid derived from the oil source, or feedstock. The fuel properties of biodiesel do depend on both the fatty acid component and the alkyl component. However, research has shown that in terms of cetane number, a measure related to the combustion properties, the fatty acid structure is the dominant characteristic. While in terms of cold flow, a measure related to the melting point, the type of alcohol has a pronounced effect. [**17**] [**18**]

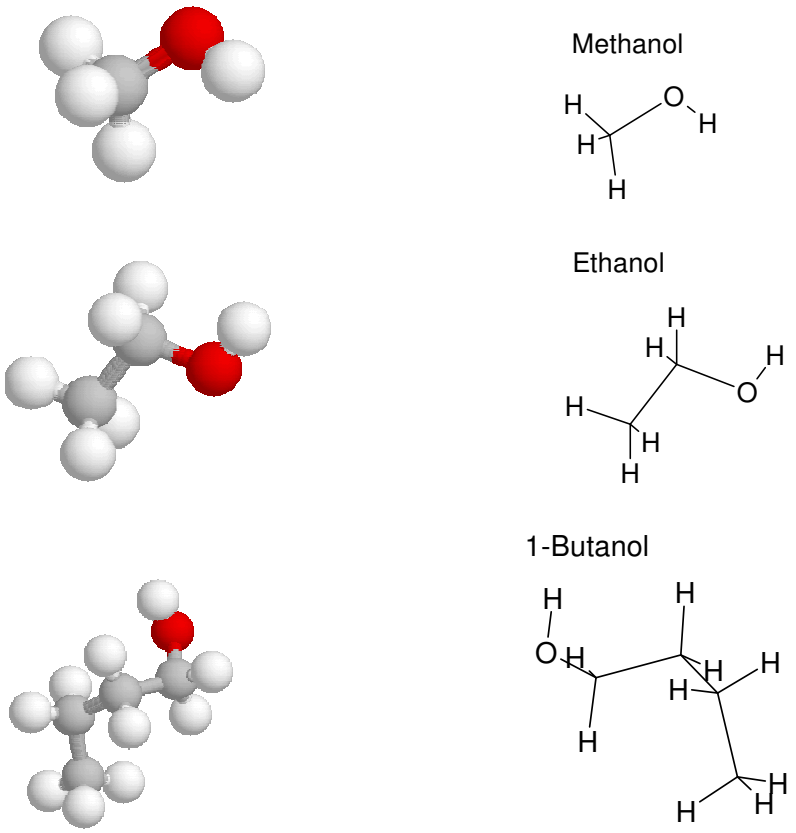

Figure **3**: Three primary alcohols representative typical alkyl components of biodiesel fuel three-dimensional illustrations (left) and chemical diagrams (right). [**15**]

Methanol, ethanol, and butanol each consist of one hydrogen bonded oxygen atom bonded to varying length hydrocarbons Figure **3** . To understand the difference related to the molecules' structure to related processing and fuel product variables it is appropriate to compare the empirical physical properties. For instance, from the molecular weight, M_r, with increasing carbon atoms it might be expected that the liquid's density, ρ, and viscosity, η, would increase. This is based on mechanical notions of mass and momentum; i.e. the heavier the molecule, the more dense and viscous the liquid. In Table **1** , this notion is evident; however, ethanol presents an apparent anomaly in this concept applied to density. While the comparison is quasi-analytical at best, this observation

indicates another property that varies between alcohols, particularly the relative permittivity, ε_r, and dipolar moment, μ_D.

Table **1**: Selected material properties of methanol, ethanol, and 1-butabnol. [**20**]

Name	Mol. form.	M_r	T_b (°C)	ρ (g/mL)	η (MPa s)	ε_r	μ_D	C_p (J / g K)	V_p (kPa)
Methanol	CH_4O	32.042	64.6	0.79142	0.544	33	1.7	2.531	16.9
Ethanol	C_2H_6O	46.068	78.29	0.78932	1.074	25.3	1.69	2.438	7.87
1-Butanol	$C_4H_{10}O$	74.121	117.73	0.80952	2.54	17.84	1.66	2.391	0.86

With a more formal discussion in a later chapter, the dielectric constant can be thought of as a potential for electromagnetic interaction and the dipole moment can be considered the strength of polarized electromagnetic field created by the atomic structure. The manifestation of the molecular polar effect in a liquid occurs through the attraction between neighboring polar molecules. In the case of the listed alcohols, the dipole moment is derived from the hydroxyl component. The oxygen atom represents a disproportional concentration of electrons compared to the positive charge in the hydrogen atom. The hydrocarbon chain is non-polar because the electrons are evenly distributed in the covalent bonds of carbon and hydrogen. This result indicates that most petrochemical products are non-polar. In turn, the degree of polarity of an alcohol compared to the hydroxyl dipole moment is offset by the length of carbon chain. This offers a possible explanation towards the density of methanol being higher than that of ethanol. While the additional hydrocarbon adds weight, the decrease in dipole moment results in less polar attraction between molecules. Thus, methanol will attract more mass in a particular volume than the heavier, yet lower dipole moment, ethanol. This effect is only evident between these species due to the similarity in molecular weight. Hence, as hydrocarbon chains are added to form butanol, the magnitude of additional mass reclaims the hydrocarbon chain length's proportionality to density.

The electrostatic attraction between molecules is important to more than just the molecular packing in liquids. For example, the looseness between various alcohols based on the inhibited strength of hydrogen bonding, or dipole moment, manifests itself as decreased vapor pressures, surface tensions, and thermal conductivities. The specific heat capacity, the amount of heat a substance can hold, is also affected by hydrogen bonding between polar liquid molecules. The hydrogen bonds represent another place where heat can be stored, in addition to the heat stored as internal vibrations associated with the translational degrees of freedom.

In practical terms, the polarity of a liquid is described in terms of its miscibility with water. Miscible agents are considered polar and the non-polar molecules do not mix with water. This notion can be useful in comparing the above alcohols in terms of miscibility with oil components. Extending this for comparison, using oil as a metric for a non-polar component, one would expect butanol to be more like oil than methanol and conversely methanol more like water than butanol. This is in essence, a comparison of the hydrocarbon chain length.

The default choice of alcohol in this work will be methanol, despite the fact that other alcohols can and are used in biodiesel production, particularly ethanol. The simple reason for this choice is its prevailing use in current industrial biodiesel practices, which stems from the low cost relative to other choices. Further reasoning will become evident after a more in-depth discussion of the electromagnetic, mechanical, and thermodynamic properties of the material.

The fatty acid portion of biodiesel is arguably a more important component to the product cost and quality. The cost of the fatty acid feedstock far outweighs that of any other component of production. [**1**] Also, as mentioned above, the type of fatty acid affects the fuel properties of biodiesel products. Standards limit the ester size, in terms of chain length, to those correlating to the properties of the hydrocarbons found in diesel fuel. This specifies the viable feedstock choices for esters, which are limited to fatty esters. The different fatty acids are commonly denoted by the number of carbons and the number of double bonds in the hydrocarbon chain, as #C : #DB. For example, the fatty acids of the above methyl esters, Palmitic, Oleic, and Linoleic, can be denoted as 16:0, 18:1, and 18:2 as in Figure **4** .

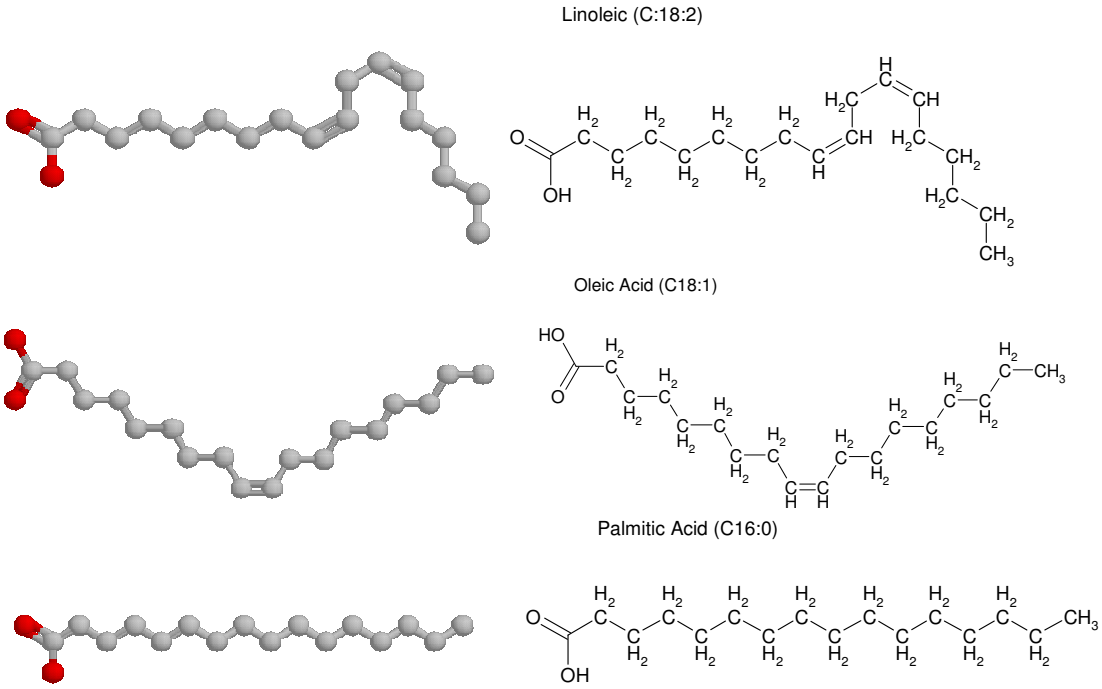

Figure **4**: Three typical fatty acids which comprise the ester component of alkyl esters in biodiesel fuel in three-dimensional illustrations (left) and chemical diagrams and (right). [**15**]

A similarity between the alcohols and fatty acids can be observed in terms of a polar component and a non-polar hydrocarbon chain. However, with the chains much longer, the bulk liquid is considerably less polar in nature than the primary alcohols. However, using the practical

notion of polarity of liquids, it can be said that fatty acids range in degree of polarity. This means that compared to the miscibility of oil and water, fatty acids are more miscible, but not to the degree of the alcohols discussed.

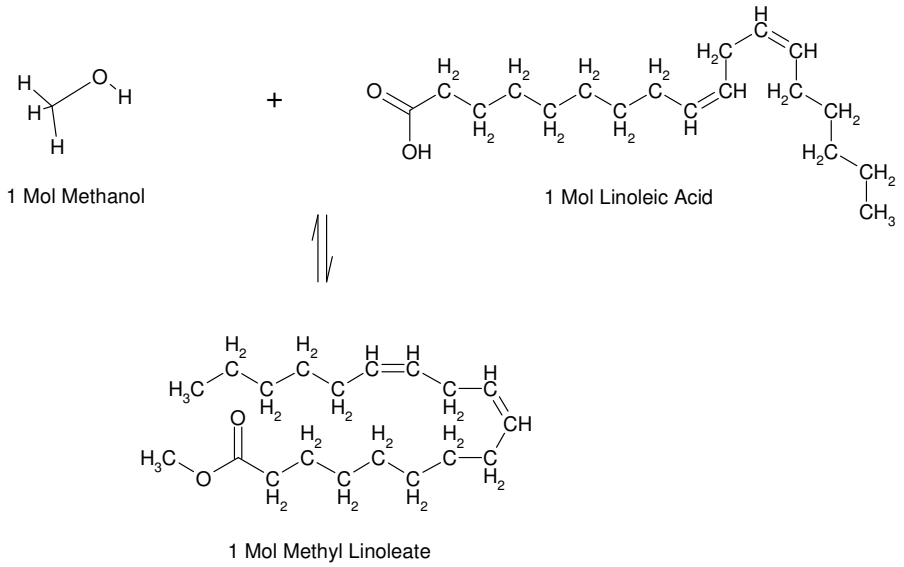

Figure **5**: Simplified chemical diagram of methanol and linoleic acid reacting to form the biodiesel fuel chemical product, methyl-linoleate in the esterification reaction.

At this point it appears that the two necessary components for the production of biodiesel are present. The chemical reaction that accounts for the combination of the alkyl and fatty acid components is termed esterification and is shown in Figure **5** . A simple balance equation seems to suggest that the only necessary reagents can combine to form the product. However, two issues must now be considered, namely the reaction kinetics and practical source fatty acids. For the moment, reaction kinetics will be limited to the discussion of acid and base catalysts. The concept of acid and base catalyst involves the presence of positive hydrogen ions and negative hydroxide ions. The combination, or neutralization of an acid and a base thus results in a water, and a salt of the ion

previously associated with the ions. Looking carefully at the esterification diagram it is noticed that a hydroxide ion is unaccounted for on the product side. For this reason, the esterification reaction would proceed quite slowly without an additional acid catalyst. The additional hydrogen neutralizes the left over hydroxide ion leaving a water molecule. Acid catalyst dissolved in methanol creates so-called protonated methanol, or the methanol molecule with an additional hydrogen atom on the hydroxyl component. Conversely, base catalyst dissolved in methanol results in methoxide, or a methanol molecule missing the hydrogen of its hydroxyl group. Given that each state is unstable, the presence of here termed carrier molecules, or salt, for the oppositely charged ion needed to maintain the unstable state of methanol. In the case of base catalyst, for instance sodium hydroxide (NaOH), the sodium ion serves this function. of the polar liquid. Before the formal discussion of reaction mechanisms begin, it is central to discuss the common sources for the fatty acids used in biodiesel production.

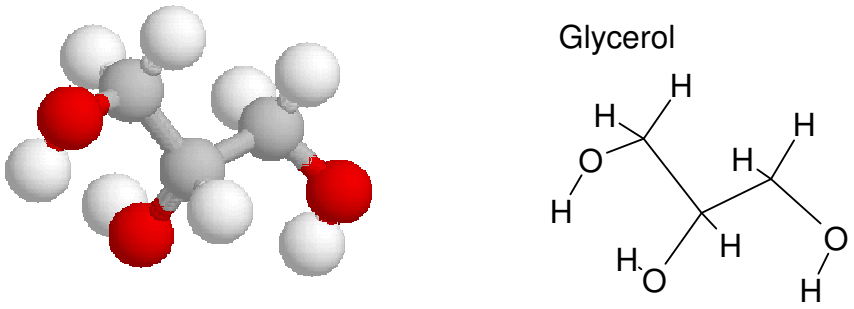

Figure **6**: Glycerol molecule which forms esters with fatty acids in typical biodiesel oil feedstock represented in three-dimensional illustrations (left) and chemical diagrams and (right). [**15**]

Up until this point the generic term "oil" has been used to describe the feedstock for biodiesel and for comparisons for liquids immiscible with water. To formalize this term is to describe the form in which fatty acids typically are found in natural feedstock, such as soybean oil,

cotton and jatropha seed oil, and algae. In such cases, the fatty acids are usually bonded to a glycerin molecule forming a glyceridic ester. Examining the molecular form of glycerin, in Figure **6** , it is observed that more than one potential bonding site is present, as represented by the three hydroxyl portions of the molecule.

This description is only important in order to visualize the natural likelihood that three fatty acids would bond to a glycerol molecule. The resulting ester from three fatty acids and a glycerol is commonly referred to as a triglyceride, as depicted in Figure **7** .

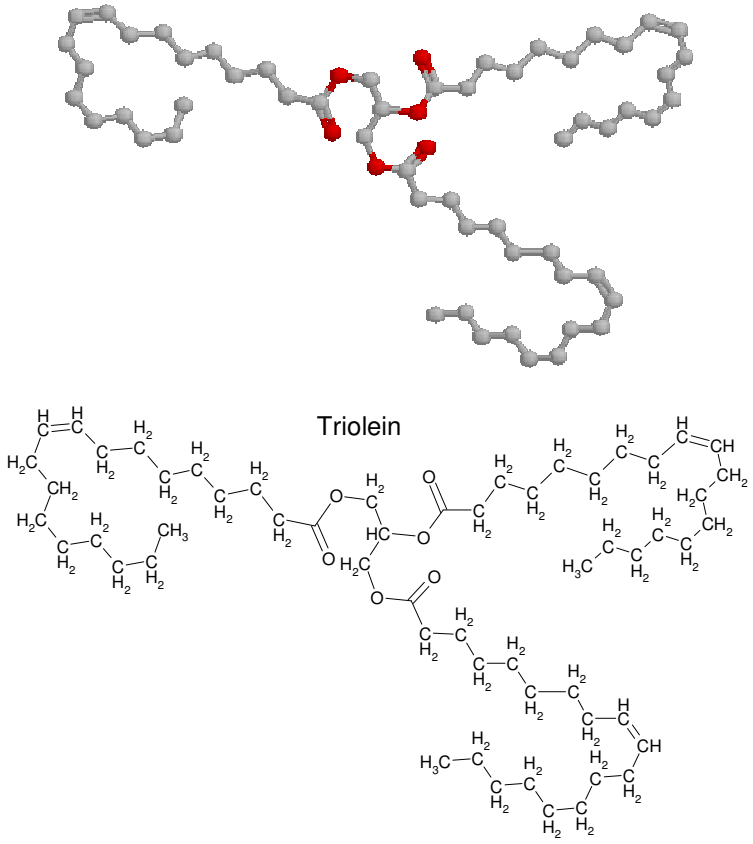

Figure **7**: Triglyceride molecule, triolein, representing the typical from that fatty acids are found in biodiesel feedstock as represented in three-dimensional illustrations (top) and chemical diagrams and (bottom). [**15**]

Just as different fatty acids can undergo esterification to form three different alkyl esters, a single glycerol can be saturated by three distinct or identical fatty acids. The types of fatty acid present in a particular oil source, soybean oil for example, will vary. The description regarding the relative concentration of various fatty acids is called a fatty acid profile. This fact alone, suggests one of the potential problems with the production of consistent fuel products. This means, in order to predict the cold pour point or cetane number for biodiesel from particular oil requires knowledge of the fatty acid profile. As a single feedstock, the variance in components can affect the bulk properties of the oil. For example, the prediction of the density, heat capacity, and other rheological properties has required extensive studies relating to the fatty acid composition. [**21**], [**22**], and [**23**]

Now instead of simply combining with a fatty acid (FA), now called a free fatty acid or FFA, to form biodiesel, the FAs must first separate from glycerol molecule. The reaction involving the change from one type of ester to another is called transesterification. Now the question of energy required for the reaction is clear. In plain terms, the FA of the glycerol ester must be coerced to change to an alkyl ester. The additional energy can come in the form of catalyst and heat. As the complications arising from these simplified descriptions have reached a peak, a critical analysis of the literature covering transesterification and esterification for biodiesel will be discussed.

2.2.2 Catalyzed Transesterification:

As mentioned before, the use of a homogenous base catalyst is the most common industrial method to achieve transesterification conversion. Though the catalyst is not present in either co-product, typical industrial practices do not involve recovery and regeneration. Instead the catalyst is removed by water washing or purification mechanisms. The result is often contaminated glycerol and water, which subsequently requires further purification to increase the value of the co-product

and remediate hazardous waste from water supplies. In addition, free fatty acids, those not bonded to glycerol molecules, will undergo saponification resulting in fatty acid salts and water. [**4**] The water created inhibits the overall reaction and fatty acids in soap products represent wasted feedstock. It is recognized the removal of catalyst from the reaction in Figure **1** results in lower cost resulting from both less reactants, post processing purification, and lost feedstock in the case of saponified products.

Initial studies regarding the process variables in the transesterification of various plant oils were performed by Freedman et al. The study indicated that a molar ratio of alcohol to oil of 6:1, twice the stoichiometric ratio, resulted in the most complete conversion. The experiments seemed to indicate that base-catalyzed reactions resulted in considerably faster conversion rates than acid catalyzed reactions. It was also noted that the presence of moisture and free fatty acids were inhibitory on conversion to esters. Evidence was also given towards the improved conversion efficiency of sodium methoxide catalyst compared to sodium hydroxide. This early study of the transesterification of fatty oils suggested several stepwise reversible reactions may account for the overall reaction rate. of mono-, di-, and triglycerides, MG, DG, and TG respectively. The triglycerides (TG) contain three fatty acids bonded to a glycerol; as one fatty acid is liberated the remaining two chains form a diglyceride (DG). Similarly, the DG then looses a fatty acid chain becoming a monoglyceride. Finally, this MG is separated into a fatty acid and glycerol (GL). [**24**]

This notion was modeled in a later study by Freedman et al, which is apparently the first formulation of a reaction rate model accounting for the individual reactions in the transesterification of soybean oil with alcohols. Using high molar ratios, 30:1, of alcohol to oil, it was observed that first order reaction kinetics showed good agreement with the stepwise reactions. When the ratio is reduced to 6:1, twice the stoichiometric amount, second order kinetics began to dominate. However,

Freedman noticed that when using methanol as opposed to butanol, second order reaction kinetics could not account for the ester conversion. More specifically, the rate of glycerol formation could not be accounted for by intermediate production of DG and MG. To account for this a shunt reaction is introduced which describes the case where three methoxy molecules simultaneously replace the glycerol in a TG resulting in three methyl esters. This shunt reaction was not necessary for modeling reaction rates with butanol at the same ratios. Freedman speculated that being a smaller and more polar molecule, methanol is more capable of a direct attack on the TG in soybean oil. Finally, this study indicated that the activation energy for the stepwise reactions in the range from 8,000 to 20,000 calories per mole, citing need for more research to investigate other process variables. [**25**]

Though the previous studies establish the reaction kinetics and recommend appropriate variables, the effect of mass transfer was ignored. This point was noticed by Noureddinei and Zhu who performed reaction kinetics experiments with different mixing intensities on 6:1 molar ratios of methanol to soybean oil with 0.2% sodium hydroxide by weight of oil. The intensity of mixing was quantified using the Reynolds number relating to the rotational speed of a mechanical impeller. The result of this study qualitatively describes three regions of reaction rates. Each region is identified by rate limiting mechanism with the first by mass transfer, the second by kinetics, and the third by equilibrium. Finally, the authors note that the mass transfer in a reaction can be further accelerated by increased temperatures, likely due to improved solubility, and ester conversion, which acts as a co-solvent. The study also reported lower activation energy of forward reaction from MG to GL than the reverse, indicating favorable reverse reactions at elevated temperatures. This was eschewed in light of an increase in reaction rates as temperatures approach the boiling point of methanol. Using a modified version of previous stepwise reaction rate model, the authors report activation energies in

the range from 8,000 to 18,500 cal/mol. The reaction rate constants are reported on the order of 10^{-1}. [**26**]

The transesterification studies above were useful in developing reaction rate equations accounting for the intermediate steps between a triglyceride, 3 FFAs, and glycerol. They also addressed the effect of moisture and FFA in the feedstock. Using the information in the above studies, researchers have gone to great lengths to systematically analyze a production process for optimal parameters. A good example of such a study was put forth by Vicente et al. This study utilized statistical design to optimize a base catalyzed reaction, using potassium hydroxide, of sunflower seed oil. The results indicated a 6:1 alcohol to oil molar ratio and 1.3 % by weight of oil catalyst.[**27**], [**28**] Despite the intricacy and success of such designs, the removal of catalyst contamination from water and the effect of FFA and water in base catalyzed reactions present a problem.

One reason the problem with base catalyzed reactions in high FFA feedstock became a repeating theme in the biodiesel literature, is due to the inherently high cost of refined feedstock, such as soybean oil. High FFA feedstocks include used fryer oil, rendered animal fats, and soap-stock from industrial edible oil refining. For a biodiesel producer to consider the cost savings of feedstock, the process has to be robust enough to handle the variable amounts of FFA and water that comes with such sources. Canakci and Gerpen presented a study covering the use of sulfuric acid in transesterification reactions, noting that reactions proceed much slower than base catalyzed reactions. The authors also note that though the acid catalyst readily converts FFA without soap formation, the resulting production of water inhibits the catalyst activity.[**29**] Haas wrote about the use of acid catalyzed conversion of inexpensive soap stock, reviewing several other studies regarding acid treatment of FFA.[**30**] Marchetti et al proposed a heterogeneous acid resin as an immobilized

catalyst for esterification of high FFA feedstock. The study showed that heterogeneous catalyst could be used to avoid later separation and purification. However, the authors admit that transesterification reactions using the same solid catalyst did not react at a reasonable rate.[**31**] A later study by the same authors provides a review of different catalyzed processes for biodiesel production including acid, base, and lipase catalyzed reactions. The lipase catalyst is an intriguing aside to production-ready processes as the cost is considerably more than chemical catalysts at this time.[**32**] Wang et al. compare processes for converting waste fryer oil finding that a two step process to remove FFA with acid esterification and follow with a base catalyzed reaction.[**33**] A recent review by Van Gerpen on biodiesel production technology provides an industry based process comparison of different methods of biodiesel production. In this review there is mention of catalyst free biodiesel production and repetition of the troubles caused by the predominant use of homogeneous base catalyst. [**5**]

In terms of striving towards atom economy, a catalyst free biodiesel process seems ideal. Clearly, eliminating catalyst from the production process would reduce cost of materials. However, aside from the cost of catalyst chemicals, the simplified separation and purifications presents an even greater savings to the process. Finally, without soap formation and dilution from water formation, the use of lower cost feedstock can be achieved with little additional process cost. Also, as new feedstock options become available, such a process may be capable of simultaneous oil extraction and transesterification. The next section reviews several reports on catalyst free biodiesel production processes at both elevated and supercritical temperatures.

2.2.3 Catalyst free transesterification:

Diassakou et al. is first to discuss non-catalytic transesterification reactions of soybean oil. Using the same stepwise reaction description, with reverse reactions ignored citing a large excess of methanol, reaction rates were calculated for catalyst free transesterification at 220 and 235 ^{o}C. The conversion rate from MG to GL observed at these temperatures is reported to be quite slow. The rate constants were reported in the on the order of 10^{-6}. [**6**]

A later study by Dasari et al. confirmed the reaction description of catalyst free transesterification. This study demonstrated the catalytic ability of metal surfaces used as reaction vessels in the following study. It is noted that a reaction catalyzed by reactor surface would likely suffer in scale up processes, as the relative volume exposed to the surface decreases with through put. Using glass capillary tubes, the reaction rates were measured at 120, 150, and 180 ^{o}C, citing results in relative agreement with the results from the work of Diasskakou et al. Discrepancies between calculated rate constants and those extrapolated from the Arrhenius model and the aforementioned results, the authors cited solubility limitations more evident at lower temperatures and conversions. [**7**]

Saka and Kusdiana report on non-catalytic transesterification in supercritical methanol with considerably higher reaction rate constants than the above studies. Studies were conducted with 41:1 molar ratios of methanol to soybean oil placed in Inconel reaction vessels at temperatures between 350 and 400 ^{o}C and pressures from 45 to 65 MPa. The authors attribute the enhancement of reaction rates to the nature of the supercritical state. The authors note specifically that dielectric constant of methanol decreases at supercritical temperatures improving the solubility in oil. However, later studies suggest that the enhancements were likely due to a reaction catalyzed by the reactor surface. While no mention was made regarding the rate of conversion of MG to glycerol, the

authors showed a unique enhancement in the type of fatty acid esters resulting from the treatment. Compared to reference biodiesel samples, both purchased and prepared conventionally, the longer retention times and higher temperatures in supercritical reactions showed disproportionate amounts of methyl linenate and methyl linoleate as compared to methyl oleate. This observation was reconciled citing that the dehydrogenation and decomposition with oils at these temperatures accounted for the shift in product composition. Interestingly, no comment is made regarding the enhancement to the resulting fuel properties, namely the reduction in cold pour point. [**34**]

Warabi joined Saka and Kusdiana in an investigation into the potential use of supercritical methanol for the esterification of FFA. The results showed that esterification of free fatty acids occurred readily and at a faster rate than the transesterification of soybean oil. This study also identified methanol as a better reactant for supercritical alkyl esterification, noting a higher pressure at test conditions. Finally, the authors present contradiction of the previous work, reporting that full conversion with supercritical methanol in a transesterification reaction took 15 minutes, as opposed tothe their previous report of 4 minutes. However, the authors again utilize a small metal, 5 mL and Inconel, reaction vessel for the experiments with no discussion addressing the potential for catalytic reactions at the surface of the vessel. [**35**]

Cao et al attempt to lower the temperature and pressure of the supercritical reaction with the addition of a co-solvent. Citing the existence of multiple critical points arising from binary mixtures, the authors add varying concentrations of propane to 33:1 molar ratios of methanol and soybean oil before a heating to temperatures in the supercritical regime. Results show that with the addition of propane co-solvent results in similar supercritical reaction rates at milder conditions than reported by Saka et al. In addition, it is shown below the critical temperature, the reaction rates are similar than those reported by Diassakou. This fact seems to contradict the claim that reaction constants

reported by Saka were catalyzed by the metal reactor surface used. Finally, Cao notes that with the addition of propane, the excess of methanol can be reduced while maintaining mutual solubility of methanol and oil, which decreases the requisite reaction pressures. [**36**]

A review soon followed on catalyst free biodiesel production, presented by Wang and Van Gerpen, which highlighted the above studies. The review ends with a list of research issues which need to be addressed. Among other concerns were, the apparent need for high excess of methanol, the question regarding catalytic activity on metal surfaces, lack of investigation into the effect of mixing and pressure, and whether mechanism of reaction rate enhancement is based on the high temperatures or improved solubility. [**9**]

A study following Wang's review, by He et al, reports careful measures the rate constants and activations of transesterification reactions of soybean oil in supercritical methanol. The authors carefully demonstrated the variation in reaction rate constants as the temperature and pressure crosses into the critical regime. In addition, the authors addressed the effect of pressure on the reaction rates. However, the use of excess of methanol at 42:1 molar ratio to oil and reaction times on the range of half an hour were reported. The authors described the enhancement of reaction rate in the supercritical region to be an effect of "the considerable changes in the physical properties of methanol." [**37**], [**38**]

Wang et al. proposed a new method to decrease the requisite temperatures and pressures of the supercritical reaction. With additions of small amounts of sodium hydroxide catalyst, between .5% and 1% by weight oil, reaction rates were shown to dramatically increase compared to those without any catalyst. The authors concluded that the addition of small amounts of catalyst allowed

for subcritical and enhanced supercritical reaction rates. However, the authors did not note a marked difference across the threshold of the supercritical point. [**39**]

Yin et al. expand the study of cosolvent and catalyst use in subcritical and supercrical processes to include the use of carbon dioxide, hexane, and potassium hydroxide. The results confirm previously claimed improvements of reaction temperature and pressure with co-solvent and small amounts of catalyst. Using only 0.1% of KOH, the authors demonstrate enhanced reaction rates at temperatures as low as 160 ^{o}C. The authors report the mixing, but do not vary the speed or discuss any need or enhancement by mixing. [**40**]

The use of peanut oil, as opposed to soy, was addressed by Cheng et al. The authors report reaction rates and activation energies similar to those reported for soybean.[**41**] To investigate the role of supercritical methanol, and the corresponding temperatures and pressures, Imahara et al recently discussed the stability of the methyl ester product using such extreme conditions. Results show that to avoid decomposition of the fatty acid chain of methyl esters, and other distortions, that the temperature should be limited to below 300 degrees Celsius. [**42**]

A comprehensive analysis of a supercritical biodiesel was put forth by D'Ippolito et al. The basis of the study was the investigation of a two step transesterification process utilizing supercritical method. While the primary contributions of the analysis were the basis for the two step process and synergistic heat recovery, the authors summarize many important aspects of supercritical methanolysis not discussed by authors of the aforementioned articles. The authors elaborate on the specific physical properties that are changed at the supercritical point, namely viscosity, density, dielectric constant, hydrogen bonding, and polarity. The result of the change in hydrogen bonding and polarity, essentially related, is increased molecular diffusivities. Finally, the reaction rate

enhancement at supercritical temperatures is actually related to the concentration of non-hydrogen-bonded methanol molecules. The authors expand on this point stating that catalyst free reactions below the supercritical point are inherently inefficient due to the immiscibility of methanol and oil. It is noted that when the two phases separate, the vapor pressure of methanol is evident, however when they are well mixed or with co-solvent the vapor pressure of the mixtures are lowered. [**43**]

To summarize, catalyst free transesterification can occur at subcritical temperatures, however the reaction rates are quite slow. The addition of small amounts of catalyst drastically increases the reaction rate in subcritical and supercritical regimes. Every study utilized alcohol to oil ratios in greater than 20:1 molar. To the best knowledge of the authors reviewed, the enhancement created by supercritical state of methanol is entirely due to the increased miscibility of the two reactants, while the temperature and pressures affect the kinetics as normal. The need or effect of mixing has not been substantially discussed. The next sections will endeavor to describe the supercritical state of methanol and general descriptions of immiscible mixtures in the form of emulsions, towards the goal of better understanding of the reactivity in transesterification reactions.

2.3 Supercritical Fluids:

The use of the term *state* to refer to a system in a thermodynamic system is inherently different to its use in other physical descriptions of systems. For instance, the thermodynamic state of a material can be described in terms of interrelated global parameters pressure, volume, and temperature without specific knowledge of spatial and temporal information regarding the mass and charge the material system. The relation between the thermodynamic functions forms the equation of state.

The equations of state represent the relations between the thermodynamic properties, in this case pressure (P), volume (V), and temperature (T). The underlying understanding involves a certain notion of equilibrium. In short, energy imparted to a system correlates to heat of the systems response. However, from these descriptions the evaporation and condensation of liquids, pressure and temperature relations, and material's response to energy is described. A useful reference covering the introduction to the theory is found in [**45**].

"When two molecules approach each other in a fluid, at a temperature where their relative speed is likely to be low, their mutually attractive forces will bring about a temporary association between them." [**46**] The author goes on to explain that this association leads to condensation to a liquid, assuming high enough density and low enough temperature. The supercritical temperature is therefore the temperature at which condensation and evaporation can no longer occur. The typical phase diagram used to depict a supercritical fluid regime is calculated as a PT curve from the equations of state. Figure **8**

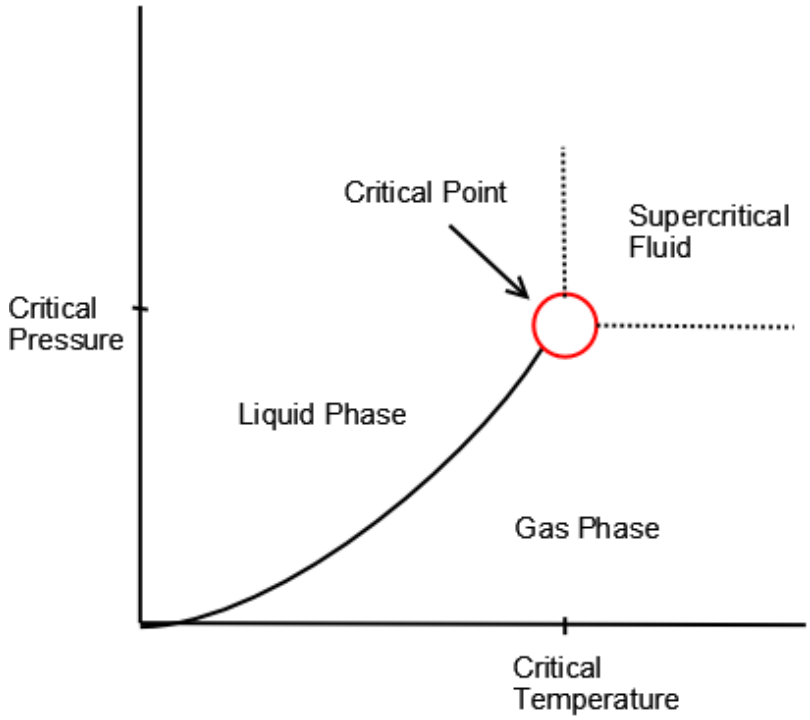

Figure **8**: Illustration of a phase diagram, on the pressure temperature plane. The diagram shows the equilibrium temperature and pressure point which the supercritical fluid phase begins, called the critical point. [**46]**

The physical description of a supercritical fluid is usually given as somewhere between a liquid and a gas. In terms of facilitating a chemical reaction there is more than one potential enhancement provided by the supercritical state. One is the solubility of the supercritical fluid with other reactants. The supercritical point represents a higher solubility than any temperature or state below it. However, the solubility of different materials will change as temperature is increased further based on their molecular properties. When a mixture of two materials with different critical points is present, the composite critical point lies on a path connecting the two.[**46**] Now the advantages of using a co-solvent like propane with methanol in a super critical process can be seen.

This does not address the energy associated with the bonding of two molecules, only the spatial separation of the reacting molecules. Once together, some energy must cause them to form

the new molecule. In some cases, the temperature needed to achieve the supercritical state is enough energy. However, from the previous literature, this would not account for the further rate enhancements by adding a catalyst. Simply put, if the thermal energy were sufficient to achieve the reaction, then adding a catalyst wouldn't improve the reaction rate assuming that the methanol is already perfectly diffused in the oil. First, to formalize the notion of improved solubility as a result of less polar molecular behavior in terms of hydrogen bonding one can observe neutron diffraction measurements which can measure distortions in the hydroxyl bond of methanol.[**47**] It is also reported that 70% of the hydrogen bonds of methanol are *broken* at the critical point and nearly 90% at 300 ^{o}C and 10 MPa.[**44**] This fact now formalizes the concept of methanol being miscible with oil at the supercritical regime. In its disassociated form the reactivity is different from the hydrogen bonded state. This clarifies the concept of sub-critical reactions being possible, but not nearly as efficient as that above the critical state.

2.4 Emulsion Science:

The discussion of emulsions is motivated by the need to understand better the notion of miscibility. It is apparent that in order for the biodiesel reaction to proceed the alcohol molecules must be in the vicinity of the fatty acid or triglyceride it is to combine or act on. However, it is not clear how and to what degree this can be achieved. Also if a mixing of two immiscible materials occurs, how does the resulting material behave?

For cases involving biodiesel production, a mixture of pure methanol and soybean oil is considered. The difference in molecular polarities indicates that they are immiscible, but one can envision an impeller dispersing drops of methanol into the oil. In a thermodynamic sense, the

system is no different than if it were two separate liquids. This description is, to a degree, accurate because as time passes the mixture will separate into two phases of pure liquids. This is a physical representation of the concept of thermodynamic equilibrium. In many ways the aim of emulsion science is to obtain mixtures of immiscible agents in as close to thermodynamic equilibrium as possible.

Emulsions are generally oil in water (o/w) or water in oil (w/o), in the case of biodiesel production the water molecule is substituted with the methanol phase. Physically, this substitution is perfectly reasonable as both represent polar molecules. The dispersed phase is of a lower volume portion and exists within the continuous, or matrix phase. In the case of typical numbers in biodiesel production molar ratios of alcohol to oil up to 42:1 represent w/o emulsions.

Since the goal is to have a perfectly mixed, or stable, emulsion, the two main topics in emulsion since are stability and methods towards achieving stability. Thermodynamically stable emulsions are considered microemulsions, with dispersed phase droplets smaller than the wavelength of light. Macro emulsions, or simply emulsions, range in scale of dispersed phase in the micrometers. As an unstable emulsion reverts back to equilibrium, several processes can occur. The types of destabilization of interest here are: ripening, creaming, flocculation, and coalescence. Figure **9**

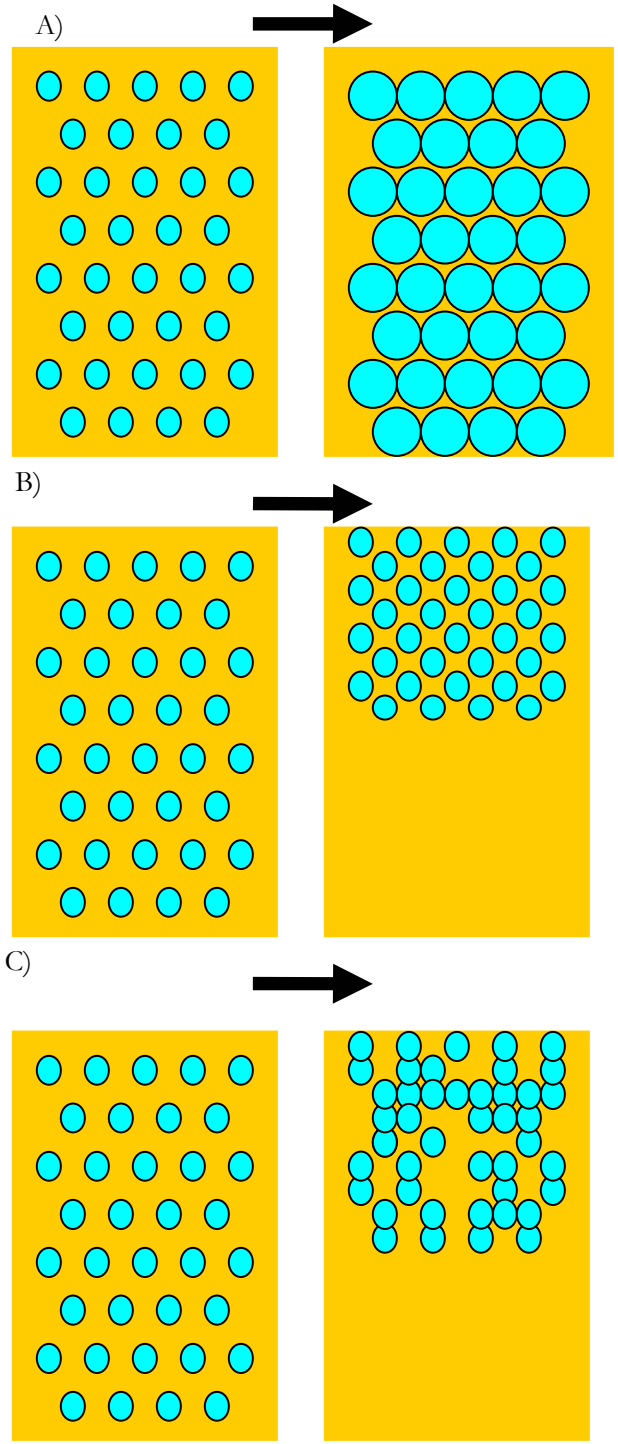

Figure **9**: Illustrations of typical emulsion destabilization mechanisms ripening (A), creaming (B), and flocculation (C) over time (from left to right).

Ripening refers to the change of the dispersed phase droplet diameter. Creaming is the motion of the lighter dispersed phase rising towards the surface. Flocculation describes the mutual attraction between particles drawing them into groups. Finally coalescence occurs when more than one dispersed phase droplet combines to form a new droplet.

Though the goal is to have a stable emulsion, the study of destabilization can be fruitful. For example, in the case of creaming, or sedimentation, Stoke's derived the rate of sedimentation of a solid sphere as Equation **1** , where u is sedimentation rate, g is the acceleration due to gravity, and r is particle radius. For two liquids, Equation **2** with a distribution of droplet sizes, r_i , becomes Equation **3** . Finally, an expression for the concentration of the dispersed phase at a given height, h, is written as in Equation **4**, where k is the Boltzman constant. [**48**]

$$u = \frac{2gr^2(\rho_1 - \rho_2)}{9\eta_2} \tag{1}$$

$$u = \frac{2gr^2(d1 - d2)}{3\eta_2} * \frac{\eta_1 + \eta_2}{3\eta_1 + 2\eta_2} \tag{2}$$

$$\bar{u} = \sum_i \frac{8\pi}{27\eta V} g n_i r_i^3 (\rho_1 - \rho_2) \tag{3}$$

$$n_h = n_0 \exp(\frac{-4\pi r_i^3 (\rho_1 - \rho_2) gh}{3kT}) \tag{4}$$

The importance of this theoretical description lies in the relation to dispersed phase radius. The stabilities of two emulsions can be compared to reveal the relative dispersed phase droplet radius. The primary method for stabilizing emulsions is to use a chemical intermediate called a surfactant. The chemical used as a surfactant is chosen based on a calculation referred to as a Hydro-Lipid- Balance, or HLB. This calculation is used to determine the extent of immiscibility of two liquids. The resulting number is used to choose a chemical surfactant, or emulsion stabilizer, to be added, which is of an intermediate HLB value. This calculation is relative to the comparisons made earlier between the chain length of a hydrocarbon and the relative miscibility with water. With a short hydrocarbon chain, methanol is similar to water, thus it replaces the water component in the terminology of emulsion science. Emulsion stabilizers include the free fatty acids and mono-glycerides that are present in biodiesel production. [**48**]

The point is best made in the review by Meher, who describes problems with emulsions forming in a biodiesel process. It was noticed that during the course of the reaction an emulsions would form and with quickly go away, when using methanol. However, with ethanol the emulsions would become more stable and frustrate the separation of products. This show seems to confirm the authors claim, and many others notion, that intermediate reactions creating mono- and di-glycerides improve the miscibility of the alcohol. However, with less polar ethanol this improved immiscibility actually stabilizes the reaction mixture. [**49**]

Chapter 3

Microwaves

3.1 Introduction:

The theory of electromagnetism represents the combination of two previously separate physical theories, namely electricity and magnetism. Stemming from Oersted's observation of electric current deflecting a compass, Ampere's proposed extension of this observation, and Faraday's generation of current from moving magnets and speculation about the electrical nature of light, Maxwell and Lorentz reconciled the two branches of physics with a concise theory. The introductory knowledge regarding Maxwell's equations and field theory that form the basis for concepts explained in this chapter is available in [**50**].

For practical purposes the electromagnetic (EM) waves will be considered to be microwaves (MW), which are characterized by frequencies of oscillation between 300 MHz and 300 GHz. For purposes here, the applications of microwaves are separated into two categories based on intensity. Low intensity MW may also be referred to as communication level and high intensity MW referred to as process level. Some communication applications include cell phones, wireless networks, non-destructive testing, and material property measurements. [pozar] Some process applications include heating, drying, sintering, chemistry processes, sterilization, baking, and pasteurization. [metaxas]

The theoretical aspects of low intensity MW are of interest in this study to describe absorption properties of materials and fundamental aspects of wave propagation. These descriptions are used to relate low intensity measurements to high intensity effects. Additionally, wave

propagation aspects are used to describe the practical design considerations of high intensity microwave applicators.

3.2 Electromagnetic Wave Propagation:

Maxwell's equations for free space of the form of Equation **5** , Equation **6** , Equation **7** , and Equation **8** , where **E** is electric field, **B** is magnetic field, μ_0 , is permeability of free space, and ε_0 is permittivity of free space, can be used to find the independent expressions for electric and magnetic field.

$$\nabla \cdot \mathbf{E} = 0 \tag{5}$$

$$\nabla \times \mathbf{E} = -\frac{\partial \mathbf{B}}{\partial t} \tag{6}$$

$$\nabla \cdot \mathbf{B} = 0 \tag{7}$$

$$\nabla \times \mathbf{B} = \mu_0 \varepsilon_0 \frac{\partial \mathbf{E}}{\partial t} \tag{8}$$

Each spatial component of the separate expressions both Equation **9** and Equation **10** , where t is time and c is the speed of light in a vacuum, satisfy the generalized three-dimensional wave equation. The resulting velocity of the traveling EM wave in free space can be shown to be the velocity of light in a vacuum in Equation **11** .

$$\mu_0 \varepsilon_0 \frac{\partial^2 \mathbf{E}}{\partial t^2} = \nabla^2 \mathbf{E} \tag{9}$$

$$\mu_0 \varepsilon_0 \frac{\partial^2 \mathbf{B}}{\partial t^2} = \nabla^2 \mathbf{B} \tag{10}$$

$$c = \frac{1}{\sqrt{\mu_0 \varepsilon_0}} \tag{11}$$

Considering now only sinusoidal propagating waves with spatial dependence in the direction of propagation, or plane waves, the time dependent traveling waves can be expressed as in Equation **12** .

$$\mathbf{E}(z,t) = \mathbf{E}_0 e^{i(kz-\omega t)} \quad \mathbf{B}(z,t) = \mathbf{B}_0 e^{i(kz-\omega t)} \tag{12}$$

It can be shown from Equation **6** , or Equation **5** and Equation **7** , that the electric and magnetic fields remain in phase and mutually orthogonal to the direction of propagation. In addition, the wavelength can be defined as the spatial distance the wave travels during the time to complete one oscillation cycle Equation **13**.

$$\lambda = \frac{c}{f} \tag{13}$$

Noting that the above electromagnetic wave travels in free space, it is worthwhile to address the energy and momentum contained within the wave. The total energy contained is equally balanced between the electric and magnetic fields. The energy flux can be expressed as product of energy density, u, and velocity, c, in the direction forming the Poynting vector, **S**, in Equation **14** , whereas momentum, $\wp$, is expressed as the quotient of the aforementioned terms respectively as in Equation **15** .

$$\mathbf{S} = \frac{1}{\mu_0}(\mathbf{E}\times\mathbf{B}) = c\varepsilon_0\mathbf{E}^2 = cu\ \hat{z} \tag{14}$$

$$\wp = \frac{1}{c^2}\mathbf{S} = \frac{1}{c}u\ \hat{z} \tag{15}$$

For practical purposes, the time averages of the above expressions are used to describe the average power and force transmitted by the wave, forming expressions for intensity, **I**, in Equation **16** and radiation pressure, P_R, in Equation **17** respectively.

$$I = \frac{1}{2}c\varepsilon_0 E_0^2 \tag{16}$$

$$\mathrm{P}_R = \frac{I}{c} \tag{17}$$

To describe electromagnetism in matter, as opposed to free space, the interactions with electrical components of the material must be taken into account. Practically, it is convenient to start with Maxwell's equations in terms of free charge and currents as expressed in Equation **18**, Equation **19**, Equation **20** , and Equation **21**, where **D** is electric displacement, ρ_c is free charge, **J** is free currents.

$$\nabla\cdot\mathbf{D} = \rho_c \tag{18}$$

$$\nabla\times\mathbf{E} = -\frac{\partial\mathbf{B}}{\partial t} \tag{19}$$

$$\nabla\cdot\mathbf{B} = 0 \tag{20}$$

$$\nabla \times \mathbf{H} = \mathbf{J} + \frac{\partial \mathbf{D}}{\partial t} \tag{21}$$

In this form, constitutive equations are needed to satisfy the system of equations. These relations are derived from the material's electronic and magnetic response to applied fields. The linear, homogenous material response is characterized electrically by the polarization and magnetically via the magnetization, Equation **22** and Equation **23**, where ε is the relative permittivity and μ relative permeability.

$$\mathbf{D} = \varepsilon\ \mathbf{E} \tag{22}$$

$$\mathbf{H} = \frac{1}{\mu}\mathbf{B} \tag{23}$$

In the absence of free charge or free currents, Maxwell's equations can be written in the form of Equation **5** through Equation **8** by simply substituting the permittivity and permeability constants of the material for those of free space. It follows that the EM plane wave solutions for intensity and radiation in free space remain valid with the same substitution. [**50**]

It should be noted here, that these assumptions do not provide an adequate description of the materials used in this study. In fact, stopping with this case would not leave the description of the effect of microwave heating. Nevertheless, despite the similarity of equations derived for free space, the possibility of a boundary created by two different materials leads to the description of wave scattering.

As a result of the conservation of charge and currents on the boundary, an EM plane wave impinging a boundary perpendicular to its direction of travel will redistribute its energy between the

two materials according to each material's electromagnetic properties. It is convenient to express the electromagnetic properties effecting wave scattering as the characteristic wave impedance, or index of refraction n, as in Equation **24**.

$$n = \sqrt{\frac{\varepsilon\ \mu}{\varepsilon_0 \mu_0}} \tag{24}$$

The resultant energies form the reflected and transmitted waves, with intensities summing to that of the incident wave. The ratio of the incident wave intensity to the reflected or transmitted wave can be expressed as the reflection, R, and transmission, T, coefficients as in Equation **25** and Equation **26** respectively.

$$R = \frac{I_R}{I_I} = \left(\frac{n_1 - n_2}{n_1 + n_2} \right)^2 \tag{25}$$

$$T = \frac{I_T}{I_I} = \frac{4 n_2 n_1}{(n_1 + n_2)^2} \tag{26}$$

When the incident wave approaches a boundary at some angle away from normal, the angle of reflection is equal to the incident angle. The angle of transmission, commonly known as the refracted angle, θ_T, is calculated from the ratio of material properties as in Equation **27**, where θ_I - Incident wave angle.

.

$$\frac{\sin(\theta_T)}{\sin(\theta_I)} = \frac{n_1}{n_2} \tag{27}$$

Now with descriptions of EM wave propagation and scattering in matter the concept of resonant geometries can be discussed. For simplicity consider a plane wave propagating between two perpendicular and perfectly reflecting boundaries. When the distance between reflectors corresponds to an integer multiple of the wavelength, the reflected waves combine constructively, creating a resonance. The concept of resonance is the basis for the design of many measurement and heating applications.

3.2.1 Electromagnetic Loss:

Now with expressions describing the propagation of EM waves in general and the generalized wave scattering solutions related to material properties, the practical application must now be considered. The assumption of absence of free charge and current requires that the electric and magnetic fields in a material resulting from an EM wave remain in phase and do not loose energy to the material. While this simplifies the expressions for waves, the preeminent presence of electrons in all matter makes this assumption fundamentally flawed. This flaw does not prevent the usefulness of the above description, noting that many simple optical problems can be described within this context. However, in the case of microwave heating, the presence of loss is a prerequisite. Consequently, communication level measurements made to analyze the potential interaction with process level microwaves must be sensitive to the origin of heating.

To formalize the mechanism of loss in real materials, Maxwell's equations in the form of Equation **18** through Equation **21** are used with out the assumptions regarding free charges and currents. For simplicity, the loss mechanisms in materials can be divided into two categories; those affecting the free current, called conductive loss, and those which arise through the free charge, called relaxation loss. Examples of conduction losses include electron conduction from free

electrons in a metal and the ionic conduction from impurities in a dielectric. From Equation **21**, the current density is related to the conductivity, σ, and the established electric field, Equation **28** .

$$\mathbf{J} = \sigma\ \mathbf{E} \tag{28}$$

Relaxation loss can be derived from Equation **21** by way of the constitutive relation in Equation **22** assuming an electric wave of the form in Equation **12** . The resulting expression for time rate of change of electric flux density is Equation **29** .

$$\frac{\partial \mathbf{D}}{\partial t} = j\omega\varepsilon\ \mathbf{E} \tag{29}$$

At this point, the forms of the expressions for permittivity and permeability must be examined. In the linear homogenous lossless material described in the previous section, these values were considered to be real constants. This assumption is reasonable in the case of permeability for the materials of interest herein. In addition, it can be assumed that the permeability is close enough to that of free space that it can be considered equal. Permittivity, on the other hand, must now be considered a complex value, which will allow for a phase difference between the electric and magnetic fields and loss to the material. The complex permittivity is expressed relative to that of free space as in Equation **30** , where ε' is the relative dielectric constant and ε'' is the relative dielectric loss factor. [**50**], [**51**]

$$\varepsilon = \varepsilon_0\left(\varepsilon' - j\varepsilon''\right) \tag{30}$$

The real term of the complex permittivity is called the relative dielectric constant and the imaginary term is referred to as the relative dielectric loss factor. Substituting Equation **30** and Equation **29** into Equation **21** an expression describing both mechanisms can be obtained as in Equation **31** .

$$\nabla \times \mathbf{H} = \left(\sigma + \varepsilon_0\omega\varepsilon''\right)\mathbf{E} + j\omega\varepsilon_0\varepsilon'\mathbf{E} \tag{31}$$

This expression can be simplified to the form found in Equation **32** , where the effective dielectric loss is expressed in terms of the conduction and relaxation losses as in Equation **33** .

$$\nabla \times \mathbf{H} = \left(\varepsilon' - j\varepsilon''_{eff}\right) j\omega\varepsilon_0 \mathbf{E} \tag{32}$$

$$\varepsilon''_e = \frac{\sigma}{\omega\varepsilon_0} + \varepsilon'' \tag{33}$$

This form provides a realistic model describing loss, regardless of its conductive or relaxation origin. As such, it is assumed herein that the expression for relative dielectric loss of a material will refer to Equation **33** , which approaches the value of pure dielectric loss at low conductivities or high frequencies. The loss tangent, $\tan(\delta)$, is a term commonly used to represent the loss of a EM system and is calculated from Equation **34** .

$$\tan(\delta) = \frac{\varepsilon''}{\varepsilon'} \tag{34}$$

While the relation to frequency of conduction losses is explicit in Equation **33**, the frequency dependence of dielectric loss is more obscure. To understand the basis for a frequency dependence of dielectric loss, the mechanism of polarization must be considered. When an electric field is applied to a dielectric medium, aside from ionic conduction, the electrons are not free to move and create current losses as in the conductive loss case. Instead, the electrons are relatively immobile, allowing them only to locally align with the external field to form dipolar regions in a material. The sum of these regions accounts for a materials polarization. In polar liquids, individual molecules form the dipoles which align to the oscillatory field resulting in a polarization field congruent with the applied field. However, as the frequency of the external electric field increases, the time taken for a dipole to rotate to equilibrium between cycle extents exceeds the period of a half cycle. This results in less external energy contributing to the induced polarization field, now out of phase, and instead

contributing to loss. The characteristic time related to polarization and depolarization of a material is referred to as the relaxation time. A relation between complex permittivity, in this case not referring to the effective dielectric loss, relaxation time, τ , of permanent dipoles in liquids, and the frequency of the applied electric field is described by the Debye equation. This relation is made using the dielectric constants at low, ε_s , and high, ε_∞ , frequency limits, as in Equation **35** .

$$\varepsilon^* = \varepsilon_\infty + \frac{\varepsilon_s - \varepsilon_\infty}{1 + j\omega\tau} \tag{35}$$

However, this solution does not approximate many dielectric materials which are not composed of dipolar molecules. For instance, the dielectric solid relies on electron transitions to form the polarization field. As a result, the Debeye model is left in favor of descriptions involving activation energies associated with various possible transitions. The resulting model describes solids and non-polar liquids more accurately, by accounting for various potential transitions.

To measure the dielectric loss of a material, an external EM wave is made to propagate within the test material in an otherwise well defined system. Before considering the system, EM wave propagation in a material with loss must be described. Without the assumptions inhibiting free charge and currents from Maxwell's equations and substituting the above expressions for current density and displacement current density, the uncoupled electric and magnetic field equations take the form of Equation **36** and Equation **37** respectively.

$$\nabla^2\mathbf{E} = \mu\sigma\frac{\partial\mathbf{E}}{\partial t} + \mu\varepsilon\frac{\partial^2\mathbf{E}}{\partial t^2} \tag{36}$$

$$\nabla^2\mathbf{H} = \mu\sigma\frac{\partial\mathbf{H}}{\partial t} + \mu\varepsilon\frac{\partial^2\mathbf{H}}{\partial t^2} \tag{37}$$

These equations can be reduced to the Helmholtz wave equation as before via the derivative relations of time varying waves of the plane wave form discussed above. However, the wave propagation constant is now given by the complex expression Equation **38** which relate the material properties to the attenuation, α, and phase, β, constants of propagation. The general electric field solution can be expressed by Equation **39**, and is accompanied by a similar expression for the associated magnetic field, where γ is the wave propagation constant.

$$\gamma = j\omega\sqrt{\varepsilon_0\mu(\varepsilon' - \varepsilon'')} = \alpha + j\beta \tag{38}$$

$$E = C_1 e^{\gamma z} + C_2 e^{-\gamma z} \tag{39}$$

To measure the electromagnetic loss of a material involves a collection of reflected and transmitted attenuation and phase constants of propagation as a wave propagates in a material of known geometry between two electric terminals. As each frequency of EM waves scatter, the reflected and transmitted energy can be correlated to the propagation constant of the material specimen. From the relation in [34] the relative permittivity and loss can be deduced from the attenuation and phase parameters. It can be seen that if no loss is present, the wave propagation constant reduces to the lossless case. In other words, the loss distorts the phase of an electromagnetic wave. [**52**]

From a practical point of view the dielectric loss measurement will relate to the relative dielectric loss and the conductivity, effectively making the dielectric loss in Equation **38** appear as the relation in Equation **33**. This means that the two effects, if present simultaneously, will not be distinguished by measurements. However, given the relation to frequency in Equation **33** and relaxation time in Equation **35** the two values can be analytically separated.

In terms of biodiesel reactants, the oil component is a relatively pure dielectric material, meaning it will not suffer appreciable loss to dipolar or conductivity mechanisms. Methanol, on the other hand, as discussed is a highly polar molecule, thus dipolar relaxation is expected. The addition of catalyst to methanol creates ionic conductivity which introduces conductive loss into the methanol material. While a more specific analysis is included in the results and discussion, the general expectation of measured dielectric loss for methanol with catalyst can be qualitatively inferred from Equation **32** with the dielectric loss term accounted for by dipolar relaxation of the form of Equation **35** as in Figure **10** .

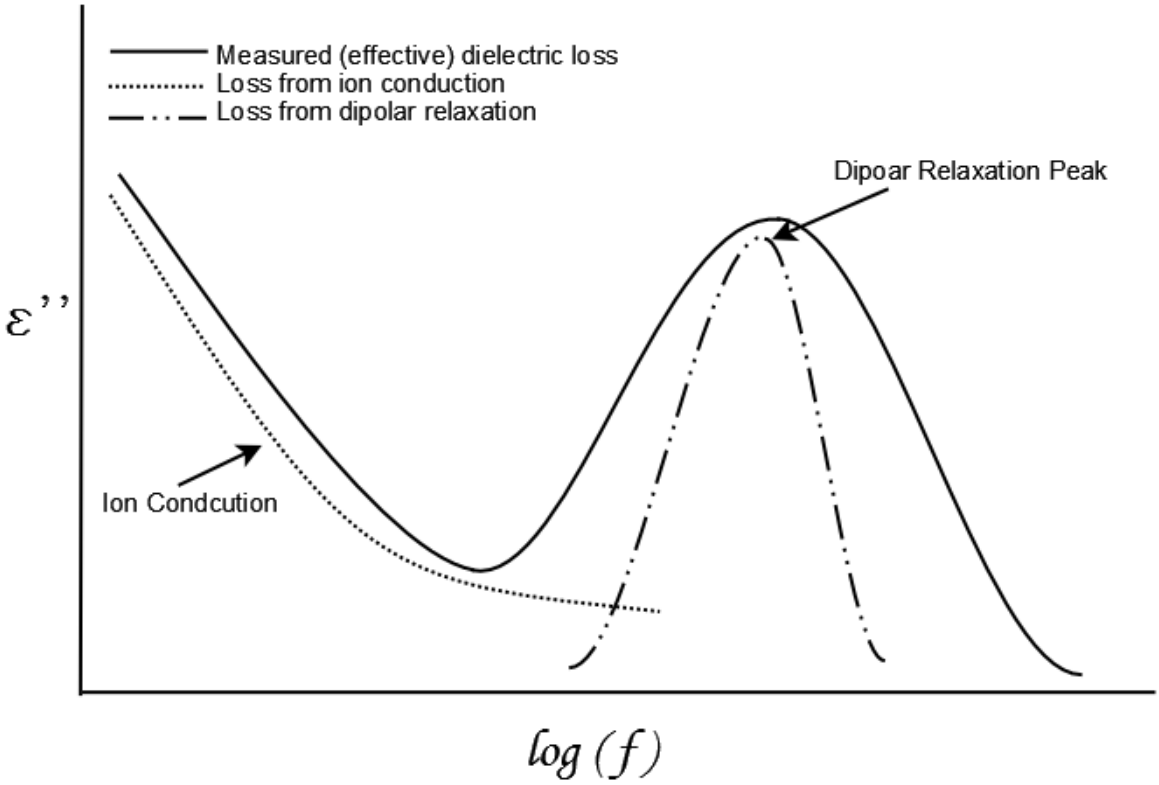

Figure **10**: A qualitative sketch of the expected dielectric loss of base catalyst dissolved in methanol. The dipolar relaxation and the ionic conduction contributions to the loss differ over microwave frequencies, similar to [**52**].

The ionic conduction and dipolar relaxations effect on the measured relative dielectric loss can be delineated based on the frequency dependence of each. As the next section explains, the measured dielectric loss is related to the amount of heating that will occur as result of the applied electric field. From this notion, it can be seen in the figure that materials such as methanol, with or without catalysts, will heat more readily at a particular electromagnetic frequency.

3.2.2 Microwave Heating:

The loss of electromagnetic energy in a material is manifested as heat. The origin of the heating is based on the type of the electromagnetic loss. As described in the previous section in the case of methanol with dissolved catalyst, both ionic conduction and dipolar relaxation contributed to the dielectric loss measured. From Equation **36** and Equation **37,** one can assume either negligible conductivity or permittivity and arrive at the diffusion or wave equations. Each simplification describes the effect of ohmic heating and microwave heating effects respectively. Though these simplifications prove unnecessary with representations resulting from Equation **31** through Equation **33** , the more familiar notion of ohmic, or inductive heating helps distinguish the heating mechanisms phenomenologically.

Whether as a result of currents in a resistive wire or surface currents from a magnetic coil, the fundamental process resulting in ohmic heating is the results of electrons causing molecular vibrations, or heat. The mechanism that makes this form of heating efficient is increase in resistively of the conductor as the temperature increases. In the case of ionic conduction in a dielectric, the function of electrons is replaced by charged ions. This phenomenon is a result of the conductivity loss entering the electromagnetic equations through the free current, **J**, represented in Equation **20** .

On the other hand, the permittivity of a pure dielectric is a result of Equation **18** and Equation **21** in the form of dielectric displacement, **D**, which relates to the polarizability of the material. In this way the polarization can be a result of the electric field slightly deforming the electron clouds to align with the external field, **E**. Since the electrons are essentially fixed, the degree of heating through this mechanism is dependent on the molecule or group of molecule's ability to align the field resulting from its electron structure. Thus, the dielectric electromagnetic heating mechanism is efficient due to its direct action on the molecular structure. However, the effect of increased absorption as the temperature increases is not necessarily the case, as the dielectric loss can decrease with temperature.

With the descriptions derived with a dielectric loss factor which accounts for both types of loss, the above description remains as such. The intensity or power absorbed by a material can be derived from the Poynting vector in Equation **14** using the relative dielectric loss portion of complex permittivity as defined in Equation **33** . Through the equation of state the relation between the electromagnetic energy absorbed and the rate of heating can be obtained in the form of Equation **40**, where T is temperature, C_p is the heat capacity at constant pressure and ρ_0 is the density. [**52**]

$$\frac{\partial T}{\partial t} \propto \frac{\varepsilon'' \mathbf{E}^2}{C_p \rho_0} \qquad (\mathbf{40})$$

3.3 Microwaves applications:

From this point the discussion of microwave heating will focus on concepts specific to the biodiesel process, limiting the materials to methanol, oil, and methanol with base catalyst. Also it is noted that the microwave frequencies available to use for high intensity heating applications are

dictated by the industrial, scientific, and medical (ISM) frequency bands, most commonly 915 MHz and 2.45 GHz. In terms of microwave absorption, and thus heating, the three materials are categorized in terms of loss mechanism. The oil component is considered a relatively pure dielectric, meaning the dielectric loss is not a function of microwave frequency. The methanol component is considered highly polar, compared to other primary alcohols, which means the microwave heating will have a strong relaxation peak at a particular frequency. The solution of sodium hydroxide in methanol would contain an additional ionic conduction loss which would contribute at lower microwave frequencies.

In chapter two it was determined that supercritical methanol was capable of driving the transesterification reaction without catalyst, which is beneficial to biodiesel production. The mechanism was based on the increased miscibility with the oil, high temperatures, and the breaking of hydrogen bonds between methanol molecules. Omitted from the discussion was research into the use microwaves to enhance the transesterification rate for biodiesel production.

The following sections will cover microwave heating effects on the materials described and microwave assisted biodiesel reactions.

3.3.1 Microwave superheating:

It follows from Equation **40** that the internal heat of a liquid undergoing microwave heating can be written as in Equation **41**. This allows the expression of microwave heating to be substituted directly in to Fourier's heat equation of the form found in Equation **42** .

$$\frac{P}{V} = 2\pi f \varepsilon_0 \varepsilon'' E_0^2 \qquad (41)$$

$$\rho C_p \frac{\partial T}{\partial t} + \kappa \nabla^2 T + \frac{P}{V} = 0 \qquad (42)$$

This description was used by Chemat and Esveld to model the microwave heating enhancement to boiling temperatures and reaction rates. Up until this point, the effect of microwave heating had been described as volumetric and only related to an improvement in efficiency as compared to classic heat conduction mechanisms. The authors cite several new studies regarding the ability to superheat liquids using microwaves. For example, the boiling point at atmospheric pressure for methanol is 65 °C, however, when heated with microwaves at the same pressure the methanol will heat to 79 °C. The authors show that under reflux the superheated boiling temperature could be maintained above the conventional boiling temperature. Further more, the study showed that the extent of superheated boiling temperature, defined as the sustained boiling temperature above the atmospheric boiling point, could be controlled.. They show that different nucleation mechanisms were capable of lowering the temperature of superheated boiling incrementally down to the conventional case. In addition, a model was developed based on Equation **41** and Equation **42** that accurately predicted the ability to increase the superheated temperature by the total MW power imparted to the sample. The authors state that microwaves used to superheat a reaction mixture at atmospheric pressure are equivalent to heating the reaction under its own pressure to the same temperature. [**53**]

The superheating of methanol represents a state of matter that is not predicted by the equations of state due to equilibrium conditions. However, the metastable state of superheated liquids is still a well studied phenomenon. In a chapter from a Supercritical Fluids textbook, author Debenedetti reviews several studies in superheated fluids. He explains that the extent of superheated is limited by homogeneous nucleation that occurs near the critical point of a fluid. As the

temperature approaches the critical point the rapid decrease surface tension and increase vapor pressure result in homogenous boiling. Many measurements tabulated seem to suggest that the limit to superheated temperature at atmospheric pressure is about 90% of the critical temperature. The derivation, omitted here, is based on microscopic vapor embryos that start near the atmospheric vapor pressure and expand thermodynamically until near the critical point and subsequently erupt, as in boiling. Perhaps, more interesting is the description of the droplet superheat method used to study the limits of superheating in liquids. In this technique, the superheated liquid is released as a small droplet and allowed to rise up through a denser immiscible phase which facilitates an ideally smooth interface minimizing non-homogeneous nucleation. The author claims that this method creates the deepest penetration into the metasable superheated region with repeatable results. [**44**]

Palacios et al studied the microwave heating profiles of several primary alcohols to determine the difference in heating based on the molecular structure. The heating rates indicated a lower dielectric loss for increasing number of carbon atoms forming the hydrocarbon chain. The study also showed decreasing dielectric loss with increasing temperatures for each alcohol. While the results are expected, the calculation of dielectric loss from heating profiles yielded values not supported elsewhere in the literature. [**54**]

Yoshida et al published a study regarding the effects of microwaves on soybean oil and free fatty acid mixtures. The results showed that under microwave heating, soybean oil oxidize rapidly. In addition, the presence of free fatty acids the oxidative rate was accelerated. Finally, the authors show that the enhanced oxidization from the free fatty acids increased with shorter hydrocarbon chains. [**55**]

The effect of chain length of hydrocarbons indicated, in both the case for oil and alcohol, that short chains are more active. These claims support the applicability of the description given in chapter two, regarding the suppression of the hydroxide ion in terms of dipole moment, to the description of microwave loss and heating presented here. The other aspect of concern to biodiesel production is miscibility. With evidence of microwaves ability to superheat methanol and the likeness of this metastable state to the supercritical state established, the last is ensuring that the energetic alcohol molecules come in contact with the oil and fatty acids.

3.3.2 Anisothermal Heating:

The other aspect to biodiesel production is the mixtures of alcohol and oil that occur. To describe the effects of microwave absorption of mixtures, mixing rules sometimes are used to scale the dielectric loss to ratios of its constituents. This may help model the overall heating trends, however the dielectric properties of each material will still lead to different heating patterns. Given a highly polar methanol droplet dispersed in low loss dielectric oil, the temperature gradient through selective microwave heating can enhance reaction kinetics at the interface. The subject of mixing rules will be discussed in the results and discussion portion; however, several interesting microwave heating studies have been conducted on mixtures of oil and water.

The studies on the microwave heating of emulsions are generally in the context of demulsification. Though this is contrary to the desired outcome for biodiesel production, the results are useful. Evdokimov et al. studied the demulsification of crude oil and water emulsions under microwave heating. The emulsions were prepared with a rotary mixer at 2000 rpm and droplet sizes were reported on the order of 8mm. The heating curves reported were widely varied and great lengths were taken in verbal description of possible reasons.[**56**] Another study by Abdurahman et al

investigated water in crude oil emulsions prepared in a 1600 rpm mixer with stabilizing agents. While the report was on deumlisification, the results reported showed longer separation time with increased temperatures from microwave heating.[**57**] A more conclusive study was conducted by Chih-Chieh et al. who report improved MW demulsification of water oil emulsions when the dispersed phase droplet size is larger, the matrix phase is of a lower proportion, and amounts of catalytic chemicals are increased.[**58**] Basak et al. support this notion by considering only droplet sizes greater than 5 micrometers. The author also cites another study which confirms the decreased effectiveness of microwaves to separate water in oil emulsions with small dispersed phase droplet diameters. [**59**]

Zhang et al. published a study regarding the natural convection that occurs within a material undergoing microwave heating. While the study did not include models for two phase systems, the result for a single phase were repeated for water and corn oil representing good and poor microwave absorbers respectively. The results are in the form of a three dimensional numerical simulation which shows that in water convection plays a significant role in temperature the redistribution of temperature gradients, while in oil they are not as significant.[**60**] This indicates the potential stabilizing nature of the oil in a biodiesel reaction mixture under microwave irradiation.

3.3.3 Microwave Chemistry:

Microwave heating for chemical applications is studied for a broad range of application. Kappe published a comprehensive review covering many reactions and microwave effects to chemical reactions of current interest.[**61**] A less recent, practical review of microwave technologies, effects, and applications was published by Straus. In this review, he discusses the use of microwave and methanol to complete reactions without catalyst. Specifically, that in the presence of microwaves, the presence of methoxide was sufficed with methanol. This fact hints at microwave

disassociation of methanol being more efficient than the thermal disassociation. The author also explains that when ionic conduction is in the mixture, at a certain temperature the conduction loss will overcome the loss to dipolar relaxation. [**62**]

Typical microwave processing systems consist of a current controlled magnetron which generates the electromagnetic waves into a wave guide. In an industrial setting, the wave guide traverses a circulator and tuning before being transmitted into the microwave cavity. The cavity, like the wave guide, is made of a conductive material and determines the mode(s) of wave propagation. The two principle types of microwave chambers are single mode and multi-mode and differ greatly in application, Figure **11.** A single mode chambers' dimensions represent a sealed microwave waveguide which creates a standing wave of the propagated mode. Though different modes have different EM distributions, single mode cavities generally exhibit very intense regions of microwave activity and are limited in sample residency volumes. Such a cavity would be most appropriate for a continuous flow system. A multimode chamber contains many superimposed standing electromagnetic modes resulting in a relatively even distribution of microwave energy. Such a system also affords large residency volume making it a suitable candidate for batch or stop flow implementation. Both methods face challenges in implementing a chemical reactor, however much research has been put into modeling MW reactors.

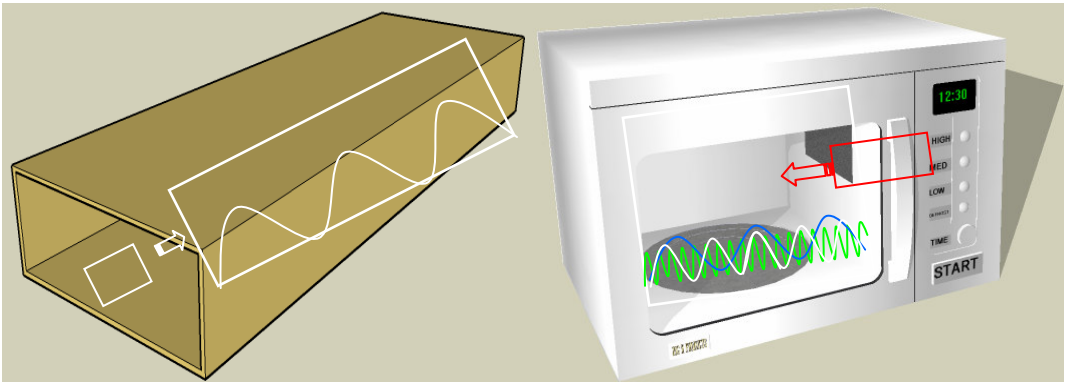

Figure **11**: Illustration of single mode (left) and multimode (right) microwave chambers.

Another review by Zhang covers the theoretical and modeling aspects to heat transfer and thermo-kinetics created by the use of MW in sterilization. His review covers many of the practical design considerations in terms of materials and dimensions of a microwave reactor from a modeling standpoint.[**63**] Several other comprehensive models for simple field simulations of microwave reactors are available in [**64**]. The modeling complexity resulting from a two phase system and continuous flow MW reactors were addressed by Lee, [**65**], and Ayappa, [**66**], respectively. Models including chemical reaction predictions were put forth by Huang. This study was unique in its use and modeling of a single mode resonant cavity and directly related the microwave energy to reaction rates.[**67**] Drexler et al presented a model for a tublular resonant chamber specifically designed for MW heating of emulsions. Within the analysis, the author recommends microwave power regulation to heat maximize heat distribution of an inhomogeneous and dynamic, reacting, phase.[**68**] Other reports of practical MW reactor designs can be found in [**69**], [**70**], and [**71**]. Finally, Benali et al has published a unique study of the effect of flow in a microwave chamber. Using infrared cameras, the author captures images of MW heating fluids as they flow through the reactive zone. These images are surely a helpful quantitative technique in the determination of optimal flow rates. The author

also demonstrates the improved absorption during flow utilizing a single mode chamber as opposed to a multimode. [**72**]

3.3.4 Microwaves for Biodiesel production:

Several reports have been made regarding the use of MW heating in the biodiesel production process. Masszocchia et al. present the use of MW heating for the both homgenous base catalyst and a heterogenous catalyst. The yields of methyl-esters under MW, determined by gas chromatography (GC), were compared to conventional heating processes. The results suggest that the amount of excess methanol required for a 99% conversion could be reduced from 18:1 stoichiometric ratio to oil to a 9:1 ratio. Results also showed much faster reaction times, from hours to minutes, as compared to conventional heating scenarios to MW heating. Finally, the amount of catalyst required was shown to reduce by a factor of three in the case of homogenous base catalyzed transesterification.[**73**] However, this study did not include any calculations of reaction rate constants or activation energies that could be compared to other techniques reported in literature.

Saiffuddin and Chua present a similar work using ethanol and used frying oil for a MW transesterification reaction. The results presented indicate a maximum yield with a 6:1 ratio of alcohol to oil and 0.5% sodium hydroxide catalyst by weight of oil. The authors also indicated that the subsequent phase separation of the glycerol byproduct and water from ester washing could be accelerated by MW heating. While this study also omitted any chemical rate analysis, it included a more in depth discussion of the potential reaction mechanism that is enhanced by MW radiation. The authors explain that MW fields cause the rotation of polar molecules which increases the accessibility of the hydroxide bonds.[**74**] This explanation is reasonable, as the hydrogen bonds formed in methanol are related to the alignment of many molecules. Under microwave heating, each

methanol molecule aligns with the field independent of its neighboring molecule. In this way, the MW heating affect weakens the hydrogen bonds at the onset of heating.

Leadbeater et al presentwork utilizing potassium hydroxide catalyst in methanol for transesterification of pure and used oils under MW heating. The amount of catalyst reported was 5% by weight of either a 6:1 molar ratio of alcohol to oil. Results were focused on demonstrating the scale up potential, which demonstrated batches as large as five liters. The use of a stirring mechanism was used in each test. The conclusion did not include reaction rate calculations and merely stated that using microwaves provided fast conversion rates at atmospheric pressure, specifically 98% conversion in one minute ate 55 ^{0}C. [**75**]

Hernando et al. present work demonstrating a flow process capable of similar conversion rates as those presented by Leadbeater and associates. The process developed, however seems more chemically intensive then other processes. The process utilizes ether, assumedly as a cosolvent, in addition to strong acid to help separated the ether and excess methanol through distillation. These chemicals are in addition to sodium hydroxide, methanol, and oil.[**76**] While the 98% conversion, resulting in fuel spec biodiesel, achieved in one minute is impressive, the amount of chemicals required for this process outweigh the conversion enhancement. The use of a cosolvent, however indicates the importance of mixing even in a MW reactor.

To summarize, it appears that the use of MW not only increases heating effiencies, but reaction rates as well. While specific reaction calculations apparently have not been conducted in the MW literature, comparisons to conventional heating methods indicated improved methyl-ester yield at similar thermal and chemical treatments. From the derivations presented in this chapter, this additional enhancement is explained in terms of anisothermal superheating of methanol. Given that

oil is less MW active then polar methanol molecules, it stands to reason that the methanol will heat disproportional to the oil. Furthermore, from description of technique used to study the superheated state, the oil phase can stabilize the superheated methanol up to 90% of its critical point at atmospheric pressure.

From chapter 2 it is known that as methanol approaches the critical point hydrogen bonds weaken and break allowing for enhanced reactivity. In this chapter it was explained that the core mechanism of MW heating of polar molecules necessarily weakens hydrogen bonding regardless of the temperature. With this knowledge, it seems that catalyst free biodiesel production should be achievable using microwaves whether in a supercritical state or a microwave superheated state. However, the description of the metastable, superheated state is completely dependent on nucleated boiling. If nucleation is prevented, then the reaction mixture will superheat, otherwise it will evaporate and boil. This would eliminate the advantages obtained by operating at atmospheric pressure. Finally, MW demulsification literature provides suggestions towards the stabilization of emulsions in microwave heating. Noting that MW would not separate emulsions with dispersed phase droplets smaller than five micrometers, a thorough and microscopically accurate mixing mechanism is sought. In addition to fine droplet dispersion, the relative size of the droplets should be as close to uniform as possible. This is a result of the anisothermal heating situation that occurs in MW fields. With different sizes of methanol droplets, it is expected that unevenly distributed temperature gradients would give rise to convection which would disrupt the metastable superheated state. So it appears that an ideally mixed emulsion with uniform dispersed phase droplets would maximize the microwave heating effects for biodiesel production.

Chapter 4

Ultrasonics

4.1 Introduction

Mechanical energy imparted to a material is dissipated analogously to electromagnetic energy. In place of the internal balance between electric and magnetic fields a mechanical body conserves energy within stress and strain. From the law of conservation of mass, momentums, and energies, the equations of motion can be derived. The generalized description of mechanical waves can be more involved in solids as a result of stresses which can be directionally dependent. In the case of ultrasound in fluids, this description simplifies significantly, as a fluid's properties are generally not directionally dependent. [77]

4.2 Ultrasonic waves in fluids

Euler's equation of motion for a hydrodynamic body can be written as in Equation **43** , where ρ is the materials density, **v** is velocity vector, F_v are forces due to viscosity, P is pressure, and $\Im$ is the potential for external forces.

$$\rho \frac{\partial \mathbf{v}}{\partial t} = -grad\ P - \rho\ \left(grad\ \Im\right) + F_{\mathbf{v}} \tag{43}$$

From the observation of conservation mass on a boundary element at equilibrium subjected to a pressure, one can derive the continuity condition as in Equation **44** .

$$\frac{\partial \rho}{\partial t} + div\ \left(\rho \mathbf{v}\right) = 0 \tag{44}$$

These equations, accompanied with the relations provided by the equations of state, can be used to derive wave behavior within the low amplitude assumptions, written as Equation **45** , where p and ρ' are the change in pressure and density from a previous equilibrium pressure and density, P_0 and ρ_0 respectively.

$$\begin{aligned} \left|\frac{P-P_0}{P_o}\right| &= \left|\frac{p}{P_0}\right| << 1 \\ \left|\frac{\rho-\rho_0}{\rho_o}\right| &= \left|\frac{\rho'}{\rho_0}\right| << 1 \end{aligned} \tag{45}$$

With the assumption of low amplitude waves comes the simplification of the velocity derivative in Equation **43** to exclude convective accelerations in the form **v**grad(**v**). The relation between the mechanical pressure and fluid velocity can be expressed as in Equation **46**.

$$grad\ \ p = -\rho_0 \frac{\partial \mathbf{v}}{\partial t} \tag{46}$$

The material properties enter into the wave behavior from the equation of state, which are linearized defining the modulus of elasticity, K, as the ratio of mechanical pressure, p, to the change in volume of an element, δ_V , in Equation **47** .

$$K = \frac{p}{\delta_V} \tag{47}$$

The speed of mechanical waves in an ideal fluid, c_0, can be related to the pressure and change in local density as in Equation **48** . For a simple fluid, the mechanical wave velocity can be expressed in terms of the heat capacities at constant pressure and volume, C_P and C_V, and the isothermal compressibility, β_T , in Equation **49**.

$$p = c_0^2 \rho' \tag{48}$$

$$c_0 = \sqrt{\frac{C_P}{C_V \rho_0 \beta_T}} \tag{49}$$

The wave equation is now written in the form of Equation **50**, which can be used to relate the mechanical pressure and the displacement.

$$div\ \ grad\ \ \mathbf{v} = \frac{\rho_0}{K}\left(\frac{\partial^2 \mathbf{v}}{\partial t^2}\right) \tag{50}$$

The use of the method of potentials provides a convenient form for wave analysis and can be performed by introducing the velocity potential, phi, and writing the relations in Equation **51** .

$$\mathbf{v} = -grad\ \ \Phi \quad p = \rho_0 \frac{\partial \Phi}{\partial t} \quad \rho = -\frac{\rho_0}{c_0^2}\frac{\partial \Phi}{\partial t} \tag{51}$$

Now the wave equation can be written in the more familiar form, as in Equation **52** .

$$\nabla^2 \Phi = -\frac{1}{c_0^2}\frac{\partial^2 \Phi}{\partial t^2} \tag{52}$$

It follows that a mechanical plane wave traveling in the x direction and oscillating at an angular frequency, ω , can be expressed in terms of pressure amplitude, p_m, and wave number, k, as in Equation **53** , with similar expressions for the velocity and thus displacement.

$$p = p_m e^{j(\omega t - kx)} \tag{53}$$

The relation between the wavelength, λ , wave number, speed of sound, and frequency are related in Equation **54** and the intensity can be expressed as in Equation **55**. [**78**]

$$\lambda = \frac{2\pi}{k} = \frac{c_0}{f} \tag{54}$$

$$I = \frac{1}{2}\frac{p_m^2}{\rho_0 c_0} \tag{55}$$

The scattering and diffraction equations follow analogously as those derived in the previous chapter. Though the relations between mechanical waves in a fluid and the material properties, once again the assumptions made to do so preclude the possibility of high intensity ultrasonic effects, such as cavitation. Before giving a description of high intensity effects, a brief description of mechanical loss mechanisms in a fluid must be presented for continuity.

4.2.1 Non-linear Ultrasonics:

From the hydrodynamic Equation **43** and Equation **44**, the generalized equation of state with quadratic parameters, and the introduction of the heat transfer equation, Equation **56** , one can write the relation Equation **57** , where B and A are nonlinear parameters related to the attenuation. [**78**]

$$\rho T\left(\frac{\partial S}{\partial t} + \mathbf{v}\nabla S\right) = \sigma_{ik}\frac{\partial v_i}{\partial x_k} + \kappa_t \Delta T \tag{56}$$

$$p = A\frac{\rho'}{\rho_0} + \frac{B}{2}\left(\frac{\rho'}{\rho_0}\right)^2 \tag{57}$$

Allowing for non-linear absorption permits more precise measurements of material properties. Davies et al presented a study which nonlinear parameters are measured ultrasonically in a specialized test chamber.[**79**] A review by Henning and associates describes several process measurements that can be conveniently made in situ through the use of ultrasonic probes. This

study describes how relatively new digital signal processing techniques and equipment have enabled a new area of research for ultrasonic process control. [**80**]

The nonlinear ultrasonic measurement that is most relevant to this study is the measurement of dispersed phase droplet diameters in emulsions and emulsion stability. Yi et al. report on the use of ultrasonic measurements to measure the stability of emulsions. The results show that ultrasonic measurements are capable of predicting the emulsion stability of a particular mixture. Emulsions in this study were limited dispersed phase diameter on the order of tenths of a millimeter as created by a rotary mixer operation at up to 600 rpm.[**81**] Wang et al. present a study of ultrasonic measurement for rapid determination of dispersed phase droplet diameter in emulsions. With a relatively simple ultrasonic measurement and automated digital signal analysis, the authors were able to distinguish between 0.5 and 1.4 micrometer droplets. The measurements were reasonably matched to the expected theoretical absorption of ultrasound.[**82**] While this measurement beyond the scope of this study, as no commercial forms are readily available, the measurement would be quite useful for in-situ monitoring of emulsion formation for various applications.

4.3 High Intensity Ultrasonics:

4.3.1 Ultrasonic Cavitation

The important effects of high intensity ultrasonics for this study are cavitation, atomization, streaming, and jetting. Each aspect is believed to be a component of ultrasonic emulsification, among other potential processes.

The assumptions made in Equation **45** are in direct conflict with the notion of ultrasonic cavitation. Moreover, the use of ultrasonics to create a cavity within a fluid is to provide pressures, p,

significantly above the ambient pressure in the fluid. It may seem that in order for a pressure wave to create a cavity within a fluid it would have to overcome the tensile strength of the fluid. However, the pressure needed to overcome the tensile strength of a fluid is often an order of magnitude more than observed in practice due to microscopic gas inclusions.

In general, ultrasonic cavitation occurs in three steps; bubble formation, growth, and collapse. The source of the initiation of an inclusion is somewhat debated, however, the following dynamics has been the subject of many exhaustive studies. The growth component is a result of the mechanical effects on the cavity enhancing gas diffusion from the liquid which further expands the cavity until it eventually bursts. The cavitation collapse is a highly energetic phenomenon, with temperatures measured on the order of 5,000 to 10,000 K and pressure of the resulting shock wave on the order of MPa. [**78**] It is well known that the contribution of such events, as depicted in Figure **12** comprises the chemical effect of ultrasound. More specifically, the enhancement to reaction rates due to ultrasonic cavitation is a result of the localized extremes in temperature and pressure. [**83**]

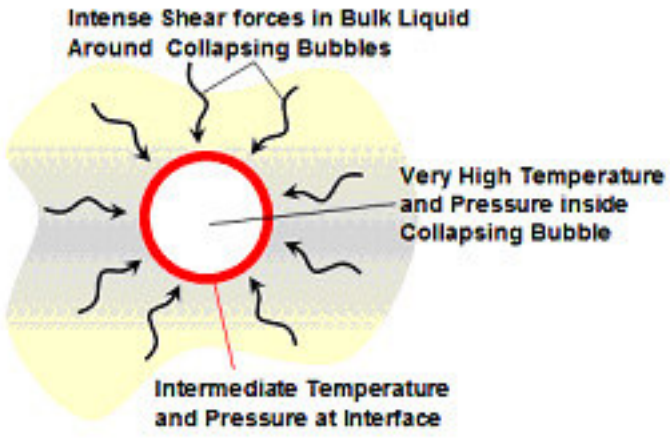

Figure **12**: Illustration of the extreme environment created in and around a cavity collapse during ultrasonic cavitation. **[83]**

More interesting to this study are the effects of high intensity ultrasonics in two phase systems; however for completeness a review of modern research into cavitation phenomena is first presented.

A comprehensive introduction to the theoretical considerations involving cavitation growth and collapse phenomena is found in [**78**]. The energy imparted from a cavity collapse is proportional to the size of the cavity during the growth phase. Many studies are dedicated to the non-linear description of bubble dynamics subjected to oscillations in a fluid. For example, Maksimov presents an exhaustive theoretical treatment of the oscillation of gas bubble. The result of this model allow for predictions of cavity collapse size, and thus energy of collapse, base on the material properties of the fluids used.[**84**] A global model of cavitation derived in terms of free energy was reported by Floris. This model focused on the free energy of cavitation which is said to contribute to the solvation energy. More specifically, this model includes the details regarding the resulting structure of solvent molecules around a solute body. As cavitation proceeds and one material is dissolved into another, the parameters for cavitation are altered. This model provides for such interactions and predictions towards the necessary cavitation energy to dissolve a material in a solvent. The applicability of this model is limited, and the results present show little improvement over more simple models. [**85**]

A simple model was described by Raman et al., which utilized the Helmoltz equations to model the localized pressures created during an ultrasonic resonance mode. However, this model did not include actual cavitation phenomena. Instead the authors establish a threshold pressure for cavitation, which when simulation results exceed the value at any location cavitation is assumed.

This type of study is useful mainly from a reactor design standpoint, as the actual cavitation phenomenon is assumed. [**86**]

Servant and colleagues have reported on numerical simulations of cavitations resulting in a two dimensional visualization of the cavitation field in a liquid. This model accounts for the reactor chamber design. The results of this study provide a useful picture of cavitation generation within a specific geometry.[**87**] The previous study could subsequently be combined with numerical models that predict the pressure emitted from a particular transducer design, such as that presented by Liauh et al., among others. This study focused the pressure waves generated from a disc shaped transducer. Although the simulation was not specific to high intensity application, the pressure waves needed for cavitation in a fluid are within the limits of the solid transducer body as described in Equation **45**.[**88**] One interesting deviation in sonochemical reactor design modeling came from Moholkar et al. In this report, a sonochemical reactor operating at two frequencies is considered. The results of this study suggest that a second ultrasonic frequency can be used to control the rate of cavitation, either by contribution or inhibition. [**89**]

4.3.2 Ultrasonic Emulsification:

To quantify the mechanical mixing effect of high intensity ultrasonics, non-linear interfacial phenomena must be considered. Aside from cavitation, high intensity ultrasonics can also create acoustic streaming. Without theoretical description, acoustic streaming involves the induced flow in fluids. This is a result of the average pressure difference created between the pressure field of the transducer and the surround liquid. This effect occurs simultaneous to cavitation phenomena. This phenomenon accounts for the bulk mixing in a fluid. For example, as products are formed in the pressure field of the transducers, acoustic streaming will redistribute them in the surrounding fluid

allowing reactant mixtures to replace the reacted products in the ultrasonic treatment zone. In general, this effect is analogous to stirring.

The ultrasonic mixing effect is not due to acoustic streaming; however it is debated as to whether the effect is derived from cavitation disruption at an interface or capillary wave atomization. In the opinion of this author, both effects occur in during ultrasonic emulsification. The dominant phenomenon appears to be that which produces the most stable emulsion. In these terms, most stable is to mean smallest dispersed phase droplet sizes. So if two competing emulsification effects are occurring, the one resulting in smaller droplets will dominate as it would reduce the larger droplets. Nevertheless, to obtain a notion of the effect of ultrasonic power and frequency both cases must be considered.

From the derivation of Equation **52,** assuming a plane wave of the form in Equation **53** , the surface displacements of a free boundary, liquid and air, can be derived as Equation **58** , where ζ is the out of plane displacement on the surface of the liquid. From this expression, viscous dampening terms, and the frequency relation to displacement amplitude, it is observed that a surface, or capillary, wave resonance can occur. The wavelength of such a resonance is described by the capillary wavelength in Equation **59**.

$$\zeta = \zeta(t)\cos(kx) \tag{58}$$

$$\lambda_C = \left(\frac{8\pi\sigma_L}{\rho\ f^2}\right)^{\frac{1}{3}} \tag{59}$$

The standing capillary wave accounts for the atomization process of high intensity ultrasound. Atomization occurs at the crest of the capillary wave when the displacement overcomes

the surface tension ejecting a certain mass of fluid. Several relations between the size of the droplets formed and the capillary wavelength have been derived. However, the simplified expression in Equation **60** is found to be reasonable for practical purposes, where the average droplet diameter is D_d and α_a is a constant determined from practical measurement.

$$D_d = \alpha_a \lambda_c \quad \alpha_a \to 0.3 \tag{60}$$

This description would not describe emulsification, as the layer created by immiscible fluid is not equal to the free surface of a fluid. It can be expected that the second layer would inhibit the ejection of water droplets shifting the droplet size towards smaller diameters. In addition, a cavity created in one fluid imparting a boundary results in a violent disruption. The result of this imploding cavity's shockwave at the interface corresponds to fluid jets. The jets created are analogous to acoustic streaming discussed above; however the flow velocity is significantly higher. While no equations exist quantifying this effect in ultrasonic emulsification, the general notion of the phenomena is accepted. In addition, the relation to frequency and droplet size derived from a capillary wave holds. [**78**]

To gain a practical description of ultrasonic emulsification, descriptions in the literature are discussed. As common to the literature the terminology for dispersed phase droplet diameters will be considered particles or droplets. An early review by Bondy et al. described the phenomena of emulsification and cavitation without specific determination of the origin of effect.[**90**] In a more recent textbook in emulsion science, Binks identified a qualitative correlation between, what he terms *oscillatory shear* and the size and variation of dispersed droplet diameters. Bink's points out that truly monodisperse droplet diameters can be achieved with sufficient amplitude. In addition, the diameter of the resulting monodisperse droplets can be decreased with increasing frequency. [**91**]

Rajagopal reported on the particle size variation over time during emulsion destabilization and formation via ultrasonic methods. The results showed a steady decrease in particle size during emulsification. The author concludes with the admission that the model for ultrasonic emulsification did not follow experimental finding. Specifically, the limit of droplet size, on the small side, was never reached.[**92**] The author followed this work with another report on the theoretical kinetics of ultrasonic emulsification. In this study, the author presents the emulsification process as a sum of competing processes. More specifically, he separates the lower intensity ultrasonic effects occurring on the bulk interface from those occurring at higher intensity through cavitation. However, the theory presented did not predict particle size or the effects of frequency of ultrasound. [**93**]

Rajan et al.conducted extensive correlations relating to the droplet size created through the ultrasonic atomization process. However the study did not include two phase systems as in the case of ultrasonic emulsification.[**94**] Behrend et al. studied the effect of continuous phase viscosity. The authors examined several other emulsification techniques in comparison to the ultrasonic technique. Results of this comparison showed ultrasonic emulsification producing smaller droplets at given energy density than most commercial emulsification. This point is worthy of noting because the ultrasonic system used was not a commercial unit. The authors also observed that without stabilizing agents the dependence on viscosity was not apparent. The results show that ultrasonic emulsification was as capable of high pressure commercial systems for continuous flow. [**95**]

Chuchevel etl al. presented a study on the effect of power on ultrasonic emulsification. The results show that the intensity of ultrasound only affects the rate of emulsification. This concept opposes the concept of the existence of a threshold for emulsification.[**96**] This concept was supported by a pair of investigations conducted by Abismail et al. The results of these studies clearly indicate the ability of ultrasonic emulsification to create smaller dispersed droplets than conventional

mixers using the same power. The authors also note that emulsions made with ultrasound are less polydispersive in droplet diameters than other techniques. The studies also utilize light scattering methods to measure the droplet size. Normally this technique requires a dilute solution of particles, so the authors compared the measurement to that without dilution. The results indicated similar measurements of diameter regardless of dilution. However, the emulsions investigated utilized stabilizing agents which would help prevent changes during dilution. The most alluring claim of the studies was the conclusion that the small, monodisperse droplet sizes created by ultrasound created more stable emulsions. [**97**], [**98**]

Timko et al. have reported on reactions occurring within microemulsions. The study utilized near critical carbon dioxide in water emulsion created ultrasonically without stabilizing agents. The study included a unique ultrasonic emulsion reactor with droplet sizes of the order of microns. The study also included several reaction rate models which were used to compare the mass transfer effect of ultrasound.[**99**] The study verifies the ability of ultrasound to disperse a supercritical reactant in a continuous phase with a higher critical point.

4.3.3 Ultrasound in chemistry:

An early review in sonochemistry described cavitation effects as decreasing boiling temperature of liquids. The early studies utilized opalescent reactions to measure the temperatures and pressure created during cavitation. Observation suggested that during cavity collapse supercritical temperatures and pressures were achieved. Studies also showed that ultrasonic waves could cause violent disruption of superheated fluids resulting in explosive boiling. [**100**]

High intensity ultrasound can be applied in several different methods. The most basic scheme involves the direct application of a transducer to the work medium. However, this technique is limited in maximum power output by the size of the transducer. In order to amplify ultrasonic power and control frequency, an applicator, or sonotrode, is often used. In general, a sonotrode is a specially designed resonant body, tuned to efficiently couple a certain frequency of ultrasound. Two common types are the wavelength stepped sonotrode and the exponential horn as in Figure **13**. The advantage of such sonotrode designs include: thermal insulation, isolated electronics, tailored surface area independent of transducer frequency or size, and acoustic power amplification.

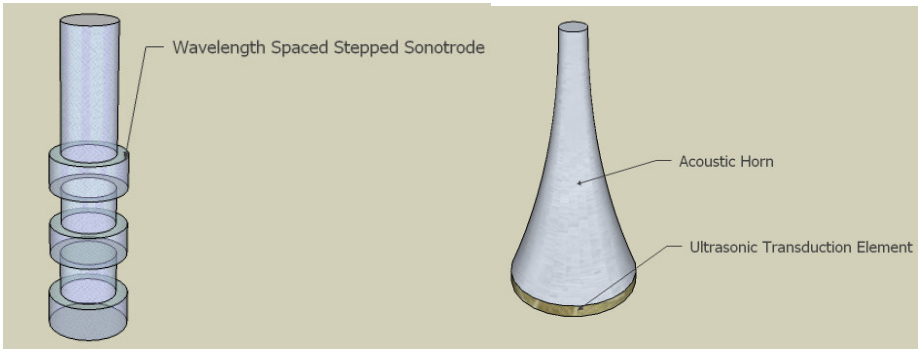

Figure **13**: Two types of ultrasonic horns are illustrated. The steped horn (left) is more common in large scale applications while the exponential horn (right) is more suitable for small volumes.

A modern and concise review regarding the chemical effects of ultrasound is given by Suslick. This report describes the high temperature, pressures, and shock wave created by cavitation and how they relate to chemical activity. In general, the temperatures and pressures contribute to the reaction as normal. However, the concentration and localization of these thermal energies make up the unique aspect of cavitation. Furthermore, the shock wave created at interfaces is sufficient to disrupt a two phase system or even coagulated nanoparticles. [**101**]

A modern and comprehensive review of the use of high intensity ultrasound in chemistry is provided by Thompson et al. This review includes the chemical contribution of cavitation to several different reactions as found in the sonochemistry literature. A short portion discusses the use of high intensity ultrasonics for phase disruption of heterogenous systems. In the case of liquid – liquid systems, the use of high intensity ultrasonics creates very fine dispersed phase droplet sizes. In addition, the review covers many different ultrasonic reactor designs. One interesting point is the discussion regarding the transduction materials which indicate that, for industrial processes, magnetostrictive elements offer better response and durability than piezoelectric material. [**102**]

The issue of using high intensity ultrasonic reactors on the industrial scale has also been addressed. Mason wrote a review discussing the applications of high intensity ultrasound to industrial processes. In conclusion, the author stated the need for optimization of industrial scale systems. Hielscher wrote a review of the process of developing an industrial size ultrasonic emulsification or sonochemical system. The author states that the ability of ultrasonics to make nano-size emulsions is already available on the industrial scale. The article covered three steps in the development of a new industrial ultrasound process; feasibility study, optimization, and scale up.[**103**] It is noted that the previous author has interest in the promotion of the ultrasound equipment recommended for each step. Never-the-less, the question of whether ultrasonic systems are scaleable is answered.

4.3.4 High intensity ultrasound in biodiesel production:

Lifka et al. compared the effect of ultrasound to that of 11,000 rpm mechanical stirrer in terms of mass transfer during biodiesel production. The comparison included acid and base catalyzed reactions. In the case of the, slower, acid catalyzed reaction the ultrasonically mixed runs

showed a considerable improvement in yield over the other methods. Under basic conditions, the reaction yields were similar at the onset. However, as yields increased and began to level off, ultrasound was shown to drive the reaction to further completion. The authors also compared power consumption, noting that the use of ultrasound achieved higher yields with less electrical power than any of the comparison methods. [**104**]

Zhu et al.reported on the use of ultrasound in biodiesel production using base catalyzed reaction. The study included an investigation into the effect of frequency. This was tested by subjecting thin foil to ultrasonic cavitation in three 100 Watt cleaning baths with frequencies of 28 kHz, 45 kHz, and 100 kHz. The foil that suffered the most damage was used for the study, which was the 28 kHz case. The remaining results indicated that biodiesel made using ultrasound performed the same as other biodiesel fuels in power output and fuel consumption measurements of diesel engines.[**105**] The frequency analysis presented in this study was based on the notion that a strong cavitation phenomenon is the good measure of sonochemical contributions to the transesterification measurement. Furthermore, it was not considered that the higher frequency ultrasonic baths operate at lower displacements given the same input power. Nevertheless, the authors did establish that little or no additional effect to the resulting fuel was created through the use of ultrasound.

Singh et al.reported studies utilizing ultrasonics for base catalyzed transesterification. The experiments utilized soybean oil, methanol, and potassium hydroxide catalyst in a power adjustable ultrasonic reactor. Authors claim improved yields compared traditional methods, yet perform no reaction rate calculations. The ultrasonic frequency used was 28 khz with powers varying from 79 to 131 kWs. The reaction time for 98% yield of methyl esters was reported to be 5 minutes. The authors claim that the reaction yields decrease with increasing power.[**106**] In a later article from the

same authors, the effect of power is reported with a similar trend.[**107**] The correlation of ultrasonic power in this study was misleading. The results show that the reaction temperatures increased with increasing power, which is known to decrease the amount of power delivered from a cavitation collapse. The authors did not account for or attempt to control the temperature of the reactions.

Stavarache et al. analyzed the use of ultrasound for biodiesel production on a variety of oil types. Using KOH base catalyst and methanol in glass flasks, the reactions were driven via an ultrasonic cleaning bath filled with water. This approach allowed for temperature control. The results indicated that under ultrasound, the limiting step in the reaction changed from the classical case. Instead of the reaction from diglycerides to monoglycerides as the rate limiting step, it was reported that the MG to glycerol step became the limiting factor.[**108**] Controlling the temperature of the reaction was an improvement to other studies, however the interface created by the water in the ultrasonic bath and the glass reaction likely dissipated the majority of ultrasonic energy generated.

Stavarache et al.followed the previous study with the development of a continuous flow ultrasonic reactor. This reactor design did not suffer the energy loss created in the previous study. The study included a small and large scale ultrasonic reactor operating at 45 kHz and 600 Watts, with working volumes of 2.6 and 6.35 liters. Optimal chemical requirements were determined to be 7.5 : 1 molar ratio of alcohol to oil and with an undisclosed amount of base catalyst. The reaction vessel was water cooled to prevent heat dissipation. The results indicated acceptable yields with a 20 minute residency which correlated to about 19 liters per hour.[**109**] The reactor presented in this study is ideal for the determination of sonochemical contribution of ultrasound, but perhaps not for the production of biodiesel. The forced cooling of the reactor while maximizing the power from a cavity collapse, limits the reaction kinetics. A hybrid approach involving an ultrasonic and heat

treatments is needed to determine the point when a mixture is more efficiently driven with heat than ultrasonic cavitation.

Siatis et al. preformed a short study using ultrasound in a combined oil extraction and base catalyzed transesterification reaction. The authors used seed cake, a valued byproduct from seed crushing facilities, to produce biodiesel. The use of ultrasound was claimed to enhance the extraction of oil from the used seed cakes while simultaneously converting to methyl esters through transesterification. [**110**]

Wu et al. recently published a unique study regarding the dispersed droplet size of ultrasonically formed biodiesel mixtures. The authors measured droplet size using light scattering techniques for both rotary mixed and ultrasonically mixed biodiesel reactant emulsions. The results showed that ultrasonic techniques produced smaller droplets that standard mixing.[**111**] This study was the first to discuss the mixing effect of ultrasound in the biodiesel process. However, the authors used surface active emulsion stabilizers, which limit the applicability of dispersed phase droplet size. Furthermore, the study focused on the comparison to convention mixing as opposed to ultrasonic optimization.

In summary, it appears that high intensity ultrasonics could provide the means to form catalyst and surfactant free emulsions of methanol and oil. The advantage of ultrasound is the ability to control the dispersed phase size and polydispersivity. In turn, it appears that the combination of ultrasonics with microwave heating may extend the superheated behavior of reactant mixtures. With extension into the superheated methanol state, reaction rates should be improved.

Chapter 5

Methodology

5.1 Ultrasonic Emulsification

Ultrasonically formed emulsions are prepared from various reaction mixtures pertinent to the transesterification reaction. The stoichiometric ratios of lab grade methanol to refined, degummed, deodorized and bleached soybean oil used were: 3:1, 6:1, and 9:1 varying from the stoichiometric ratio to a typical industry ratio. To calculate the molar mass of soybean oil, reference values for the fatty acid profile are utilized from the contribution of various carbon chains that make up the triglycerides of soybean oil.[**16**] In addition, Sodium Hydroxide base catalyst was used in varying concentrations as dissolved in the appropriate volume of methanol. The catalyst is measured on a precision scale and stored with desiccates to prevent any humidity from being adsorbed. The base catalyst concentrations vary from 0%, .1%, .5%, and 1% wt-wt soybean oil and are chosen to span from relatively slow catalyst free reaction rates to typical catalyst concentrations used in industrial batch processing. The intermediate catalyst concentrations correspond to reaction conditions reported in the literature in chapter 2.

The choice in ultrasonic equipment was dictated by the desire to investigate the amplitude and frequency parameters' affect on emulsification. The two instruments utilized represent the two most common types found in a laboratory, namely an ultrasonic cleaning bath and an ultrasonic homogenizer, or horn. The Sonix Systems cleaning bath is powered with a non-adjustable 600 Watt, 44 kHz auto-tuning amplifier with remote on/off functionality. The capacity of the ultrasonic bath is more than five gallons, and after initial attempts, it was determined that at least 1 liter of fluid was

necessary to ensure reasonable distribution along the basin of the bath. The bath verifies the ability to apply high intensity US to larger volumes than with more sophisticated horns. The ultrasonic energy is transmitted through the thin, metal bottom of the vessel by a parallel network of tuned, compressed piezoelectric, longitudinal stack actuators, Figure **14** .

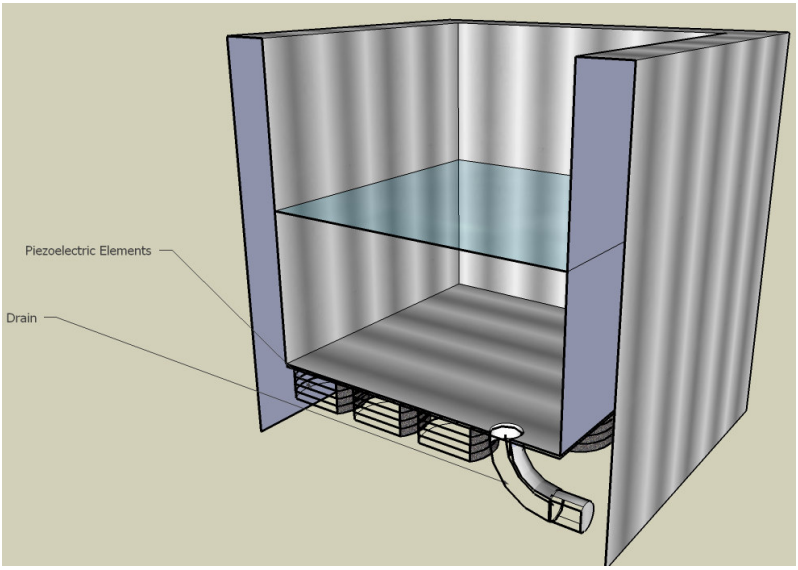

Figure **14**: Illustration of the 600 Watt ultrasonic cleaning bath used for 44kHz ultrasonic emulsification.

The same mixtures are emulsified using a Branson brand 20 kHz ultrasonic transducer attached to an exponential type horn and a power adjustable 600 Watt manually tunable amplifier. This horn is found to be more convenient for small sample preparation as it is more portable, allowing closer proximity to measurement devices. This advantage, however, must be considered in terms of emulsion stability. Because it is expected that different ultrasound treatments will vary the resulting emulsion's stability, the appropriate time must be kept between emulsification and measurements for the horn and the bath, if measurements are to be used to compare techniques. For example, though it may be convenient to make emulsions with the portable ultrasonic horn near

the measurement device and follow with immediate measurements. However, if the bath is less conveniently located the time between emulsification and measurement will be inherently longer.

The goal of this procedure is to analyze the dynamic effects of ultrasound as evident through mixing. With the knowledge of the relation between mechanical result of high intensity ultrasonics and the affected bulk material properties, an optimized process can be chosen to facilitate a particular effect of a subsequent treatment. The primary goal is to extend the stability of the emulsion and superheating of dispersed methanol during microwave heating.

5.2 Optical Analysis

As a means to measure resulting emulsion microstructure from various ultrasonic treatments, specifically the diameters of the dispersed phase, optical microscopy is employed. Two microscope systems are utilized in the optical analysis, one utilizing a 200x objective and a .3 Mega pixel CCD and the other a 100x objective and a 2 Mega pixel CCD. The first microscope requires manual calibration for digital image analysis and several images of each trial to encompass enough measurements. To calibrate, a reference grid is imaged at the magnification to be used several times to establish an average value for micrometers per pixel. Using imaging software more than forty measurements are made in pixels from the start of one reference bar to the start of the next. The number nearest the reference bar indicates the quantity of the measured distance within a centimeter. For example, the representative measurement in the below figure is approximately 270 pixels, therefore 18*270pixels is 4,590 pixels per centimeter or between 4 and 5 pixels per micrometer.

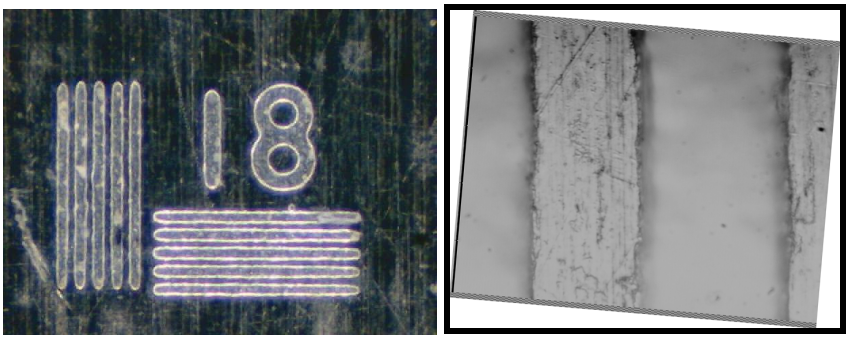

Figure **15**: Digital image of the reference grid using 100x and 500x optical magnification.

The second microscope automatically saves the pixel length reference for each magnification. Using a lower magnification objective, more dispersed droplets are captured on a single image. The increased resolution of the CCD maintains a degree of precision that would otherwise be lost at lower magnification. To ensure the previous measurements based on a manual reference coincide with this microscope, independent trials of the same preparation routine are measured for continuity.

When obtaining optical images of emulsions, care is taken to: isolate regions with large populations of the dispersed phase, avoid focal planes near the surface of the optical slide or cover, and avoid any contaminants or aggregates such as large air pockets. Though subjective, this is thought to reduce measurements based on interactions created by the measurement as opposed to the process. Once digital images are obtained, each bubble on the focal plain of the optical objective is measured across its diameter. To obtain enough measurements to encompass the statistics, a goal of 300 measurements per trial is set. The resulting measurements are analyzed in a population distribution with bin widths related to the maximum possible resolution of the image.

5.3 Dielectric Measurements

Permittivity measurements are made by monitoring the material response to low intensity external electromagnetic (EM) energy. The source and receiver for this function is generally a vector network analyzer which generates a frequency band of low intensity EM signals while simultaneously recording the scattered energy at two electrodes at each of two terminals. The voltage ratio of a wave incident to one given port to a wave initiated from another given port, defines the scattering parameters. These scattering parameters are written as S_{ij} where the indices i and *j* indicate the incident and source ports respectively. Thus S_{11} represents the sum of the reflected energy with components due to the reflection at the material boundary and the propagation within the material as internal reflections contribute. The transmission terminal, S_{21}, represents the transmitted energy as the sum of the propagated waves including internal reflections. Thus, the resulting scattering parameters are representative of compilations of all of the internal reflections within the material as in Figure **16**

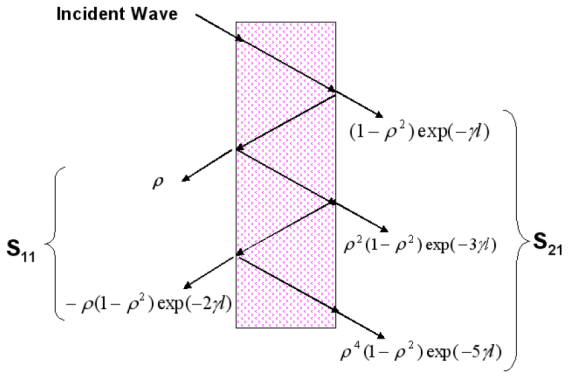

Figure **16**: Illustration of the composition of the scattering parameters obtained via dielectric resonance spectroscopy. [**112]**

The measured scattering parameters provide attenuation and phase from the incident and scattered fields. These values quantify the interaction between the EM energy with the sample

material through wave propagation to the complex reflection and propagations terms ρ and γ respectively, Equation **61**

$$S_{11} = \rho \frac{1-\exp(-2\gamma l)}{1-\rho^2 \exp(-2\gamma l)} \quad S_{21} = \frac{(1-\rho^2)\exp(-\gamma l)}{1-\rho^2 \exp(-2\gamma l)} \tag{61}$$

The analysis is not straightforward, and often requires an initial guess, manual fitting, and iterative regressions to quantify the contribution of the material to the overall response. For example, an initial estimate of the effective permittivity can be obtained using Equation **62** to estimate the reflection term ρ.

$$\rho = \frac{1-(\varepsilon^*)^{\frac{1}{2}}}{1+(\varepsilon^*)^{\frac{1}{2}}} \tag{62}$$

Then, using a measured scattering parameter and Equations 5 at a given frequency, the propagation term γ can be calculated. These values can then be used to calculate the next frequency scattering parameters and iterated to fit the measured data within a predetermined threshold. In the end, the adjustments to the initial values needed to match measurements are used to calculate the complex permittivity over the range of frequencies. To ensure the accuracy of the measurements, known loads are used in calibration routines before samples are measured. [**112**]

To accurately measure the dielectric properties of a particular material, the reflected and transmitted signals are designed to be altered only by the material load, in this case the liquid sample. This is commonly achieved by placing the sample material within a resonant body or transmission line. However, liquid permittivity measurements at microwave frequencies presents the technical challenges of the containment of the liquid in a resonant body, the calibration of the technique, and the analysis of the scattering parameters. One method involves modifying a reference 10cm coaxial transmission line to house liquid in place of air. In this study, however, a reflection mode sensor

specifically designed for liquid permittivity measurements in robust conditions surmounts these challenges. The Agilent 85070D dielectric probe and associated software integrates the HP8510C wideband vector network analyzer for liquid permittivity measurement Figure **17**.

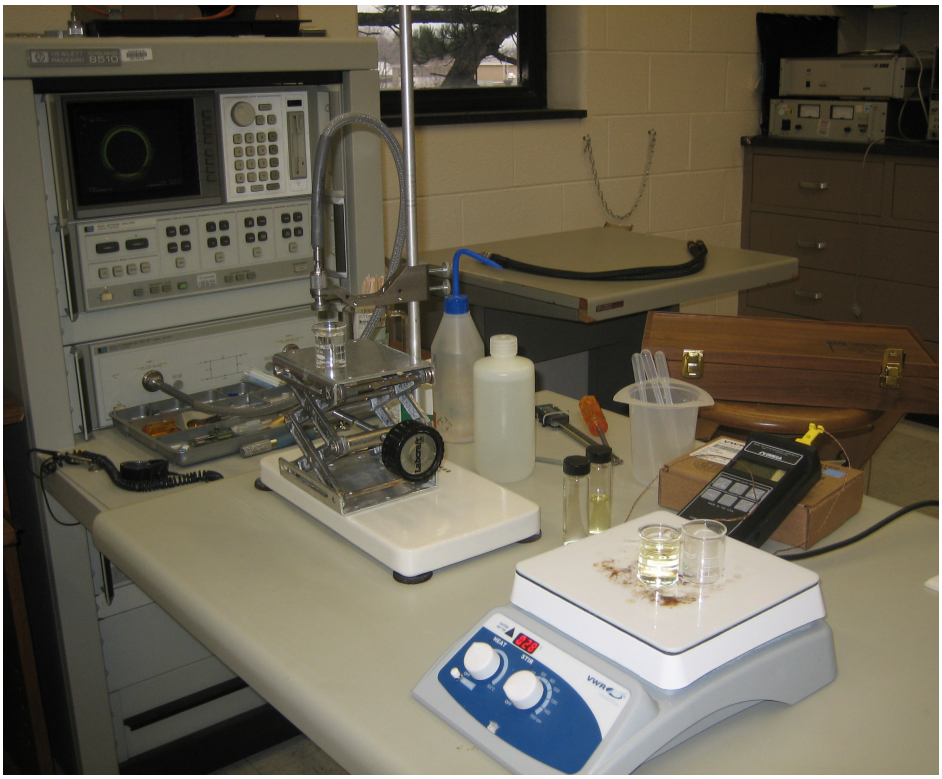

Figure **17**: Image of dielectric measurement set up including, from back left to front right, the wideband vector network analyze, liquid permittivity probe and stand, digital thermocouple, and temperature regulated hotplate.

A serial GPIB cable connects the network analyzer and probe to a PC running software included with the probe. In this configuration, the frequency range, calibration routine, and data analysis are completed through PC interface. The probe, in Figure **18** , terminates into the liquid specimen from specially arranged terminals ensuring a consistent correlation to material properties. The calibration routine consists of an open, short, and water load to the sensor. The water portion of the calibration is used to calibrate for temperatures up 300 Celsius. In this calibration process,

deionized, degassed water was maintained via thermocouple and hotplate at the appropriate temperature for calibrations.

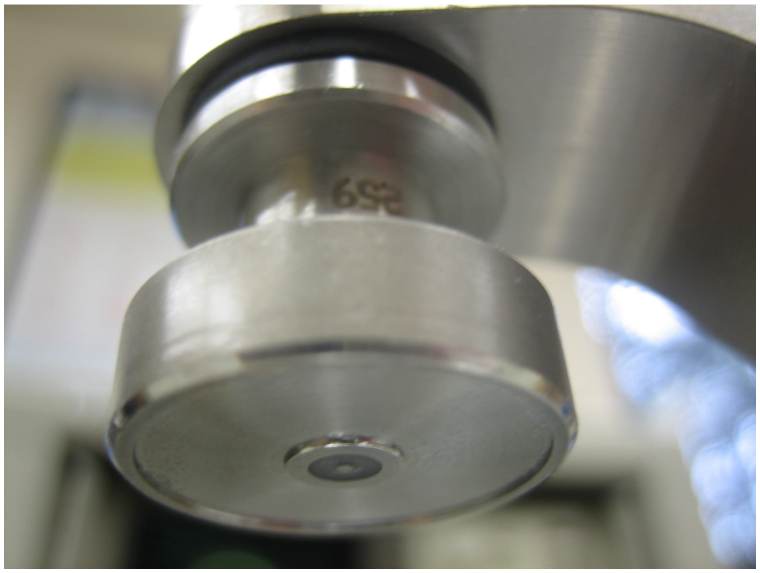

Figure **18**: Image of Agilent 85070D liquid permittivity measurement probe.

The real and imaginary terms of the measured complex permittivity are recorded in the frequency range from 50 MHz to 5GHz, chosen to include the 2.45 GHz and 915 MHz microwave bands for industrial heating. Each measurement is repeated at least three times and averaged curves are calculated for later analysis. The imaginary component of the complex permittivity, referred to herein as dielectric loss, is proportional to the microwave heating rate of a material.

The purpose of this measurement is to relate the effects of ultrasonic emulsification to microwave absorption. The dielectric properties of soybean oil and methanol remain the same when mixed in certain proportion, thus it is reasonable to expect only the relative quantity of one to the other to determine the mixtures permittivity. However, this assumption does not account for the reduction in net polarization as manifested through the dispersion of the polar methanol phase into fine droplets. In this form, the polar phase is inhibited by the low loss dielectric substrate until the

dispersed droplets are of sufficient size to regain noticeable polarization. Accordingly, permittivity measurements will help quantify the electromagnetic stability of an emulsion over time.

5.4 Microwave Heating

Each ultrasonically formed emulsion will then be subjected to high intensity 2.45 GHz microwaves provided through a current controlled magnetron from a domestic microwave oven. The multimode oven is retrofitted with an infrared (IR) thermocouple, manual rheostat hard wired to the magnetron power circuit, in integrated data acquisition in National Instruments Labview via a USB carrier. The IR thermocouple is calibrated to a NIST traceable thermometer before each trial at cool and warm temperatures. The appropriate calibration requires a blackbody radiation source with a known emissivity, which is available for the reported MW heating profiles. The heating profiles are repeated for each mixture and technique of preparation at four power levels roughly correlating to a range from 75% to 100% power of a 1.2 kW magnetron. A schematic diagram of the measurement setup is in Figure **19**

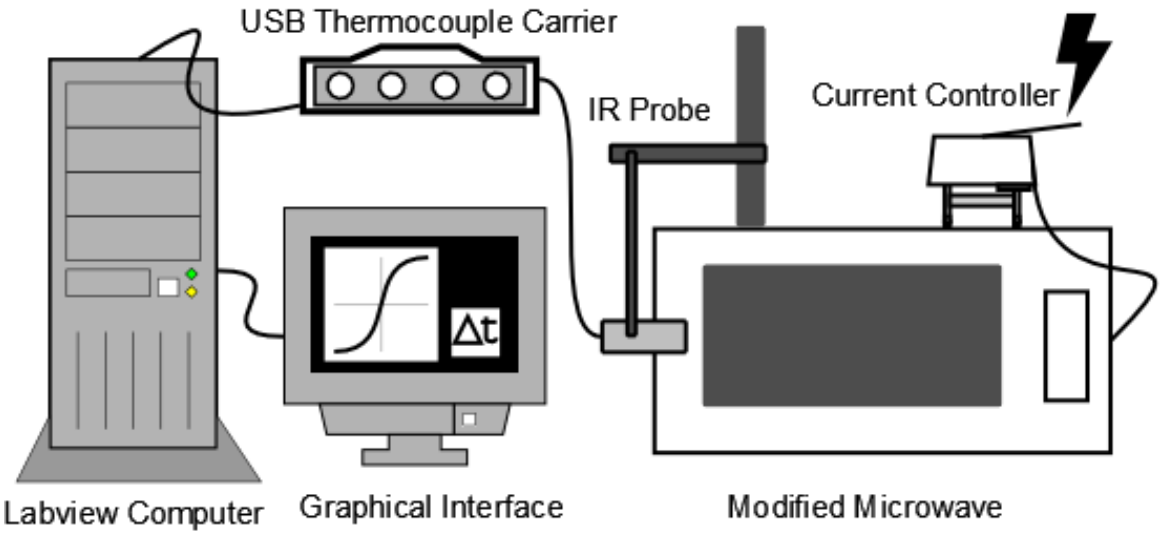

Figure **19**: Schematic diagram of domestic microwave oven modified for current control, Infrared temperature measurement, and automatic data logging used to monitor the temperature of microwave heated samples.

A very important observation is the temperature at which the mixtures reach a boil. As described earlier, microwave heating can result in superheating which is evidence of the enhancement of reactions kinetics achievable. As the extent of superheating, in the ideal case, is related to the incident microwave power, control is needed to experiment with this relation. The quantitative correlation between the electrical power provided to the magnetron and the power absorbed by a body relies on predictable magnetron performance, monitored reflected power, and homogenous field distribution. The magnetron performance is considered to be sufficiently consistent in the sense of repeatable results at various power settings. However, it is noted that this assumption forbids utilizing the provided electrical power to calculate the field emitted. To make this correlation without direct measurement of reflected power, the electrical efficiency of the magnetron and its performance over ambient temperature fluctuations need be known. In addition, when using modified domestic microwave ovens, microwave field in-homogeneities arise in the multimode chamber. These field gradients manifest so called hot spots or dead spots in the cavity which lead to uneven heating of samples. This issue can be addressed by a rotary table or microwave mode stirring

fan. In this study, however, this problem is address by repeatedly heating samples of deionized water at various locations. Ultimately, a location convenient for the incorporation of the IR thermometer is chosen. Once the sample zone is identified and the thermocouple installed, it is marked for reference for all subsequent measurements.

The microwave heating profiles will act as the litmus test for measurements and conclusions through analysis regarding the ultrasonic optimization of emulsions for microwave heating. For instance, dielectric loss measurements can be used to compute theoretical heating curves for comparison with measurement. In turn, the material parameters contributing to microwave heating can be calculated from this measurement and compared to a direct measurement. The goal of this measurement is to correlate the ultrasonic process parameters for specific mixtures to the actual microwave heating.

5.5 Biodiesel Analysis:

Several types of analysis are dictated by the ASTM biodiesel fuel specification; however, for purposes of this study the measurement of methyl-ester production is of sole interest. Admittedly, the analysis made does not constitute a fuel quality assessment resulting from the process technique; however, the treatment of samples are intentionally deprived of separations and purifications normally used in the production of a biodiesel fuel product. Instead, reactants are subjected to certain ultrasonic and microwave treatments over a short period of time, and the complete mixture analyzed to compare either relative reaction rates or, in some cases, to investigate whether *any* reaction occurred. The other aspect is to simply verify that the product associated with observed glycerol formation is in fact the expected methyl-esters from the transesterification reaction. With

this confirmation, the reaction rates can be compared on the measurements of mass of separated glycerol.

The objectives for the analysis are as follows:

1. Measure methyl ester formation in catalyst free reaction schemes
2. Compare chemical formations to standard to confirm transesterification reaction
2. Use low amounts of catalyst to enhance the reaction rates for comparison of techniques based on glycerol formation

As mentioned above, the ultrasonic and microwave treatments will be conducted over only short periods of time. This is a result of using atmospheric conditions without reflux. The heating times are limited by the boiling of methanol. As it was shown in chapter 2, the reverse reactions will occur if excess methanol is not present to shift the reaction equilibrium towards product. Accordingly, the ideal reaction mixture, microwave, and ultrasonic treatments, in terms of stability of superheating, may not be feasible with the current reactor design. For instance, if 6:1 molar ratios of alcohol to oil superheat to the greatest degree, the equilibrium towards products could literally evaporate during a single boiling event.

To investigate catalyst free transesterification, the results of the microwave heating studies will be used to determine the best reaction mixture and ultrasonic treatment. Several samples are heated with varying microwave power until near or just to the superheated boiling temperature. Samples will then be quenched and collected for Gas Chromatography (GC). Along with these samples, reactions utilizing low catalyst amounts (< .3% NaOH wt-wt oil) will also be subjected to ultrasonic and microwave treatments, quenched, and collected for GC analysis. As mentioned,

neither samples will be purified, separated, or otherwise washed. The goal is to capture the reaction progress at the desired temperature and time.

The GC analysis is conducted off-site at an independent laboratory utilizing the ASTM D6751 standard for GC determination of free and bound glycerol. The samples are prepared in 10mL sample vials and the prescribed reference samples are added. The GC unit also utilizes internal standards. The results are reported in terms of weight percentages of mono-, di-, and tri-glycerides making the bound glycerol, and glycerol molecules accounting for the free glycerol measurement. The data is also presented in the form of chromatograms, for a qualitative view of the results of a particular treatment. This technique, aside from being standardized, has been tested for repeatability.[**113**] Furthermore, the correlation of the chromatograph peak locations to the chemical it represents is well known using known reference chemicals.[**114**] The horizontal axis in the chromatographs refers to the retention time in the column while the vertical axis correlates to the amount of molecules detected at the associated time. In general, the larger molecules take longer to reach the detector and appear to the right side of smaller molecules. For the purpose of description, a GC chromatograph of a partially reacted mixture of soybean oil, methanol, and NaOH catalyst is presented in Figure **20**.

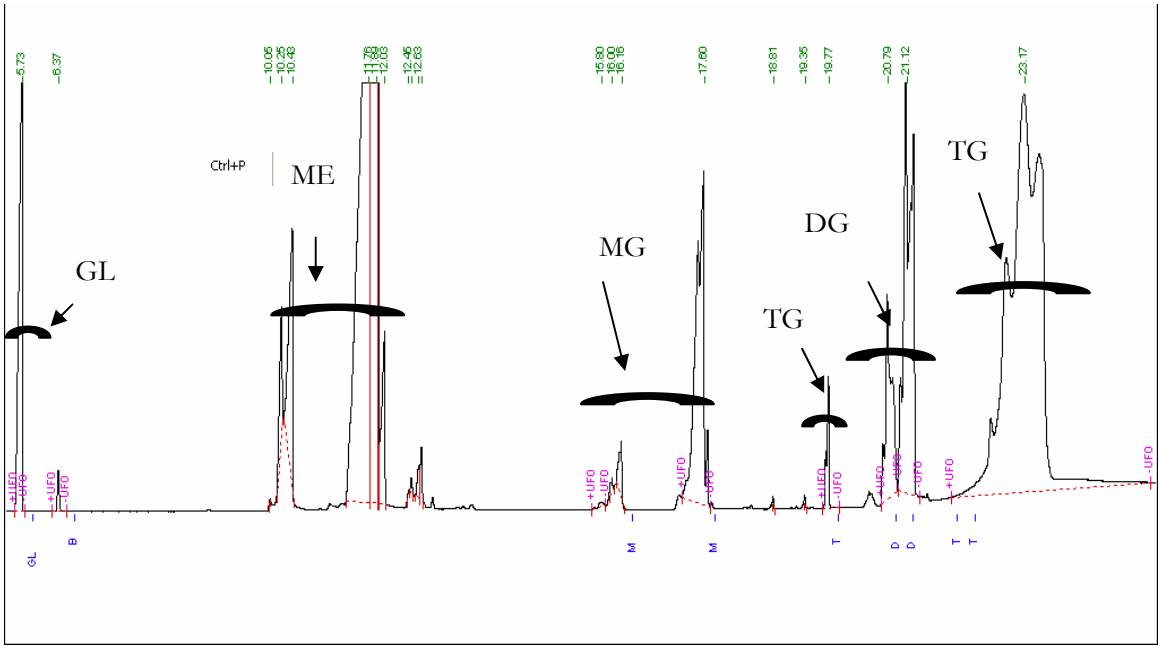

Figure **20**: Gas Chromatagraph of partially transesterified soybean oil with methanol and base catalyst. This shows the separation by retention time of the individual components of the mixtures. Where the acronyms are represented as follows: GL - glycerol, ME - methylester, MG - monoglyceride, DG - diglyceride, and TG - triglyceride.

Data in this form show the progress of the stepwise reactions described in the literature. It will also confirm that the products that form when glycerol settles are, in fact, the expected methyl esters. By comparison, the catalyst free samples with relatively small methyl ester peaks, can be detected qualitatively from the GC chromatograph.

The second experiment conducted is the direct measure of glycerol formation by weight in bulk reactions. This test is used to compare the methyl ester production of ultrasonically mixed samples and rotary mixed samples under microwave heating. The object of this measurement is to ascertain the advantage of ultrasonic emulsification for microwave heated samples over conventional mixing techniques.

Chapter 6

Results

6.1 Optical results:

Each emulsion was prepared as described in the previous chapter. However, all the emulsions made for the optical imaging tests contained no catalyst. This choice was made to avoid possible stabilization effects from the catalyst or the reacted products during mixing. All emulsions were methanol to soybean oil in molar ratios of 3:1, 6:1, or 9:1. The normalized distribution is used to express the frequency of droplets measured within 0.5 micrometer bins and was calculated by dividing the number of occurrences in a range of diameter by the total number of measurements.

6.1.1 Emulsion Destabilization:

The first round of images were taken using the 22 kHz ultrasonic horn at half and full power, roughly 300 and 600 Watts electrical power. The first observed effect of ultrasonic emulsification is the destabilization process. Without using any stabilizing agents, the stability of the emulsion relies on the droplet size distribution and volume fraction alone. The first evidence of destabilization was not apparent until after microscopic image processing was completed. The data indicates that in about 3 minutes dispersed phase droplets sizes shifted to larger values by nearly two micrometers as seen in Figure **21** .

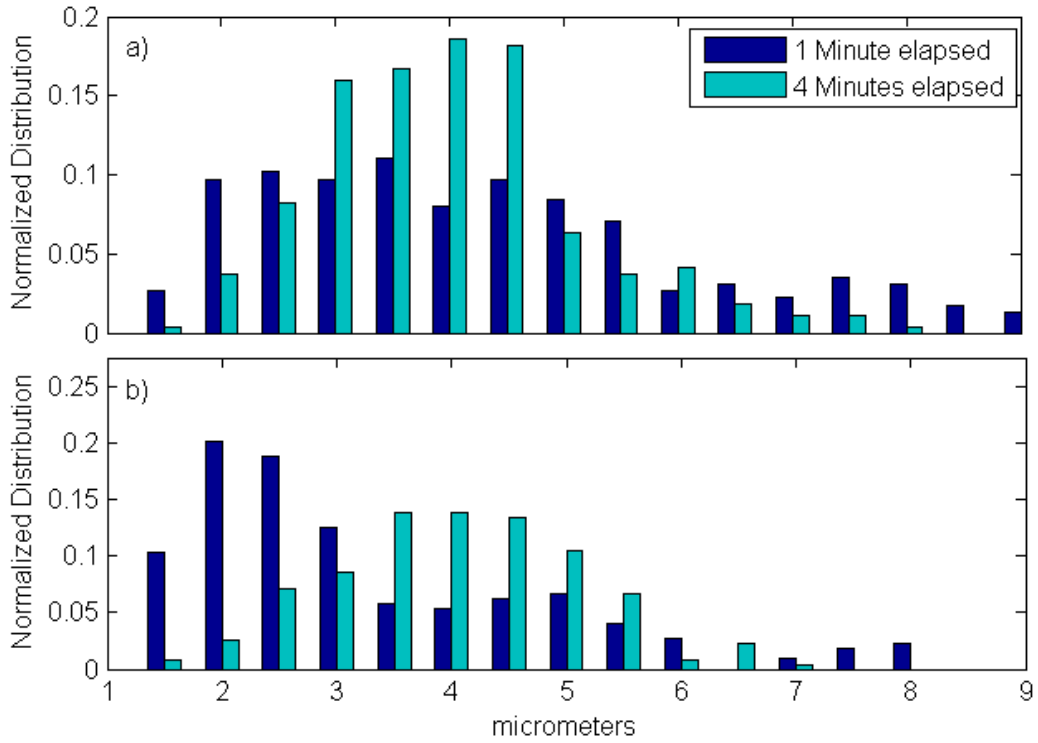

Figure **21**: Destabilization of ultrasonically formed emulsions of a 6:1 molar ratio of methanol to soybean oil over time, as measured by diameter of dispersed methanol droplets. Graph a) 22 kHz ultrasound at full power and b) 22 kHz ultrasound at half power.

It appears that the dispersed methanol droplets created at half power enlarged just as those created at full power. However, it appears that the half power case preserved its distribution. This could be due to enhanced stability in the half power case. The broadening and increase in center diameter would correspond to coalescence, as smaller droplet combine to form larger droplets. The shift to larger diameters without broadening corresponds to ripening, as the distribution equally swells. The rate of coalescence is determined by creaming, flocculation, or both. This follows from the relation to dispersed droplet diameter from the equations presented in Chapter 2. To investigate the instability more thoroughly, an emulsion formed with 22 kHz at half power was set aside and a series of images were taken and analyzed as over a period of twenty minutes, Figure **22** .

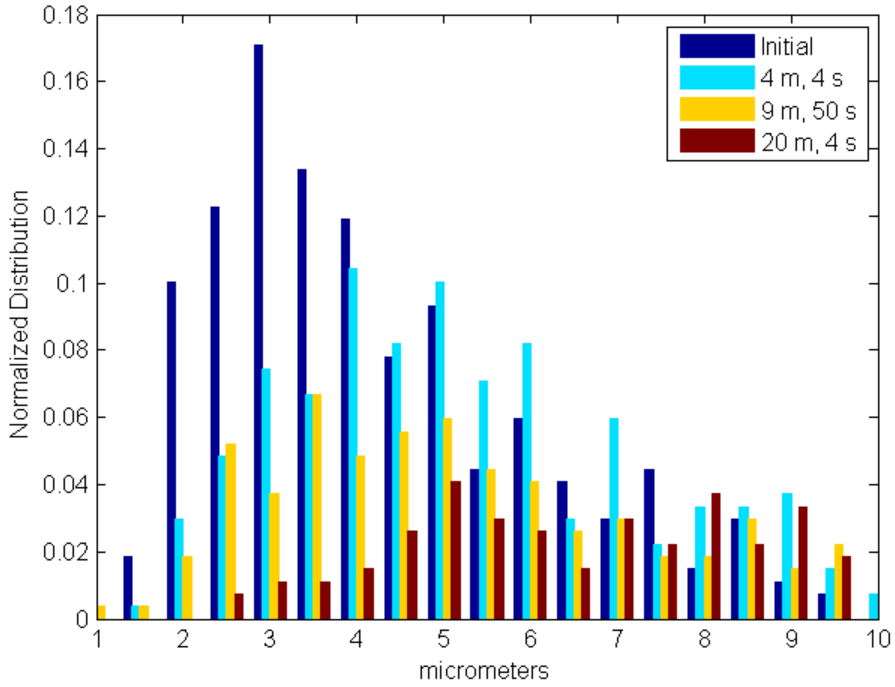

Figure **22**: Measured dispersed methanol droplet diameters over 20 minutes. The plot indicates that dispersed phase droplets both grow in size and spread in distribution of size as the emulsion destabilizes. The emulsion was prepared with the 22 kHz ultrasonic horn at half power.

The results indicate a consistent shift and broadening towards larger dispersed droplet diameters. Note that not all of the droplets remain accounted for as coalescence and creaming creates a continuous methanol phase on the surface which is either evaporated or at least no longer countable. As a result, it becomes increasingly difficult to measure the goal of 300 droplets in a single image.

6.1.2 Repeatability:

Having observed the effects of destabilization, the next experiments are conducted to investigate repeatability. To avoid variation due to the instability, consistent timing is maintained throughout the trials. It was determined that the time taken to locate an area on the microscope

slides accounted for about a one minute variation in measures. From a practical standpoint, practice is necessary to maintain reproducible methods. For example, the total volume of the sample and the time it is subjected to the treatment are parameters which can vary the emulsion. To estimate which parameters are successful without imaging, the destabilization of the emulsion is observed. The molar ratios, volumes, and times of treatment maintained for each of the following repeatability experiments were chosen based on such practice.

The repeatability experiment conducted with the 22 kHz horn utilized 6:1 molar ratios of methanol to soybean oil and the full power setting to create emulsions on three separate occasions. The experiment confirms the ability to reproduce methanol in soybean oil emulsions at a 6:1 molar ratio, with the mean dispersed droplet size of 3.947 micrometers and a standard deviation of deviation of 1.972, as in Figure **23.**

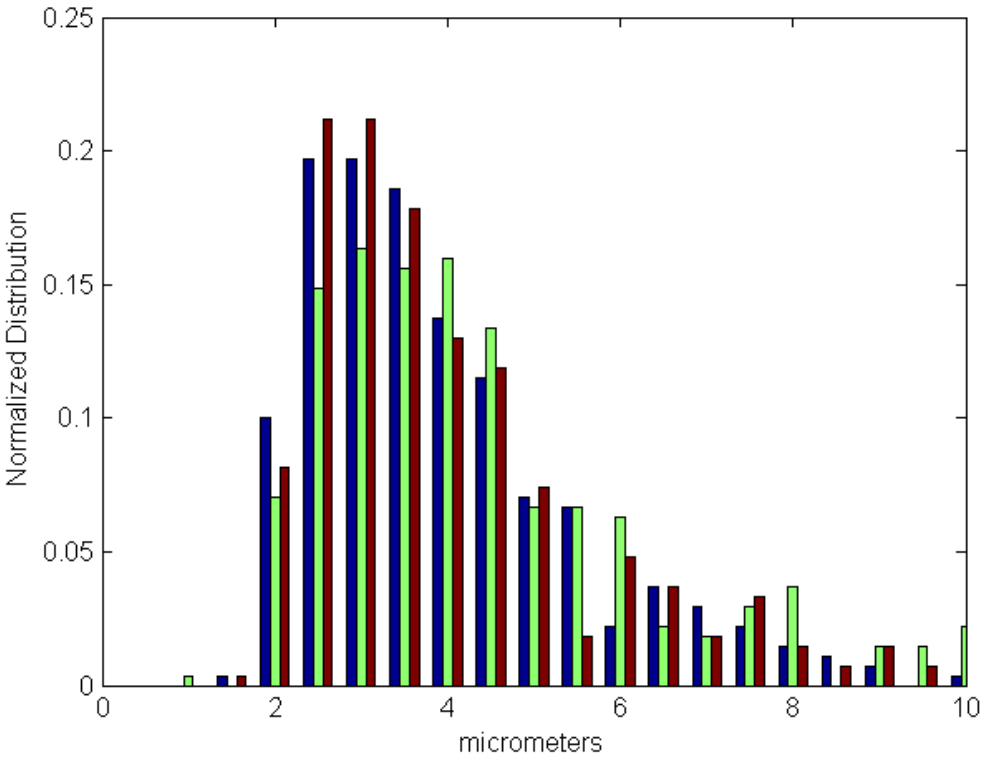

Figure **23**: Dispersed methanol droplet diameters with a mean value of 3.947 micrometers and standard deviation of 1.972 in 6:1 molar ratio emulsions as prepared in three identical runs with 22 kHz ultrasonics at full power.

The repeatability experiment using the 44 kHz ultrasonic bath for emulsification, utilized 9:1 molar ratios. The higher ratio of alcohol was used with the ultrasonic bath do to the large area of ultrasonic activity. The mixture forms a thin layer spread across the ultrasonically active basin which caused atomization to occur. In this configuration, with ultrasonic transducers aiming up through the liquid to a free surface, the effect of atomization is visualized as liquid droplets spraying upwards and out of the bath. To inhibit this, larger volumes of the mixture were used. In comparison to the horn, emulsifying samples of about 40 milliliter, the bath required at least on liter in order to avoid spraying. The experiment indicates smaller dispersed phase droplets with a mean of diameter of 2.121 micrometers and a standard deviation of 1.379, as in Figure **24**

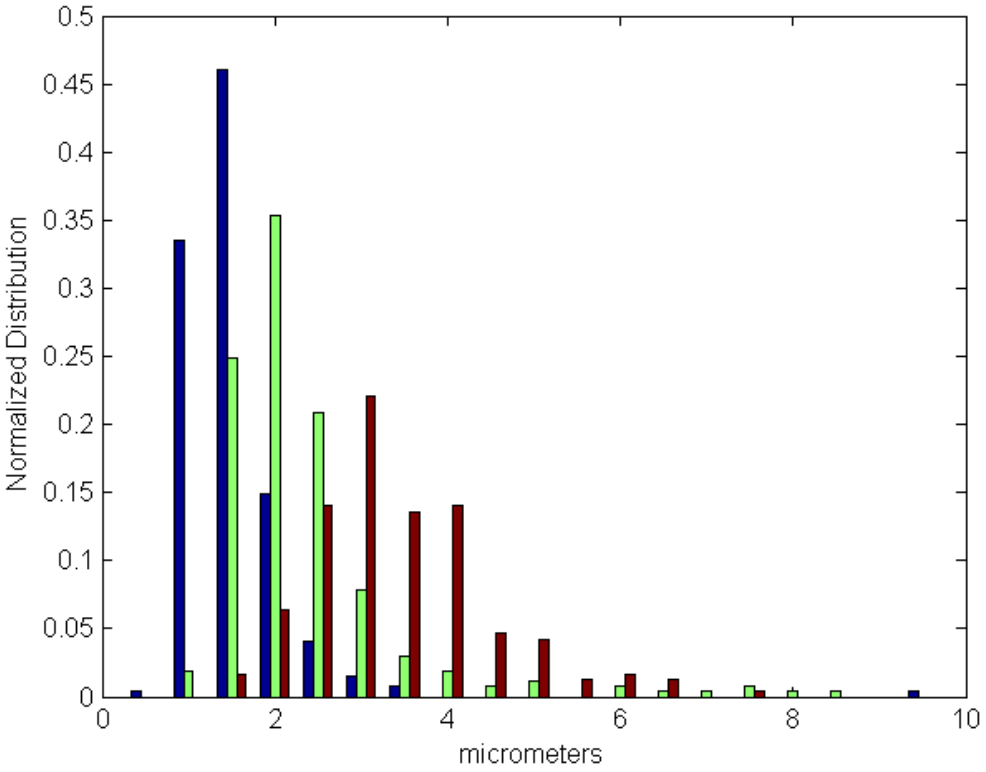

Figure **24**: Dispersed methanol droplet diameters with a mean value of 2.121 micrometers and standard deviation of 1.379 in 9:1 molar ratio emulsions as prepared in three identical runs with 44 kHz ultrasonics at full power.

6.1.3 Effect of Ultrasonic Power:

Using the 22 kHz ultrasonic horn at half and full power, emulsions of 3:1, 6:1, and 9:1 are prepared in 20 mL glass vessels. Abismail et al have shown that with increasing power the droplet size decreases.[**97**] However, Abromov indicates that decreasing power causes droplet distributions to shift to smaller values.[**78**] The data in Figure **25** seems to support the correlation to smaller dispersed phase with lower intensity ultrasonics. The half power case has a mean diameter of 3.362 micrometers and a standard deviation of 2.178. While the full power emulsions have a mean diameter of 4.179 and a standard deviation of 2.373. Another noticeable observation from the above

data is the effect of dispersed phase volume. At both ultrasonic intensities the 3:1 molar ratio emulsion tend to have smaller radius droplets than in the 9:1 molar ratios. With the 3:1 emulsion the mean diameters are 3.387 and 3.167 micrometers with standard deviations of 1.481 and 1.870 for the full and half power cases respectively. However, with the 9:1 emulsions the mean diameters are 4.562 and 3.556 micrometers with standard deviations of 2.747 and 2.205 for the full and half power cases respectively.

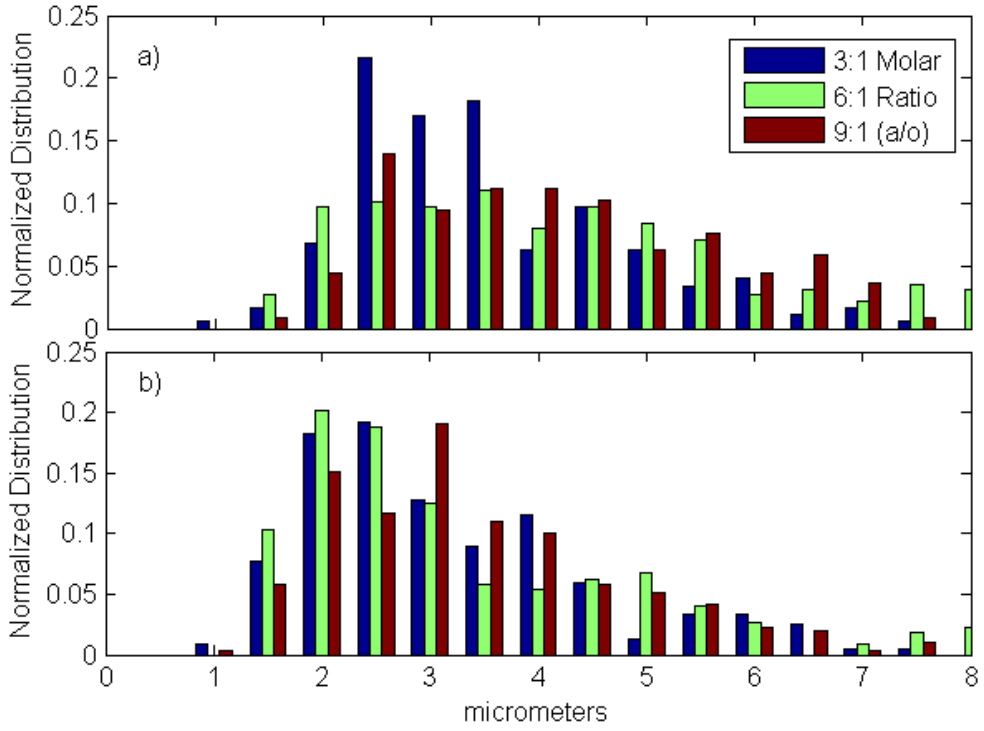

Figure **25**: The effects of ultrasonic intensity on dispersed methanol droplet diameters indicate smaller diameters with lower intensity in 9:1 molar ratio emulsions prepared with 22 kHz ultrasonics. Graph a) Full power setting yields a mean droplet diameter of 4.562 micrometers with a standard deviation of 2.747. Graph b) Half power setting yields a mean droplet diameter of 3.556 micrometers with a standard deviation of 2.205.

6.1.4 Microwave Demulsification:

Chih-Chieh explained that smaller dispersed droplets in an emulsions decreases the efficiency of microwave demulsification.[**58**] Basak stated that emulsion droplets under 5 micrometers were difficult to separate using microwaves.[**59**] In the course of this study, the opposite seemed to happen. That is, that emulsions became more stable after microwave heating in absence of catalyst or stabilizing agents. It was hypothesized that the microwave heated larger droplets preferentially, causing them to evaporate before the smaller droplets. So long as the microwave treatment stops before the entire volume of methanol boils out, the resulting emulsion should contain only the smaller droplet sizes. This hypothesis is tested using the ultrasonic bath, which is shown to create smaller droplets. The result, in Figure **26** , shows that all of the dispersed phase droplets above 3.5 micrometers in diameter are eliminated through microwave heating. Statistically, the mean diameter before microwave heating was measured to be 3.534 micrometers with a standard deviation of 2.595. After microwave heating the mean diameter was measured to be 2.150 micrometers with a standard deviation of 0.506 micrometers. This measurement confirms that smaller droplet sizes will allow better stability in the microwave. In addition, this could be utilized to reform emulsions that are polydisperse by eliminated the larger droplets.

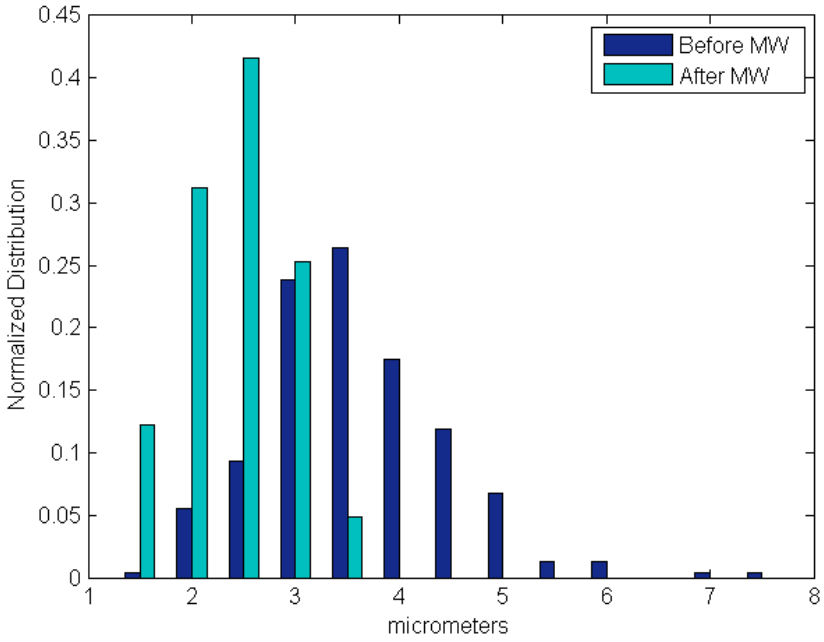

Figure **26**: Selective microwave demulsification as shown by a decrease in dispersed phase droplet diameter from a mean of 3.534 micrometers and a standard deviation of 2.595 to a mean of 2.150 micrometers and a standard deviation of 0.506.

6.1.5 Comparison to conventional mixers:

Nearly all of the ultrasonic emulsification literature reviewed included comparisons to rotational mixers and impellers. To replicate this result, a high shear rotary mixer adjustable up to 10,000 rpm was used for comparison. The impeller used was custom made out of rigid, yet thin plastic strips. This adjustment was made after the original impeller did not produce sufficient mixing. The mean diameter of dispersed drops was measured as 4.406 micrometers with a standard deviation of 5.036. The results can be visualized in Figure **27** compared to the emulsions created by the ultrasonic bath and is in good agreement with the literature.

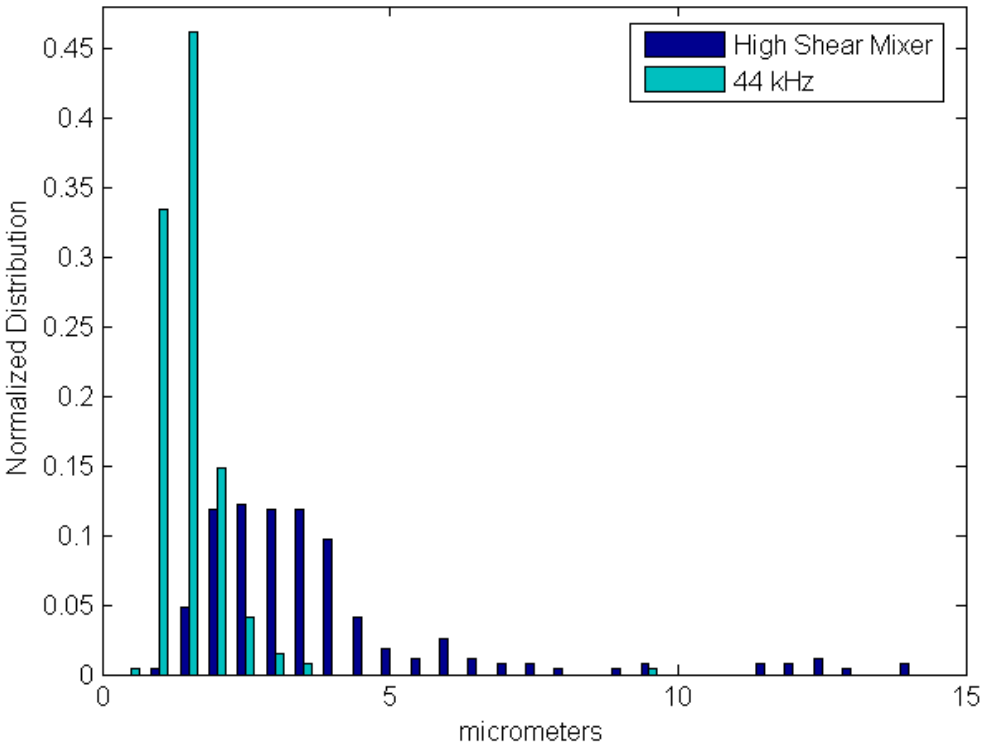

Figure **27**: Comparison of the dispersed droplet radius of methanol in soybean oil at a 9:1 molar ratio emulsions as prepared by conventional mixing and 44 kHz ultrasonics. The 44 kHz ultrasonic method produces smaller droplets and a narrower distribution of diameters.

To summarize, the destabilization processes of emulsions were observed and accounted for in subsequent repeatability studies. The effect of power had a slight effect on decreasing the dispersed phase droplet size. The higher frequency ultrasonic source created the smallest droplet sizes. A new result regarding the use of microwaves to selectively demulsify an emulsion to refine droplet size is presented. Finally, it is shown that ultrasonic emulsification creates less dispersion and smaller mean diameters of the dispersed droplets as compared to conventional mixing.

6.2 Microwave Permittivity:

6.2.1 Permittivity of pure materials:

First, the complex permittivity of methanol is measured six times and averaged. The standard deviation of the real and imaginary parts of the complex permittivity at each frequency is calculated and plotted with the average as error bars with widths twice the standard deviation. The averaged complex permittivity measurements of pure methanol are compared to literature reports. In the case of pure methanol, a single value is obtained from Von Hippel et al. measurement at 3 GHz.[**115**] In addition, experimentally calculated values for relaxation time, τ , low permittivity limit, ε_s , and high frequency permittivity limit, ε_∞ , were taken from Mashimo et al. and inputted to Equation **35** to obtain a point by point comparison in the measured frequency range. The correlation coefficient between the calculated data and the measured data is calculated as 0.9895 for relative dielectric constant, ε' , and 0.9878 for relative dielectric loss factor, ε'' . The data indicates the polar loss mechanism is present and reaches its peak at nearly 3 GHz. For this reason methanol is an ideal candidate for superheating at the commercially allowed microwave frequency of 2.45 GHz, as shown in Figure **28** .

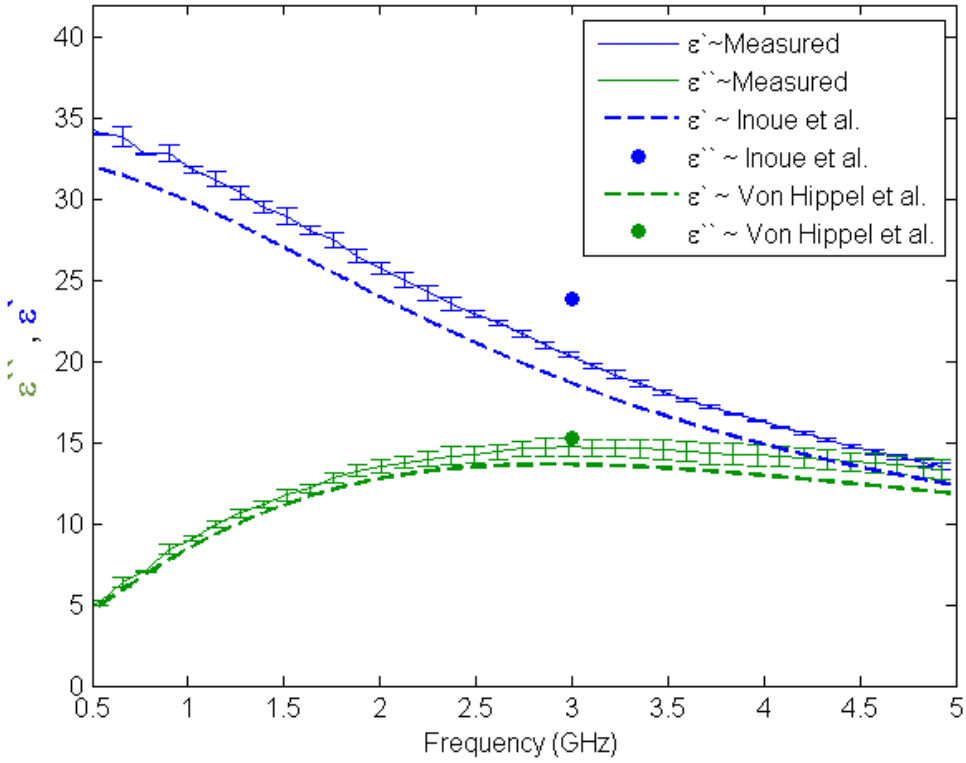

Figure **28**: Complex permittivity measurement of methanol compared to literature values. The error bars represent the standard deviation of measurement averages. The dielectric relaxation peak of methanol is located near the microwave heating frequency of 2.45 GHz.

Next, the complex permittivity of soybean oil is measured six times and plotted with the standard deviation values as before. The dielectric properties of soybean oil were reported by Inoue et al. at lower frequencies, so the highest frequency measurements are also included as single points, in Figure **29** .[**116**]

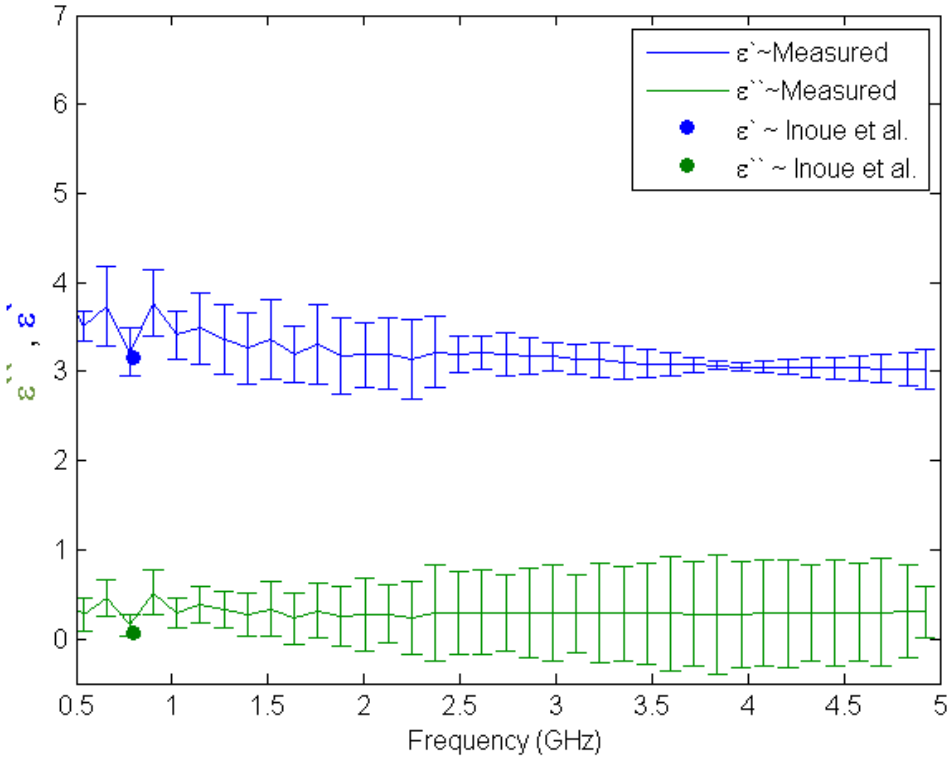

Figure **29**: Complex permittivity measurement of soybean oil compared to literature values. The error bars represent the standard deviation of measurement averages.

For a simple comparison, the same measurement was repeated using unrefined Jatrohpha seed oil. The measurement was taken to obtain a general notion of the sensitivity to refining processes and fatty acid composition. To the best knowledge of the author, these measurements are for the first time reported in Figure **30** .

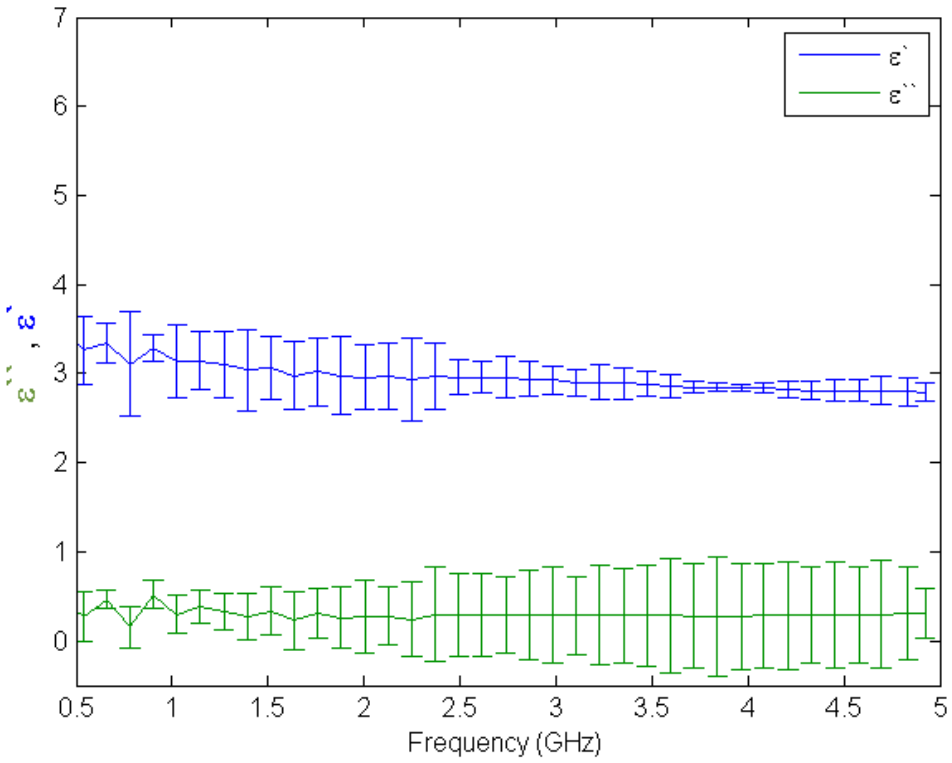

Figure **30**: Complex permittivity measurement of jatropha seed oil. The error bars represent the standard deviation of measurement averages.

Starting with the following comparison, the complex permittivity will sometimes be expressed as the loss tangent, as calculated from Equation **34,** when more than one series is being plotted. This will preserve the information regarding both dielectric loss and dielectric constant, while condensing the information to one line per test. The complex permittivity of a 0.210M solution of methanol and sodium hydroxide was measured. This concentration is representative of .1% NaOH by weight of oil for a 6:1 alcohol to oil ratio reaction mixture. This amount of catalyst is would be considered a low amount of catalyst compared to production levels. The data indicates that at this concentration the ion conductivity from the catalyst dominates the loss compared to the polar relaxation mechanism as in Figure **31** .

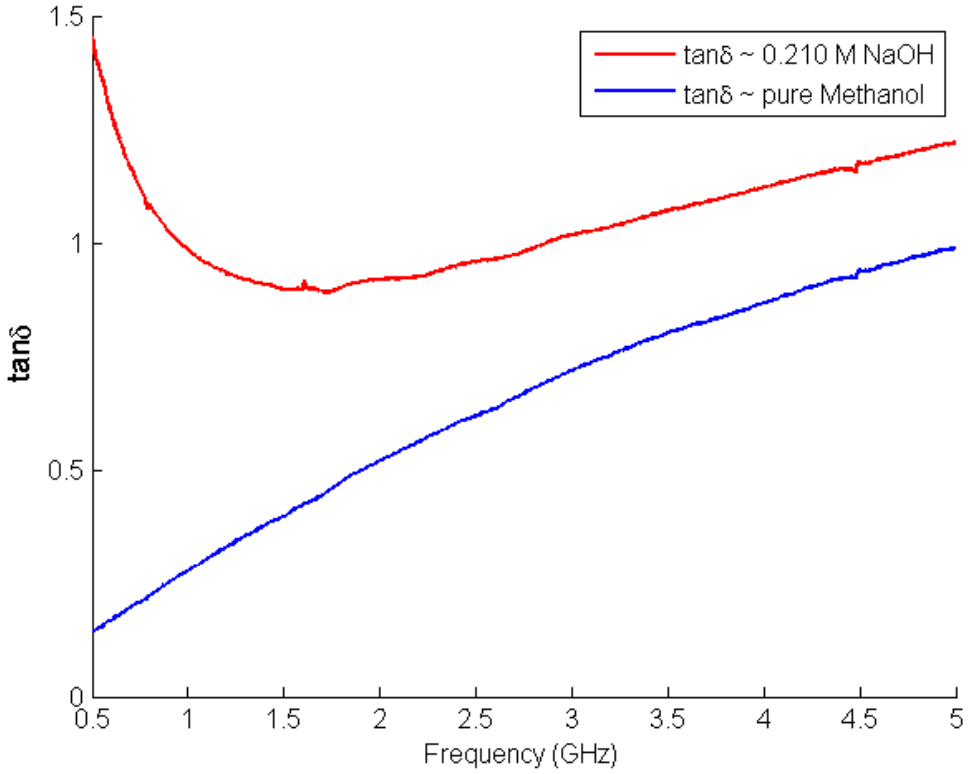

Figure **31**: Complex permittivity of pure methanol and 0.210 M solution of methanol and sodium hydroxide expressed as loss tangents. The ion conduction losses from the dissolved base catalyst begin to dominate the loss.

According to Equation **33** , the contribution of conductivity to the dielectric loss can be separated by subtracting the measured dielectric loss of pure methanol from that of the solution of methanol and catalyst. The dielectric loss due to conductivity should take the form of Equation **63** . Figure **32** shows the effective, conduction, and dipolar relaxation losses that result from the simple calculation.

$$\varepsilon_e'' = \frac{\sigma}{\omega\varepsilon_0} + \varepsilon'' - \varepsilon'' = \frac{\sigma}{\omega\varepsilon_0} \qquad (\mathbf{63})$$

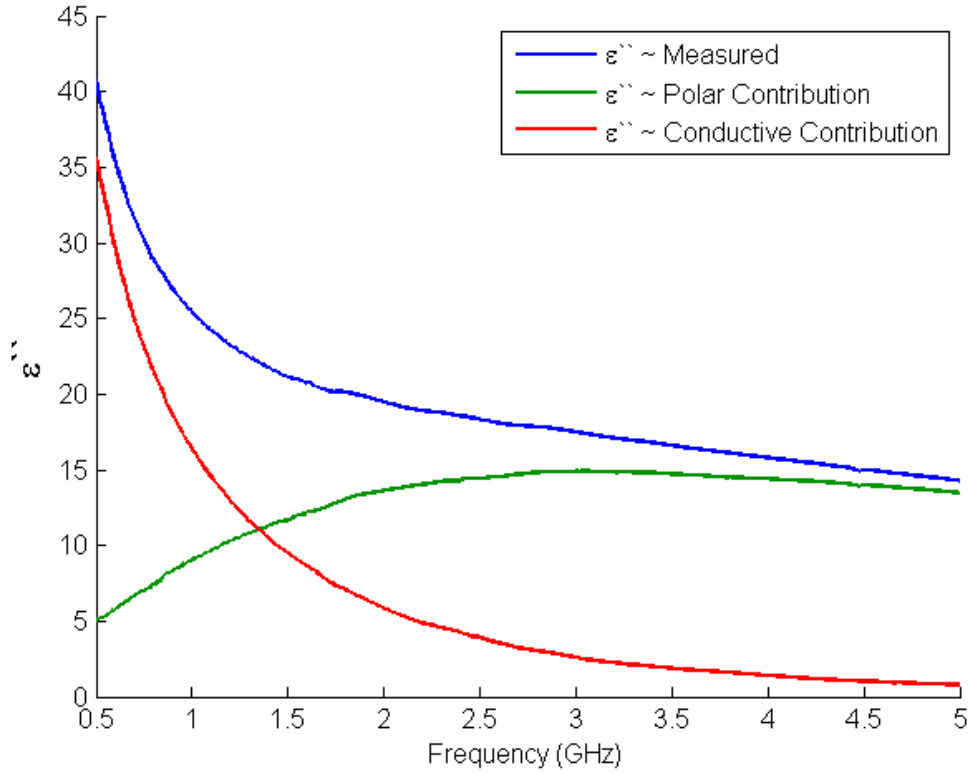

Figure **32**: Measured dielectric loss constant of 0.210 M solution of methanol and sodium hydroxide with the mathematically separated contributions from polar relaxation of pure methanol and ion conduction from catalyst ions.

Using Equation **63** as the solution form, a least sum squared curve fitting algorithm can solved for the conductivity, σ, as in Figure. It can be seen that the fit is less accurate in the frequency range corresponding to the dipolar relaxation. This disparity is a result of the simplified notion of the resultant dielectric loss of two mechanisms is equal to the sum. To account for this, expanded relations have been derived in terms of shape functions. For example, Mashimo et al. have investigated the dielectric loss interference of two overlapping polar mechanisms.[**117**] Another investigation by Lane et al. deals with the interference of ionic and dipolar dielectric loss mechanisms. To obtain a calculation of the conductance associated with the ion, κ, the authors measure over a range of temperatures. This helps to separate the two contributions as the dipolar

relaxation and ion conductivity depend differently on temperature. More specifically, at the ions at low frequency undergo current like motions while aligning with the electric field. As the frequency increases, the ions have less time to move between cycles, thus they can be considered stationary. Thus, at high frequencies the ion contribution to loss is more like dielectric loss then conductive losses. Elevating the temperature of the solution impedes the dipolar mechanism allowing a closer measurement of the loss due to ions at higher frequencies. [**118**]

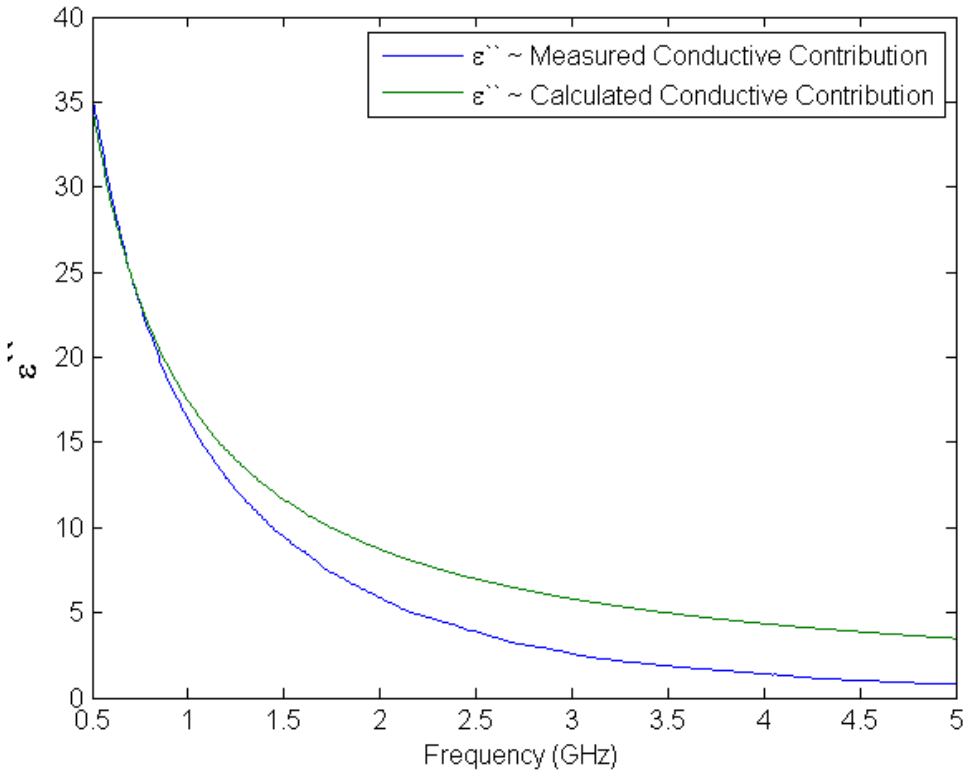

Figure **33**: The ion conductivity contribution to the dielectric loss constant theoretically calculated does not fully account for the loss as deduced from measurement. The interaction of ions with methanol molecules create an additional loss within the region of dipolar relaxation, namely from 2 to 5 GHz.

Mathematically, Equation **63** does not adequately model the ion contribution in the region overlapping with the dipolar relaxation because the form of loss approaches that of a dielectric loss,

as seen in Figure **33**. Physically, the ions can locate in complex solvent molecular structure and the relaxation of the combined system governs the loss.[**119**],[**120**] However, since the goal of this research is to eliminate catalyst from biodiesel production, the importance the measurement of ionic conductivity is secondary. Thus the pertinent result is the observation of ionic conductivity becoming the dominate mechanism of microwave absorption at relatively low catalyst concentration.

Finally, to gain a visual perspective of the sensitivity of microwave loss to ion concentration, the concentration of NaOH to methanol is incrementally increased between the above regions. The results indicate that at .04 M concentration, the microwave absorption at lower microwave frequencies approaches that of the dielectric loss due to dipolar relaxation in pure methanol, as in Figure **34** . Practically, this means that in order to achieve the microwave heating rate obtained with 2.45 GHz and pure methanol, at 915 MHz the addition of catalyst would be necessary.

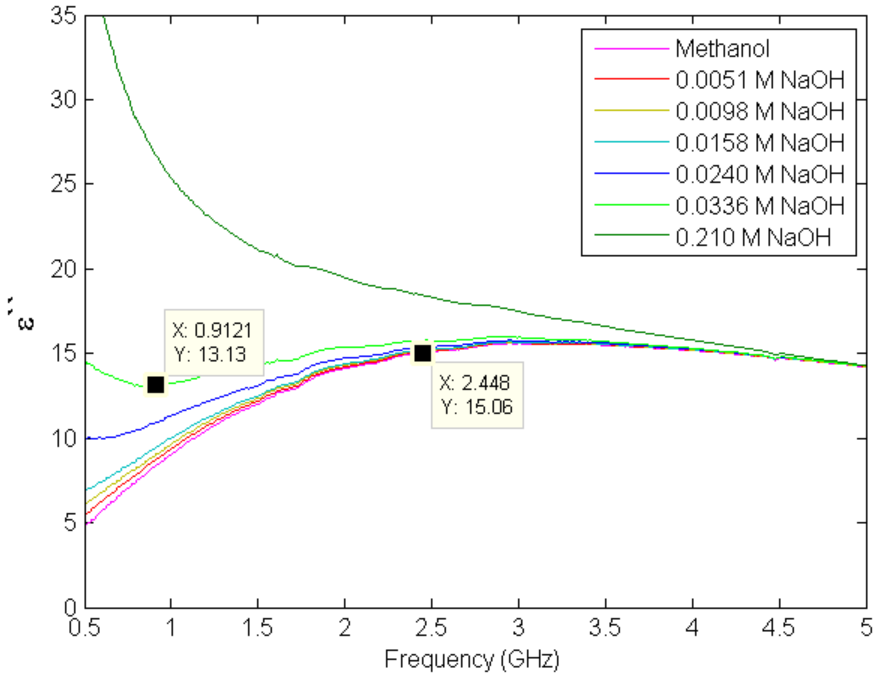

Figure **34**: The dielectric loss constant of methanol as sodium hydroxide solution is incrementally increased. At .04 M the dielectric loss at low frequencies increases to the level of loss created by the dipolar relaxation in pure methanol at 2.45 GHz.

6.2.2 Measurements at temperature:

The primary importance of measuring the dielectric loss of methanol as a function of temperature is observe the heating properties of methanol at elevated temperatures for microwave processing operational concerns. The permittivity of methanol as a function of temperature has been discussed topically in the supercritical fluids discussion in chapter 2. The decrease in dielectric constant, particularly above the critical point, is given as the reason for improved miscibility with oil phase. Practically, the improved miscibility and reactivity of methanol at elevated temperatures was related to breaking a percentage of hydrogen bonds which account for the overall polarization of a collection of methanol molecules. This concept is clarified now with a discussion of the activation

energy for a thermally excited vibrator. The individual molecules of methanol represent single oscillators aligning with the external frequency. The relaxation time, τ, corresponds to the time between consecutive alignments of a single dipole subject to external electric field. The activation energy, E_a, describes the quantum of energy needed for a single dipole oscillation to occur at a given frequency as in Equation **64** . [**121**]

$$E_a = hf \tag{64}$$

In general the availability of energy to a molecule in a body of molecules is prescribed by Bose-Einstein statistics. In analogy, the molecules can be pictured as people waiting in line for some event, the activation energy as the number of steps taken to traverse the gate, the available energy as the number of entrances, and relaxation time as the time taken for the crowd to enter. The lengths of lines resulting from few available entrances represent the number of hydrogen bonds between polar molecules. As more entrances become open, the wait is less and shorter lines result. The minimum time waiting, when ample entrances are afforded, is the time taken to walk through the entrance. In the same way, as more energy becomes available, the relaxation time shortens and hydrogen bonds break. With ample energy the relaxation time corresponds to the activation energy of a single molecule.

To formalize, the Debye equation predicts a single frequency, ω_c, corresponding to the relaxation time associated with a particular available energy. Thus, by measuring this frequency over a range of temperatures allows the calculation of the relaxation time, ω_0, and activation energy of a single molecule. This is accomplished through Equation **65** , which is derived from a similar form in the work of Von Hippel. [**121**]

$$\ln(\omega_c) = \ln(\omega_0) - \frac{E_a}{k}\left(\frac{1}{T}\right) \tag{65}$$

First, the results for the complex permittivity of methanol in the range between room temperature and its boiling point are represented as loss tangents in Figure **35**. The measurement of the center frequency of the dipolar relaxation peak is measured from the dielectric loss data.

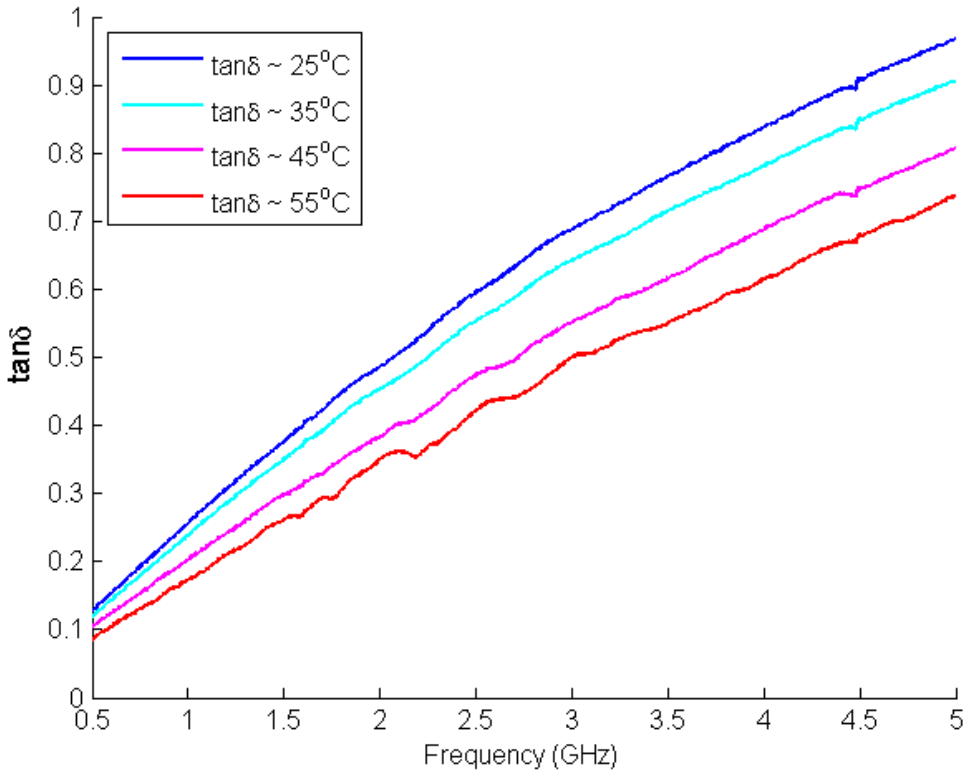

Figure **35**: The complex permittivity measurement of methanol over elevated temperatures expressed as the loss tangent. As the temperature increases the dielectric loss decreases as a result of methanol molecules disassociated from their polar bonds.

The points at the center of the dipolar relaxation curve in the plot of dielectric loss constant are plotted and fit with a linear curve as in Figure **36** . Using the slope of this curve, Boltzman's constant and Equation **65**, the activation energy for the rotation of a single methanol molecule is calculated to be 0.0961 eV.

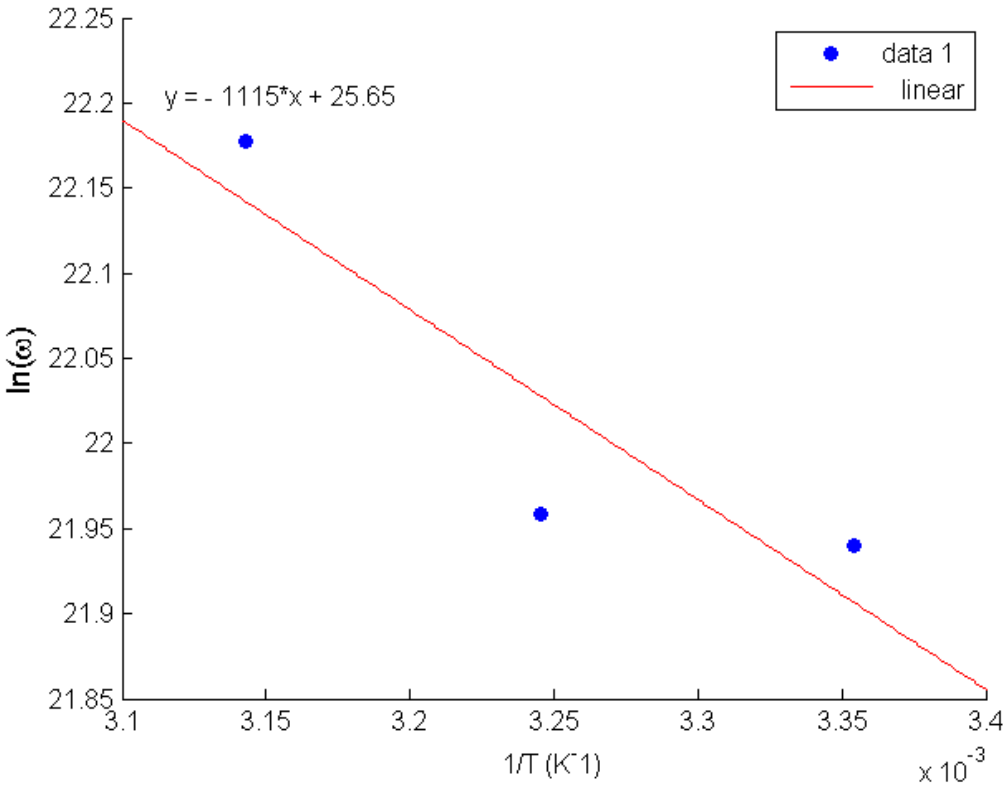

Figure **36**: Linear approximation of the log of frequency associated with the center of the dipolar relaxation peal of methanol over inverse temperature. The slope of this line is related to the activation energy of a single, freely rotating methanol molecule.

The complex permittivity of soybean oil was also measured over temperatures; however no observable change was recorded. In general, it appeared as if the dielectric loss lowered, but the noise of the measurement increased to a point which the decrease was no longer statistically evident.

6.2.3 Complex Permittivity of Mixtures:

With a detailed study of the complex permittivity of the individual components of biodiesel production established; the measurement of ultrasonically formed emulsions of the reactants is performed. The relation between the complex permittivity and the emulsion microstructure has been investigated by Holtze et al. with surfactant stabilized water in oil emulsions. His results indicated

that as dispersed water droplets decreased in size, the relaxation peak decreased in magnitude and shifted to higher frequencies. The report claimed that the stabilizers did not affect the droplet size; however it did amplify the surface conduction at the water oil interface. He also discussed the control of microwave heating through droplet size design.[**122**] The most interesting point is that the size of polar droplets affects the polar relaxation peak in a similar manner. The calculation of activation energy of methanol a single methanol droplet relied on elevated temperatures to decrease and shift of the polar relaxation peak. In short, making finer emulsions allows methanol molecules to oscillate as if there were more available energy. However, it only *seems* like there is more available energy because the physical separation from other molecules provided by the oil inhibits dipole interactions.

Once again the issue of emulsion stability is of primary concern. Without the use of emulsion stabilizers the various emulsions undergo ripening, creaming, and coalescence as described in Chapter 2. In one way, these mechanisms frustrate the accurate determination of the complex permittivity of the emulsions. On the other hand, the permittivity measurement offers a new and highly sensitive tool for observing and comparing emulsion stability. For example, in Figure **37** , a 9:1 molar ratio emulsion shows a sudden jump in dielectric loss, which is evidence of a coalescence event. This means that while the measurement was being made, a group of methanol droplets combined to form a large droplet. Since the rate of creaming Equation **4** is correlated to the size of droplet, it is understood that such a large droplet would immediately rise to the surface, where the probe is in contact with the fluid. The reason this even is evident at a frequency only by coincidence; as the network analyzer takes time to sweep through the measured frequencies.

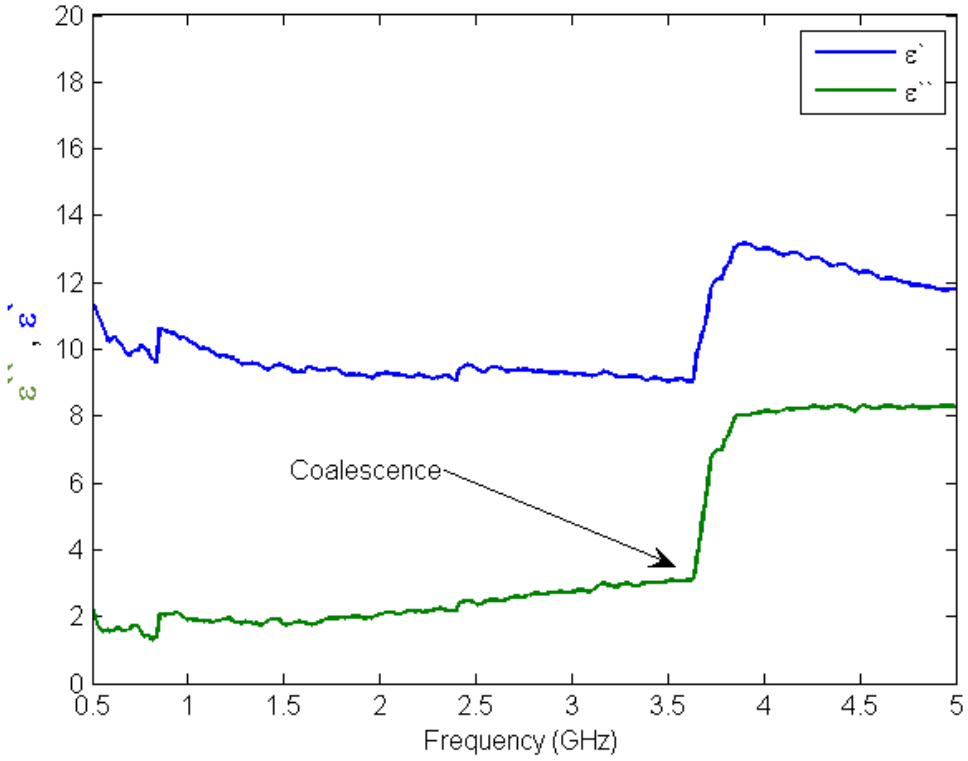

Figure **37**: Complex permittivity of an emulsion with a 9:1 molar ratio of methanol to soybean oil as a destabilization in the form of coalescence occurs. During the time the network analyzer takes to analyze the frequency spectrum several droplets of methanol join and rise towards the sensor.

First, the 22 kHz ultrasonic horn was used at full and half power to form emulsions of 3:1, 6:1, and 9:1 molar ratio in 40mL glass vessels and measured three times. The measurements were averaged and plots with standard deviations are available in Appendix 1. The full and half power ultrasonic treatments are compared for each molar ratio emulsion in Figure **38**, Figure **39** , and Figure **40.**

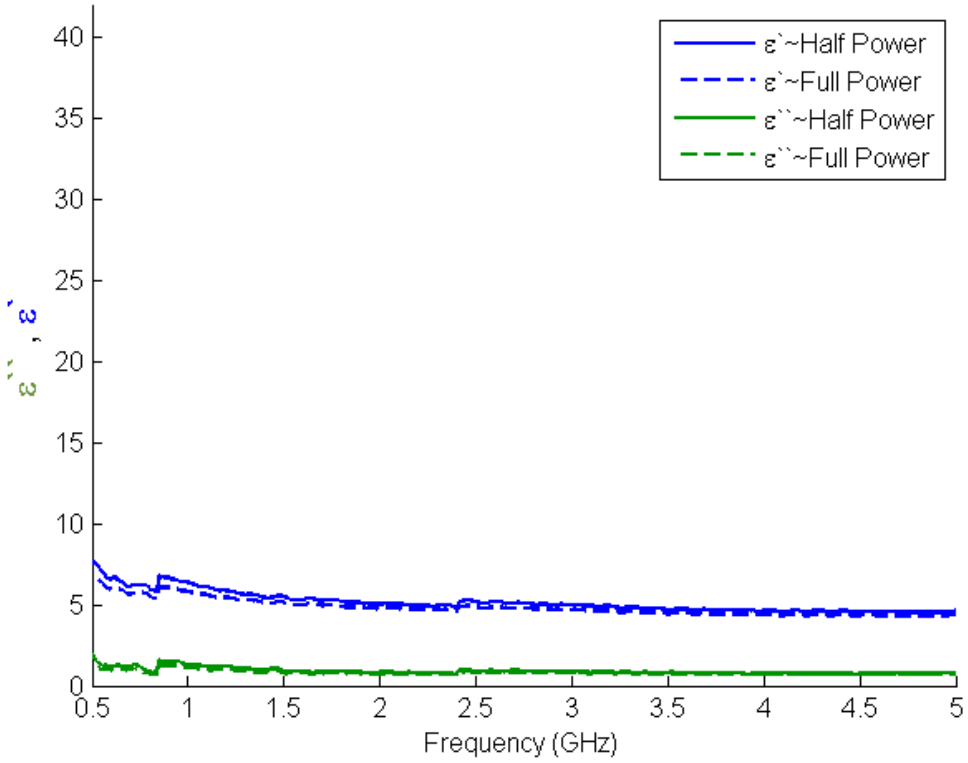

Figure **38**: Complex permittivity measurement of 3:1 molar ratio emulsions of methanol and soybean oil as prepared with 22 kHz ultrasound at full and half power. The lower values obtained in the full power case suggests smaller dispersed methanol droplets.

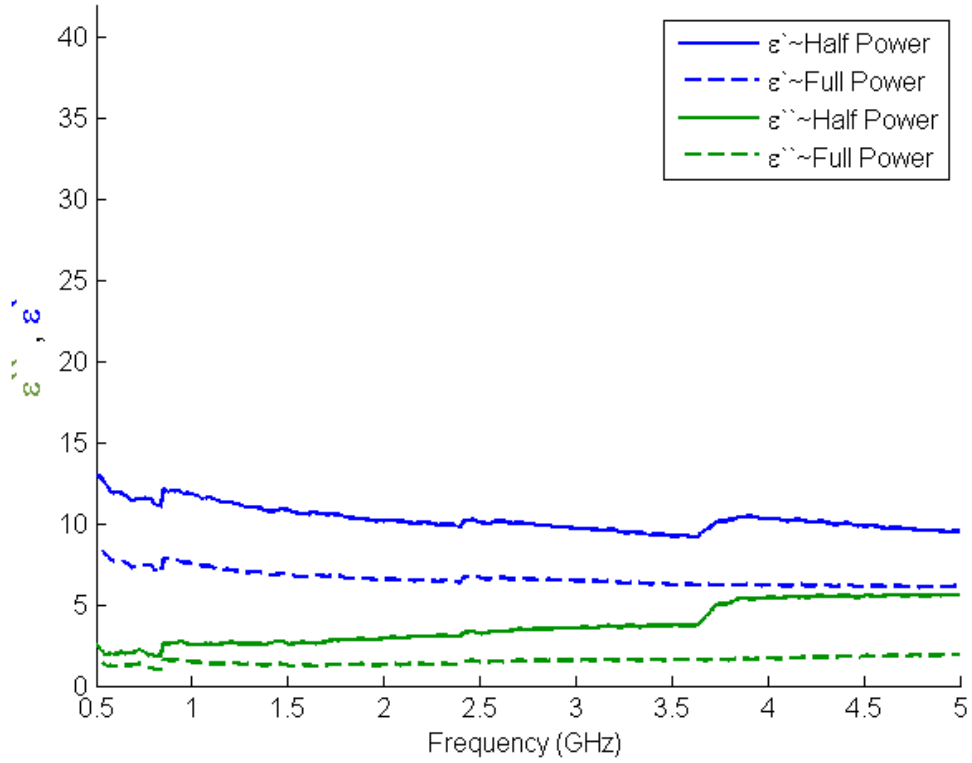

Figure **39**: Complex permittivity measurement of 6:1 molar ratio emulsions of methanol and soybean oil as prepared with 22 kHz ultrasound at full and half power. The lower values obtained in the full power case suggests smaller dispersed methanol droplets.

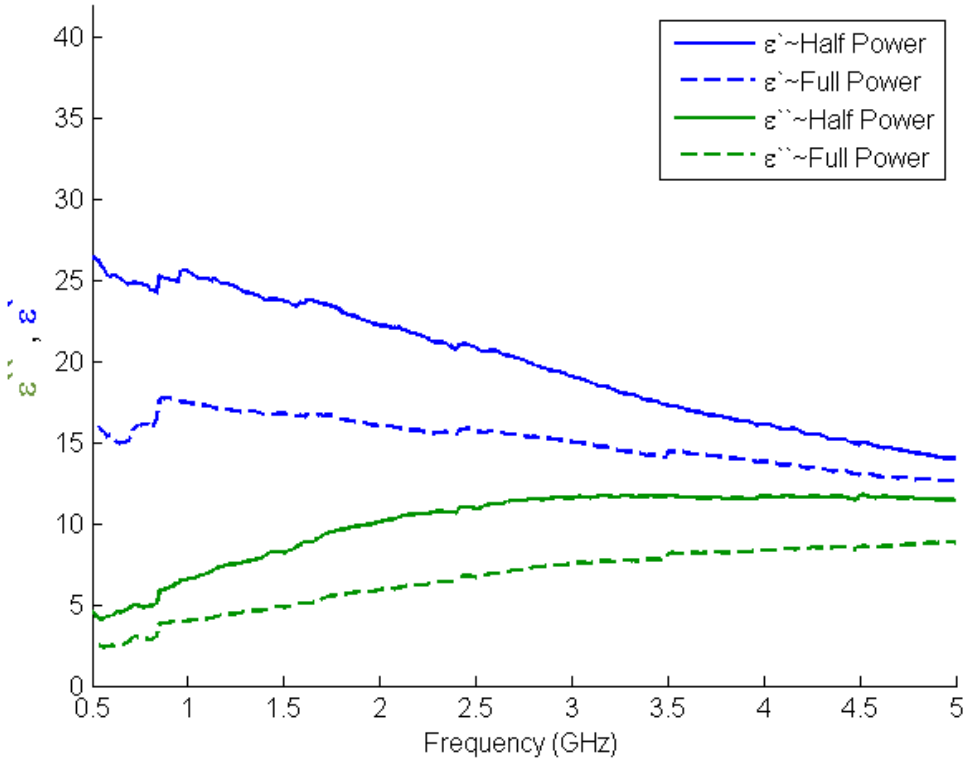

Figure **40**: Complex permittivity measurement of 9:1 molar ratio emulsions of methanol and soybean oil as prepared with 22 kHz ultrasound at full and half power. The lower values obtained in the full power case suggests smaller dispersed methanol droplets.

The results in the above figures support the conclusion made in the previous section regarding the effect of molar ratio on the dispersed droplet size. The dipolar relaxation peak emerges with higher volume concentration of methanol as the size of droplets and overall quantity of methanol increases. However, the effect of ultrasonic intensity seems to be in contradiction to the observations in the previous section regarding dispersed phase diameters. In the above figures, the half power results each coincide with higher dielectric loss. This would suggest that larger methanol droplets resulted from higher ultrasonic intensity. However, the comparison can not be made due to the difference in sample preparation volumes. As described in chapter 4, the intensity of ultrasound affects the rate of emulsification as well. Thus a larger volume may not be completely emulsified over the same period of time as a smaller volume.

Next, the same molar ratio emulsions as above are prepared with the 44 kHz ultrasonic bath and the complex permittivity. This experiment quantifies the observations discussed regarding the stability of emulsions at lower concentrations of methanol, as indicated by the maximum dielectric loss occurring with the 3:1 molar ratio, as in Figure **41** .

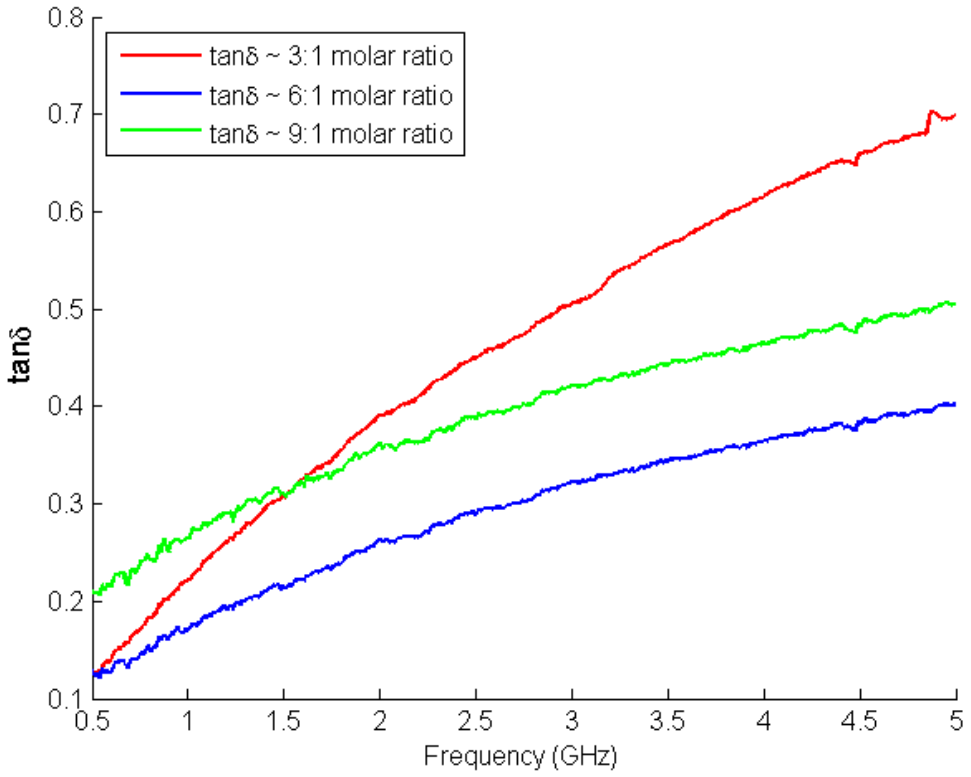

Figure **41**: Complex permittivity measurement, expressed as the loss tangent, of 3:1, 6:1, and 9:1 molar ratio of methanol to soybean oil emulsions prepared with 44 kHz ultrasonics. The 3:1 emulsion indicates the highest loss, suggesting larger dispersed droplets of methanol.

Next, the stability is observed for 9:1 molar ratio emulsions formed by 22 kHz ultrasound and 44 kHz ultrasound. Each emulsion placed immediately under the probe and complex permittivity measurements are repeated continuously as the emulsion destabilizes. The emulsion formed with 22 kHz ultrasound exhibited creaming which can be observed in Figure **42** as dielectric loss rapidly takes the form of the methanol dipole relaxation peak. As the methanol droplets saturate

the upper portion of the vessel the change in dielectric loss slows. The emulsion made with 44 kHz ultrasound exhibited ripening during destabilization. The change in dielectric loss due to ripening is distinguished from that of creaming by the smaller magnitude and constant rate overtime, as in Figure **43** .

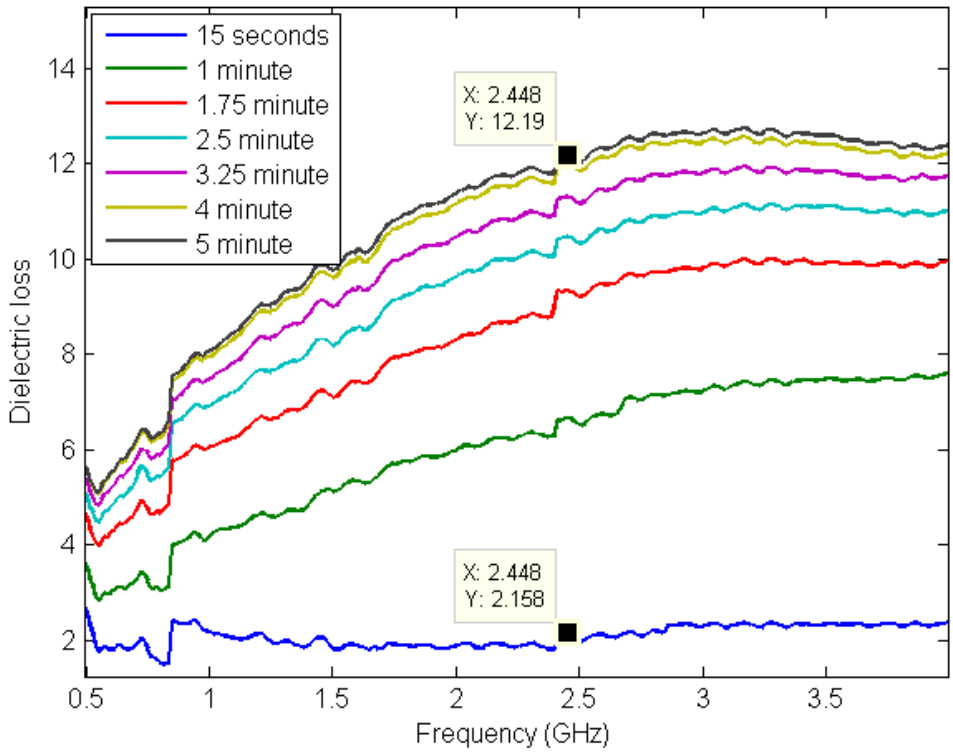

Figure **42**: Measured dielectric loss of emulsion prepared with 22 kHz ultrasound as destabilization in the form of creaming increases the amount of methanol near the surface of the vessel where the probe is located.

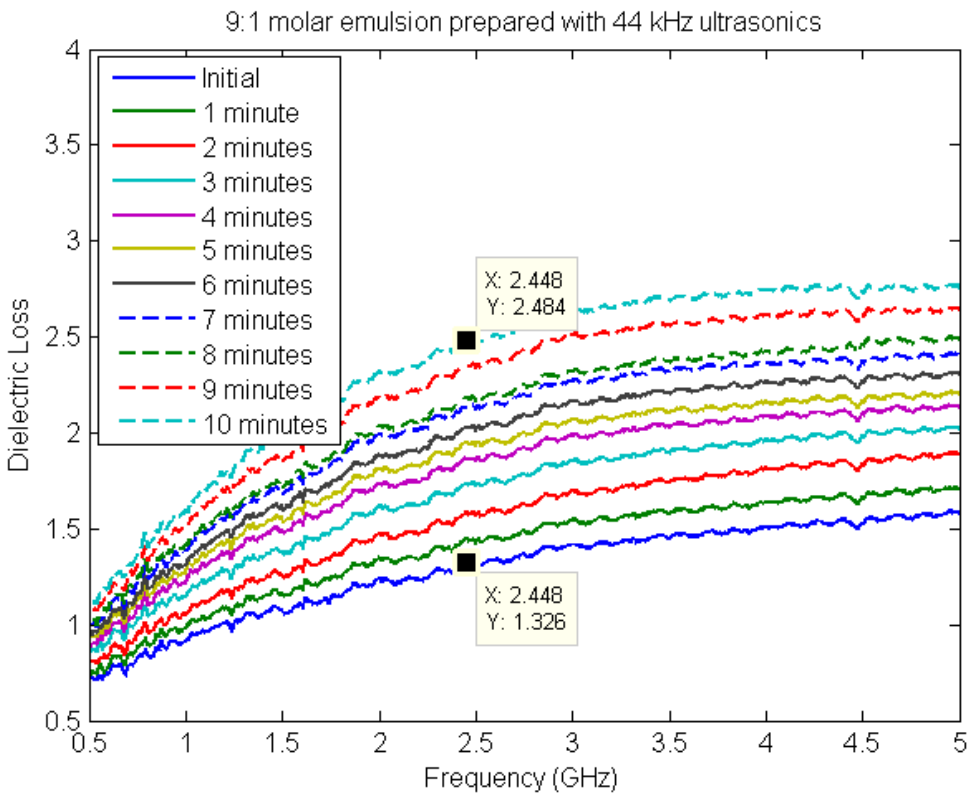

Figure **43**: Measured dielectric loss of emulsion prepared with 44 kHz ultrasound as destabilization in the form of ripening increases the size of methanol droplets in the oil. The slow and low magnitude increase in loss differentiates the ripening process from the creaming process.

6.2.4 Process Comparisons:

Finally, a high speed rotary mixer is utilized to prepare a 9:1 molar ratio emulsion representative of a conventionally mixed case. The loss tangent is calculated and compared to the ultrasonically formed emulsions and the constituent materials. The comparison indicates that despite differences measured between ultrasonic treatments, all of the treatment exceeds the performance of a conventional mixer, Figure **44**.

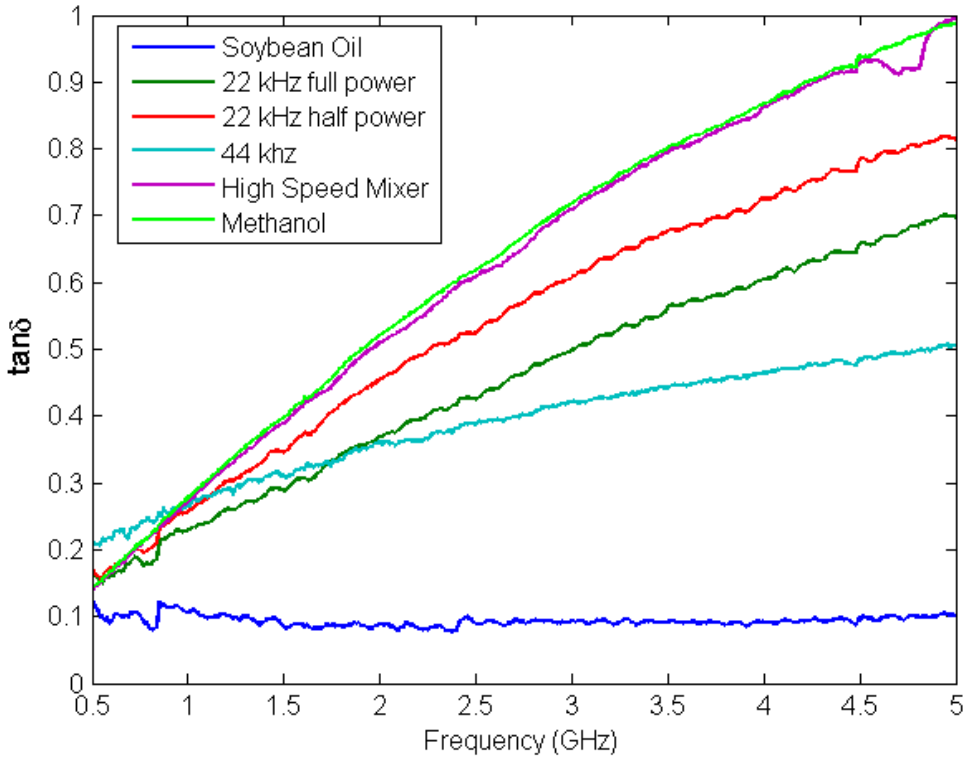

Figure **44**: Complex permittivity expressed as the loss tangent for emulsions prepared by 22 kHz at two powers, 44 kHz ultrasound, and a high speed mixer. The dielectric loss of the emulsion formed with conventional mixing closely corresponds to the loss of pure methanol indicating large dispersed droplets of methanol.

To summarize, the permittivity measurements indicate that the dipolar relaxation peak in the dielectric loss is near a maximum at 2.45 GHz. The ionic conduction contribution to dielectric loss from the addition of base catalyst to methanol is observed at various concentrations. From analysis, the presence of catalyst can not be completely accounted for by the conductivity term of effective loss. The dielectric loss of methanol over temperature was related to hydrogen bonds and the activation energy of a single methanol molecule. The dielectric loss measurement allowed the monitoring of emulsion destabilization effects in situ. Finally, the ability of an ultrasonically formed emulsion of biodiesel reactants to affect the microwave absorption at heating frequencies is distinguished from conventional mixing.

6.3 Microwave Heating:

6.3.1 Superheated Boiling:

The microwave heating measurements will be concerned with three measurements. The first measurement is that of the temperature at the onset of boiling. This will be referred to as the superheated boiling point and represents the limit to superheating at atmospheric pressure. The second measurement is the measure of microwave heating rate, which correlates to the material properties through Equation **40** . Finally, the third measurement is of the of reaction completion at a given microwave treatment and time. These measurements are used to correlate to the advantages of the combined approach and investigate attempts at catalyst free multi-energy optimized production.

The stability of the superheated state now becomes the primary concern. This stability is related to the emulsion stability, but only to the extent which the destabilization of emulsions increases nucleated boiling. To sensitivity to nucleation can is demonstrated in Figure **45**, which shows two microwave heating curves of pure methanol. In one case, the sample begins to boil at the standard boiling point at atmospheric pressure, representing a sample affected by nucleated boiling. In this case, the nucleation sites were provided by paper towel residue from drying the flask. The second curve demonstrates the ability to superheat methanol when nucleation is prevented. This sample vessel was carefully rinsed methanol before microwave heating to over twice the classical boiling point.

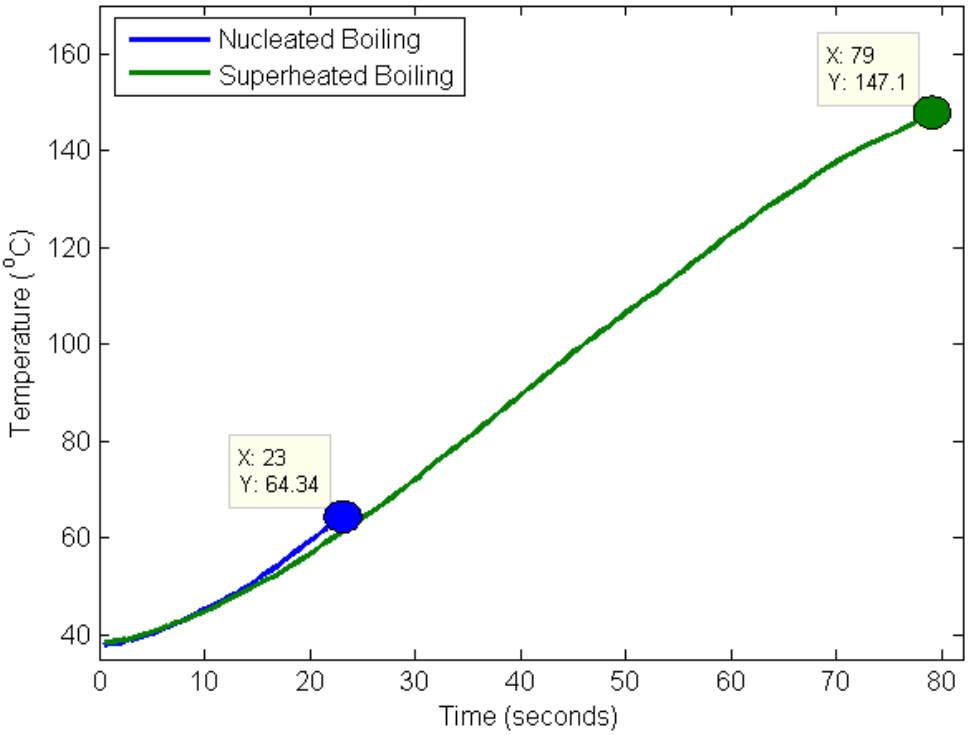

Figure **45**: Microwave heating curves of methanol at atmospheric pressure with and without nucleation sites. Without nucleation, methanol becomes superheated under microwave radiation.

The sensitivity to nucleation is of critical importance to the design of microwave reactor, as the ability to superheat enables the reaction kinetics inaccessible with conventional heating. Furthermore, the amount of pressure maintained to reach the superheated temperature conventionally, is representative of energy that can be saved using microwave superheating. For example, the superheated methanol from above, which reached more then double the classical boiling point at atmospheric pressure at 147 degrees Celsius, meaning the pressure of a classically heated reactor would need to be more than twice atmospheric pressure to achieve the same kinetics. Any skepticism regarding the resulting magnitude of energy stored in a superheated fluid is quelled during the observation of the final boiling event in such a scenario. In a process known as bumping, nearly the entire sample of superheated methanol suddenly evaporates at once. In Chapter 3 it was stated that the extent of superheating dictates the sensitivity to nucleation. In an ideal case with no

surfaces for nucleation, the entire volume of fluid would evaporate at the same instant. This is realized practically when a layer of super heated fluid contacting a uniformly smooth vessel begins to evaporate and in turn rapidly nucleates the boiling of the remaining fluid.

To illustrate the fluctuations in superheated boiling point measurements of methanol over various MW powers, the average temperature is shown with error bars representing the standard deviation of the measured values of two consecutive trials, Figure **46** . From Chemat's work, it is expected that the microwave power will increase the superheated boiling temperature. However, the microwave systems used in his work utilized much lower power. The microwave used in this experiment is equipped with a magnetron with 1.2 kilowatt output. The power output is adjusted with a rheostat; however, the minimum output with this method is still 800 Watts. In Chemat's work, the maximum power output of the magnetron was 600 Watts.[**53**] Accordingly, it is assumed that the boiling points at each power setting will be saturated indifferently. However, the rate of heating that is slower at lower powers may allow the superheated methanol to come to thermal equilibrium with the glass vessel as it heats, prolonging nucleation from the temperature gradient. This concept will be discussed more at the end of this section.

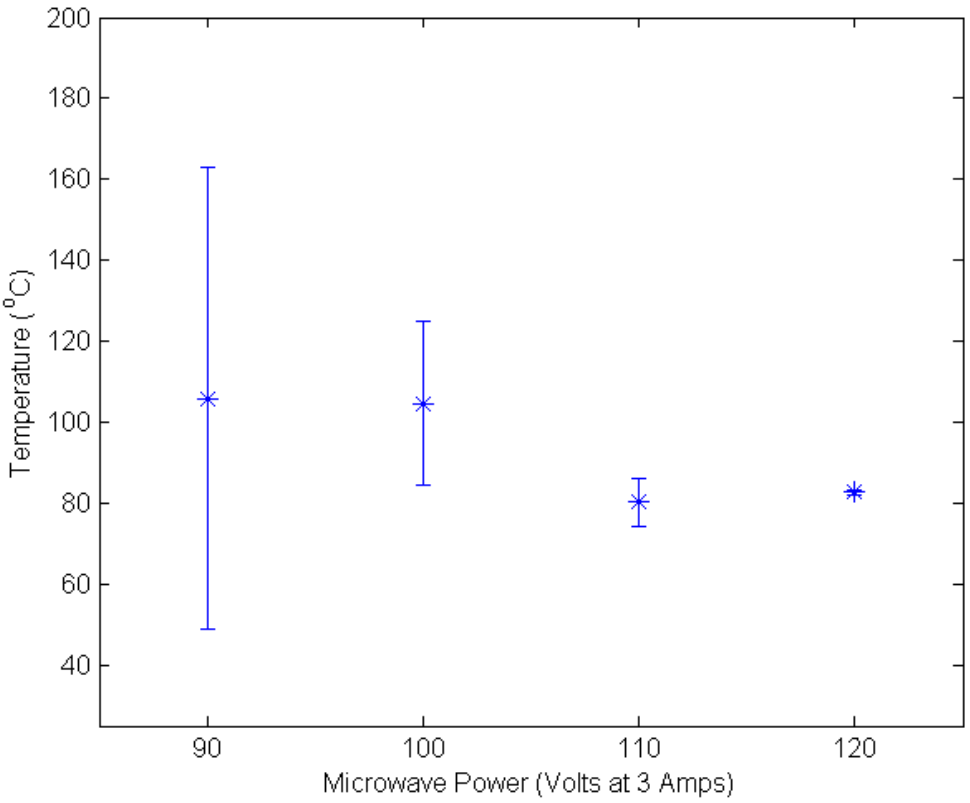

Figure **46**: The average superheated boiling temperature of pure methanol at atmospheric pressure as a function of microwave power does not increase with increased power. The error, representative of the standard deviation of the measurement, indicate unequal heating at lower power settings.

Next, the goal of enhancing the microwave superheated temperature is pursued using emulsions with molar ratios of methanol to soybean of 3:1, 6:1, and 9:1 and 0%, .1%, .5%, and 1.0% sodium hydroxide catalyst by weight of oil. Each sample is subjected to the four microwave powers until boiling twice. The boiling point associated with each catalyst concentration is averaged and the standard deviation calculated. The results are compared to the averaged values for pure methanol to indicate which samples extend the superheated boiling point of methanol in Figure **47** . The result of the comparison indicates that catalyst free ultrasonically formed emulsions were most capable of extending the superheated boiling point of methanol. The addition of catalyst created

nucleated boiling and thermal instability while heating, resulting in lower average boiling temperatures than without catalyst.

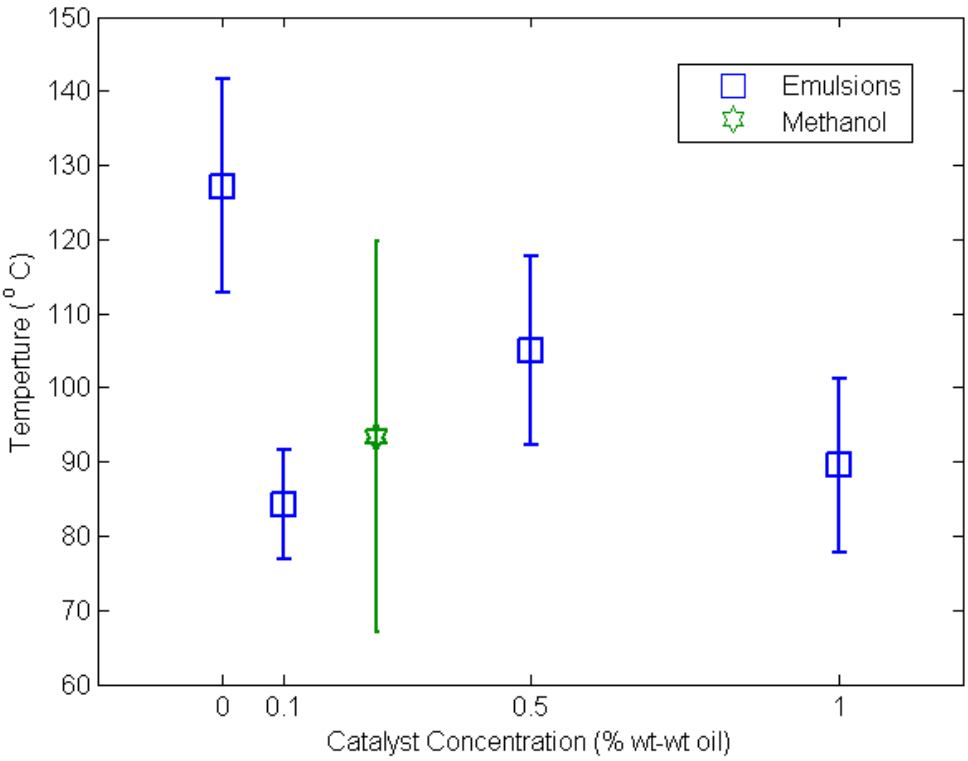

Figure **47**: The average superheated boiling temperature of ultrasonically formed emulsions with varying concentrations of sodium hydroxide catalyst compared with the average superheated boiling temperature of pure methanol. The superheated temperature of methanol is enhanced when ultrasonically dispersed in a catalyst free emulsion.

6.3.2 Anisothermal heating:

The next measurement involves measuring the rate of heating for catalyst free emulsions created with the 22 kHz ultrasonic source at full power in samples of the same volume used in the permittivity measurements. The heating rate is related to the dielectric loss constant and microwave power as in Equation **40**. To calculate the heating rate, the heating curve is fitted with a linear

polynomial by method of least squares. The resulting fit is then compared to the measured heating curve by way of cross correlation. The correlation coefficient of this measurement is used to describe the error in the approximation and each fit resulted in a correlation of 0.977 or greater. The slope of the linear fit for a particular material corresponds to the product of microwave power and dielectric loss constant.

First, this analysis is performed on pure soybean oil and methanol to obtain functions of microwave power for each material. The results plotted in Figure **48** indicate that the heating rate of methanol reaches a maximum at the 100 volt power setting while the heating rate of soybean oil continues to increase across the power settings. The reason soybean oil does not reflect saturation of microwave radiation is due to the low dielectric loss constant as measured in the previous section.

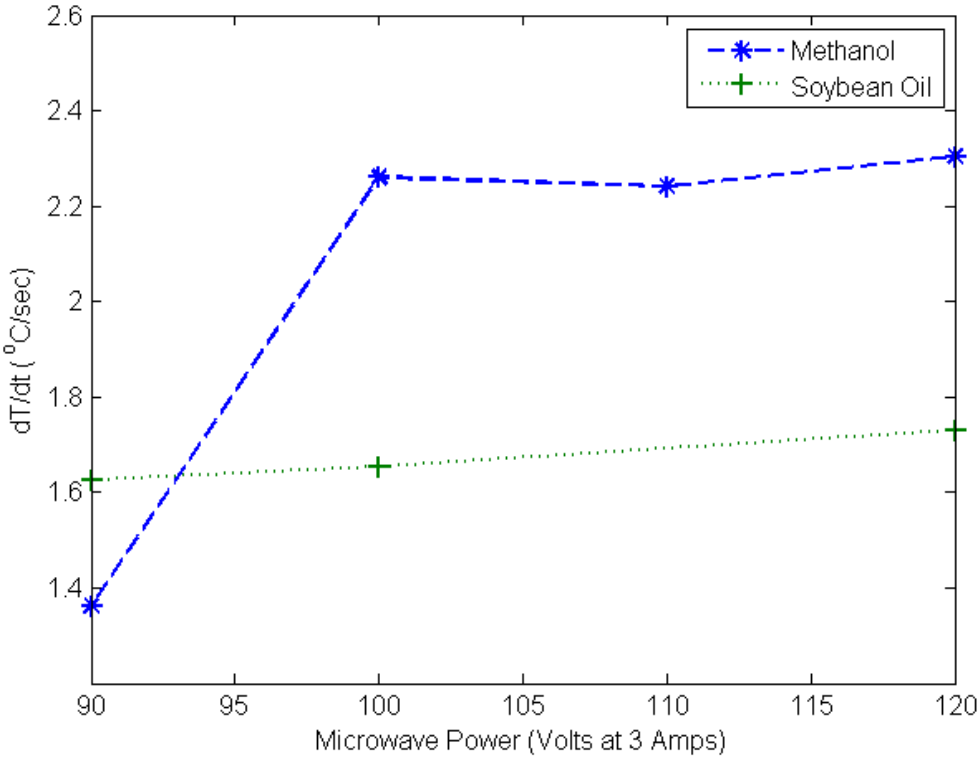

Figure **48**: Microwave heating rates of pure methanol and soybean oil at different microwave power settings. Soybean oil has a low dielectric loss which results in the heating rate experiencing little change with microwave power. Methanol has a large dielectric loss which causes the large change in heating rate.

The heating rates calculated for the pure materials can now be compared to the ultrasonically prepared emulsions. Where the superheating test verified the ability to stabilize superheated methanol, this test indicates if the emulsion enhances the dielectric loss practically. The results in Figure **49** indicate that heating rates above that of methanol can be achieved with ultrasonic emulsification. The result can be explained in terms of anisothermal microwave heating. As the dispersed methanol heats, the surrounding oil is heated through heat conduction allowing the emulsion's heating rate to exceed that of methanol. The heating rates are difficult to directly relate to the permittivity measurement due to anisothermal heating. For example, as methanol is heated its dielectric loss changes which is accounted for in the microwave heating rates of pure methanol.

However, as the methanol transfers heat to the oil, the rate at which the heating affects the dielectric loss is reduced. The net result is a mixture that can achieve heating rates and superheated temperatures above its dispersed phase.

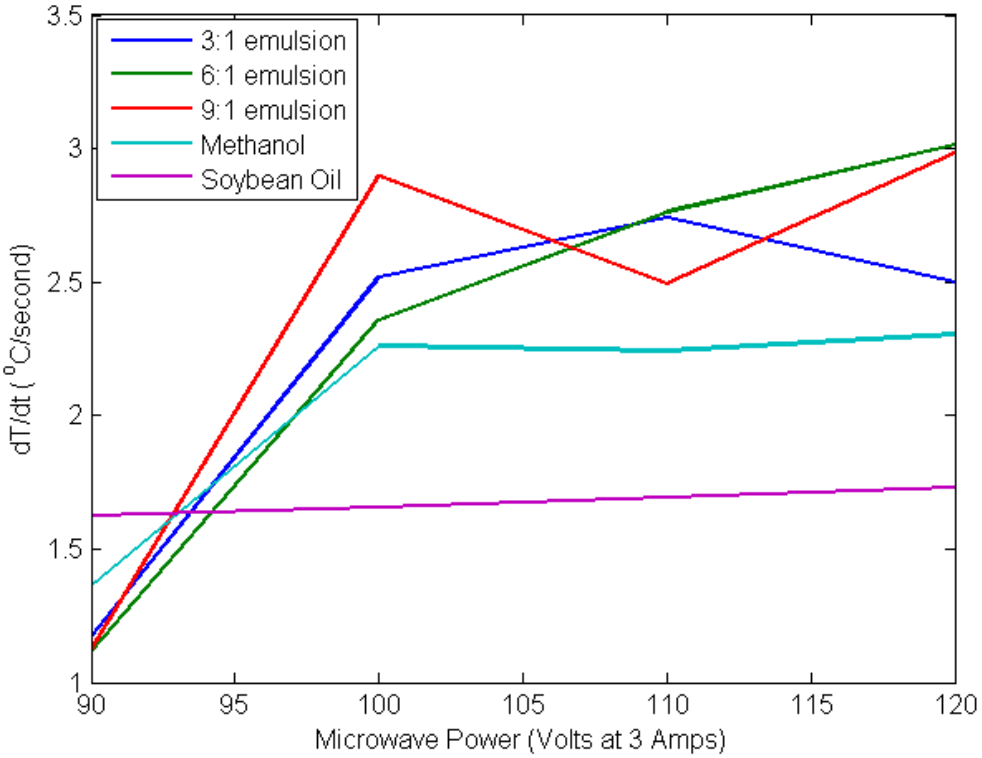

Figure **49**: The microwave heating rate of ultrasonically formed catalyst free emulsions consisting of methanol and soybean oil compared to the pure components indicates anisothermal heating effects. As the suspended methanol droplets rise in temperature, the heat conducted into the surrounding oil delays the limiting effect of decreasing dielectric loss with temperature.

6.3.3 Transesterification Experiments:

First, the advantage of an ultrasonically formed emulsion as compared to a classical mixed emulsion is demonstrated. The molar ratio of 9:1 is chosen to ensure that an excess of methanol remains if any boiling occurs and .3% sodium hydroxide catalyst by weight of oil to accelerate the reaction. The ultrasonic horn at 22 kHz and full power is compared to the rotary mixer at 10,000 rpm. The reaction completion is measured by weight of glycerol byproduct. The precision scale was determined to measure to within 0.00005 grams. The measurement correlates to only the last of the stepwise reactions described in Chapter 2, namely the conversion of mono-glycerides to glycerol. The products that form when glycerol is observed were confirmed by GC analysis, as shown in Chapter 5, to be the expected methyl esters resulting from transesterification.

Three samples were mixed utilizing each technique and microwave heated to near the boiling point of methanol and maintained at that temperature for three different amounts of time. The results of the study, in Figure **50** , show a dramatic improvement in reaction rate in the case of ultrasonically mixed emulsions.

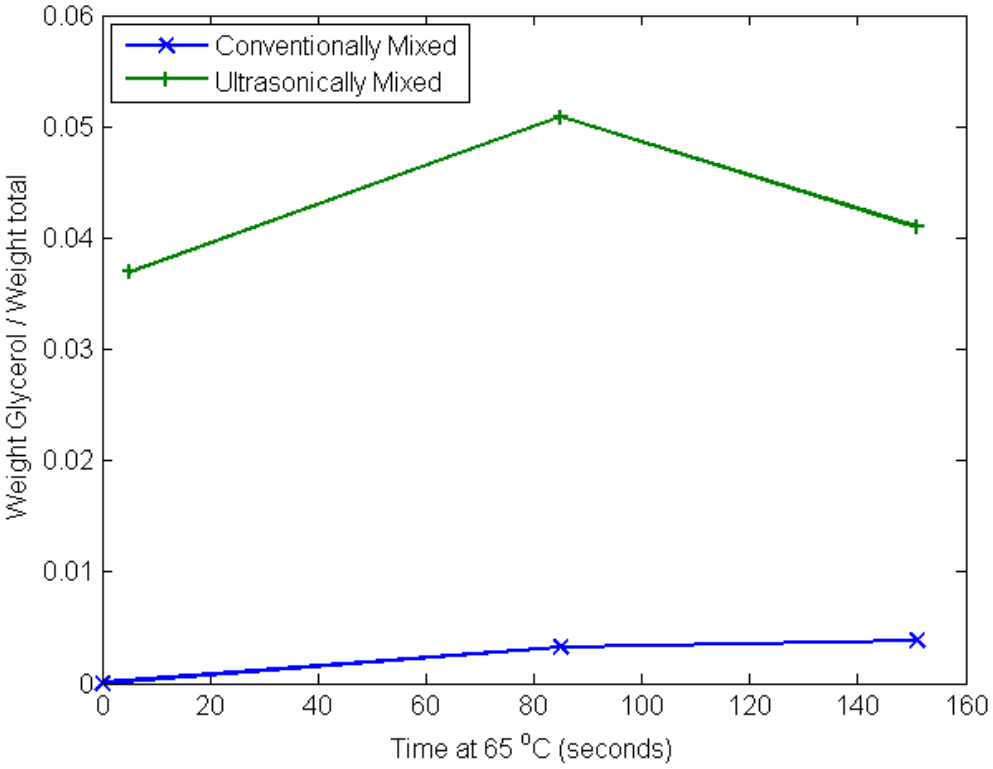

Figure **50**: Comparison of the rate of formation of glycerol resulting from the transesterification reaction between conventionally mixed and ultrasonically prepared emulsions heated with microwaves. The emulsions are of 9:1 molar ratio of methanol to oil catalyzed by 0.3% sodium hydroxide by weight of oil. The faster rate is indicated in the case of the ultrasonically prepared sample due to the optimization of microwave heating.

Finally, catalyst free ultrasonically formed emulsions are heated with microwave radiation for the purpose of transesterification. Admittedly, many attempts were made without positive results. Initial attempts focused on reaching as high of temperature as possible. To prevent boiling the microwave power was adjusted during the process by observation. This means that when boiling first begins, the power to the magnetron is reduces or turned off. As the solution stops boiling, the microwave power is slowly increased until another boiling event. One such attempt resulted in the solution to reaching over 240 °C, which is above the critical temperature. At this temperature, the remaining methanol boils out in very fine bubbles which are evenly distributed throughout the mixture. A similar description is given in the case of the superheated limit as described in [**44**].

However, the subsequent GC analysis indicates no detectable methyl ester peaks. For comparison this GC result is presented in Figure **51** .

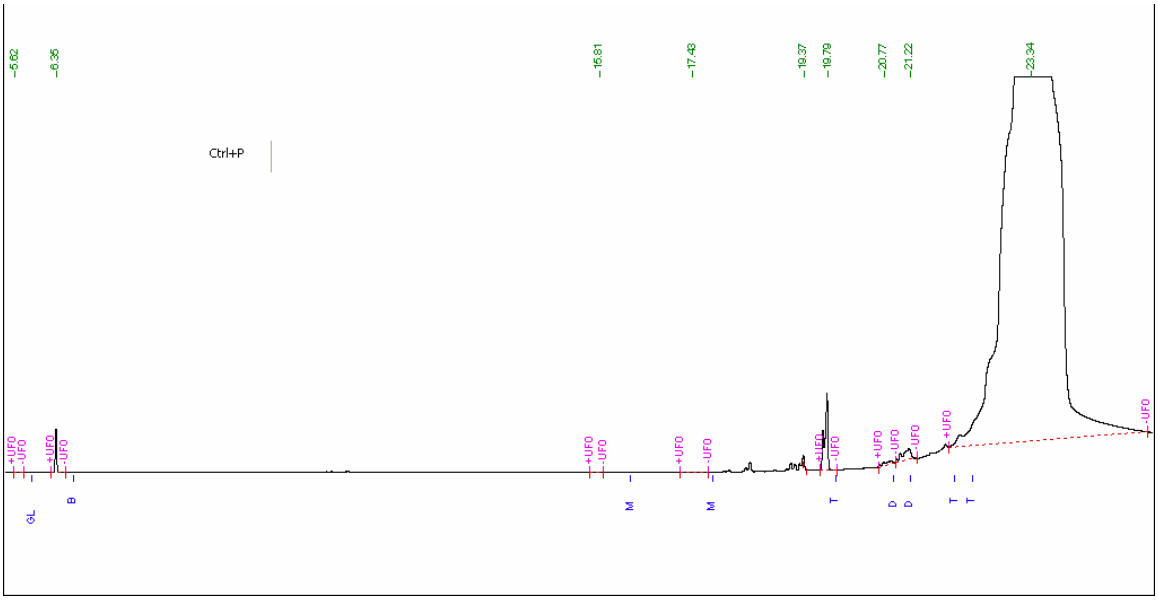

Figure **51**: GC analysis of the result of an ultrasonically prepared catalyst free reaction mixture heated with microwaves causing the methanol to boil out. The result contains no noticeable amount of methyl esters.

The lack of transesterification is likely result of methanol evaporation, which encourages back reaction to triglycerides. The next experiments still utilized controlled microwave heating to maximize the superheated temperature; however, they were removed and quenched at the onset of boiling. A 9:1 molar ratio of methanol to soybean oil ultrasonically mixed with the 22kHz horn at full power for thirty seconds, heated in the microwave to 85 °C for 220 seconds indicated a small, but noticeable methyl ester peak in the GC chromatograph, as in Figure **52** . It is noted that in this trial, nearly no free glycerol was formed, indicating that only the first of the stepwise transesterification reactions occurred, namely triglyceride to di-glyceride with the fatty acid molecule released converted to a methyl ester.

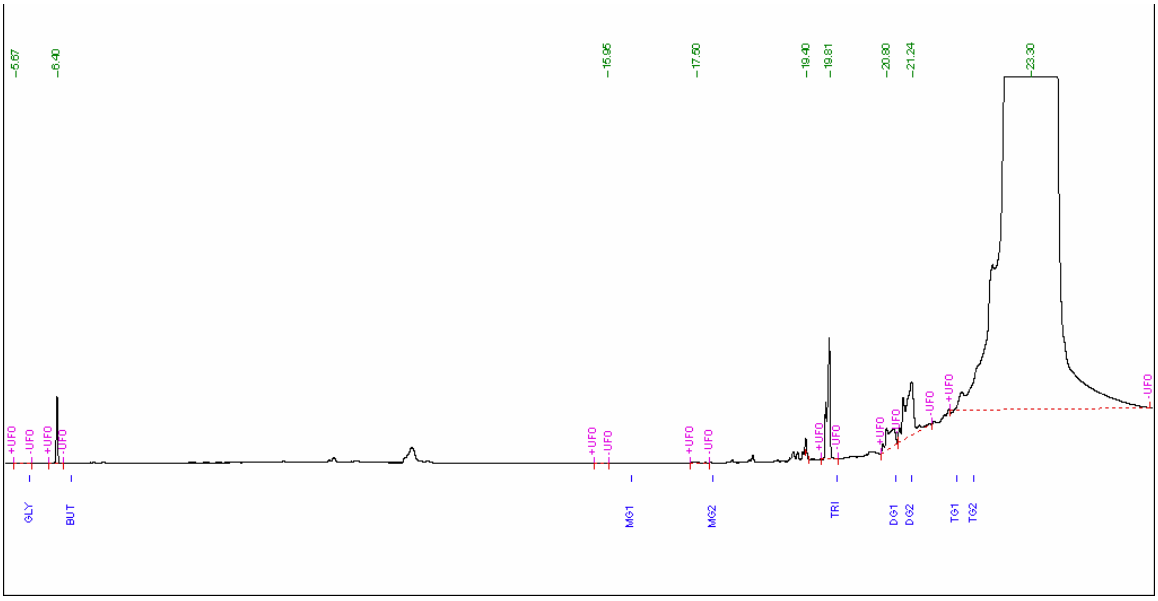

Figure **52**: GC analysis indicating successful transesterification using 22 kHz ultrasonic emulsification for thirty seconds and microwave superheating to 85 °C for 220 seconds. Sample is of 9:1 molar ratio of methanol to soybean.

To ensure the result was not due to catalyst contamination, the experiment is repeated with similar results, found in the APPENDIX. Finally, the same experiment is replicated using jatrohpha seed oil resulting in more significant methyl ester production, as in Figure **53** . Again, to rule out possible catalyst contamination this result is repeated twice more with similar results, available in the Appendix.

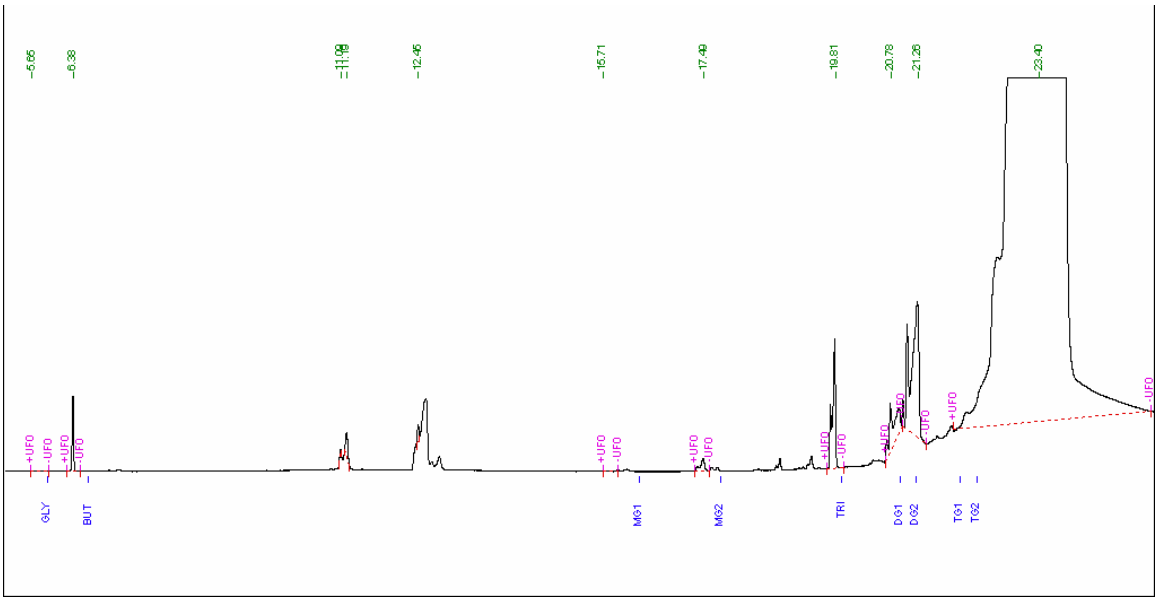

Figure **53**: GC analysis indicating successful transesterification using 22 kHz ultrasonic emulsification for thirty seconds and microwave superheating to 85 °C for 220 seconds. Sample is of 9:1 molar ratio of methanol to jatropha seed oil.

In summary, the experiments in this section confirmed the ability of ultrasonic emulsification to optimize microwave superheated as measured by the extension of the superheated boiling point. The use of catalyst inhibits the extension of the superheated boiling temperature. The catalyst free ultrasonically formed emulsion is shown to increase the rate of heating through anisothermal effects. The use of ultrasonics to prepare tradition base catalyzed reactants for microwave heating is shown to enhance the reaction kinetics as evident from glycerol byproduct formation. Finally, the combined use of microwaves and ultrasound are shown to enable catalyst free transesterification is verified by GC analysis.

Chapter 7

Conclusions and future work

7.1 Review of thesis objectives and contributions:

7.1.1 Thesis objectives

Biodiesel fuel is becoming an integral part of transport fuels industry. As a renewable resource, biodiesel is sought to offset the carbon dioxide emissions from petroleum fuels. To achieve the benefits that could be afforded from biodiesel, the research community must continue to investigate novel process strategies to eliminate the wasteful use of chemicals in production. Microwaves, ultrasound, and the combination have been identified as processes for green chemistry. However, the synergistic effects of the combination has not been addressed or suggested for biofuel processing. The aim of this work was to improve the understanding of how microwaves and ultrasonics improve a chemical process and demonstrate the technique as a method for catalyst free biodiesel production. To review, the individual goals of this thesis were:

- Measure the effect frequency and intensity of ultrasound during emulsification of biodiesel reaction mixtures in terms of dispersed methanol droplet size
- Measure the complex permittivity of methanol, soybean oil and ultrasonically formed emulsions over microwave frequencies
- Measure of microwave heating profiles of ultrasonically formed emulsions with dispersed polar phase

- Evaluate enhancement microwave superheating through use of ultrasonic emulsification
- Combine the use of microwaves and ultrasound for catalyst free transesterification at sub-critical temperatures.

7.1.2 Thesis contributions:

1. Investigation of catalyst free biodiesel production

The work began with a literature survey covering the known works concerning catalyst free transesterification. This included the use of super critical methanol for biodiesel production. The reactivity of methanol in the supercritical state was described as a function of weaker or broken hydrogen bonds, allowing molecules to freely rotate and bond without influence of near neighbors. Theoretical aspects of emulsion science were included to make up for the lack of discussion in the biodiesel production literature.

2. Description of microwave heating

From elementary derivations from Maxwell's equations the development of microwave dielectric loss mechanisms was presented. The dipolar relaxation was described as the loss mechanism of pure methanol. This was differentiated from the ionic conduction losses that would occur from the addition of catalyst. The theory of microwave heating led to the description of two enhancements uniquely provided by microwaves. The first is the ability to heat a liquid above its boiling point in atmospheric pressure, or microwave superheating. The limit to the superheated temperature, at atmospheric pressure, due to nucleation is identified as

roughly 90% of the supercritical temperature. The method used to arrive at this limit involved stabilizing small droplets of the superheated liquid in oil. The second effect is anisothermal heating resulting from two materials with different values of microwave loss. Finally, a review of applications to chemistry and biodiesel production provides the context for reasearch. This analysis led to the description of an ideal biodiesel reaction mixture which would maximize the benefit of microwave heating.

3. Description of high intensity ultrasonics

From the equations of ultrasound in a fluid, the theoretical origin of cavitation and atomization are given. A review the literature regarding modern research in ultrasonic emulsification provided the advantages unique to ultrasound. The chief advantage reported was the ability to create emulsions with uniform dispersed phase droplet size. However, the lack of conclusive relations between ultrasonic parameters, intensity and frequency, and dispersed droplet size justified the current work. Finally, a review of applications in chemical and biodiesel production yields no evidence of studies focused on the use of ultrasound to optimize reaction mixtures for microwave heating.

4. Evaluation of ultrasonically formed emulsions of biodiesel reactants

The size dispersed methanol droplets in soybean oil resulting from ultrasonic emulsification were measured to compare frequency and intensity. The results indicate that smaller dispersed phase droplets could be achieved with higher frequency treatments. The less pronounced effect of ultrasonic intensity was determined to lower dispersed droplet size with

lower intensity in samples of small volume. The uniformity of dispersed phase droplet sizes was compared to conventionally mixing, confirming the advantage of ultrasonic emulsification. The repeatability of dispersed phase droplet size was determined for commercial laboratory ultrasonic sources. It was demonstrated without specialized equipment, that ultrasonic emulsification could faithfully produce emulsions with dispersed phase droplets in the range of 2 to 4 micrometers without stabilizers. However, the repeatability test for the 44 kHz source indicated that with improved design, dispersed droplets under 1 micrometer could be achieved. This study verified the ability of ultrasound to form the emulsions identified as ideal for microwave heating.

5. Modification of complex permittivity of mixtures by ultrasonic emulsification

The complex permittivity, correlated to microwave heating, was first measured for soybean oil, methanol, and jatropha oil. The dielectric loss of unrefined jatropha seed oil was similar to the refined soybean oil. The dielectric loss of pure methanol indicated the dipolar relaxation peak overlapping with the microwave heating frequency of 2.45 GHz. The addition of catalyst to methanol showed that at low catalyst concentration, the ion conduction is greater than the dipolar relaxation loss. Monitoring the dipolar relaxation peak of pure methanol over elevated temperatures provided a measurement of the disassociation of hydrogen bonds.

The dielectric loss of mixtures of soybean oil and methanol were shown to vary due to the degree of mixing. The rate of destabilization of ultrasonically formed emulsions was measured as the dispersed methanol droplets swelled and rose to the surface of the mixture. This provided a comparison of dispersed phase droplet size through the type and rate of destabilization. Finally, the results quantitatively show that ultrasonic emulsification, in contrast to conventional mixing, can be used to alter the bulk complex permittivity.

6. Enhancement of microwave heating due to ultrasonically formed emulsion

The measurements of complex permittivity were practically tested through the measurement of microwave heating profiles of ultrasonically formed emulsions. The ability to inhibit nucleated boiling and extend the superheated temperature was confirmed using ultrasonic emulsification. Measuring the heating profiles of emulsion with different volumetric ratios, catalyst amounts, and ultrasonic treatments indicate the highest superheated temperatures result with no catalyst and a 3:1 molar ratio of methanol to soybean oil.

7. Proof of concept for the use of ultrasound to create ideal reaction mixtures for microwave heating and catalyst free biodiesel production

The ability of ultrasound to maximize the effectiveness in a microwave heated transesterification reaction was demonstrated using 0.3% base catalyst and 9:1 molar ratios of methanol to soybean oil. The weight of glycerol byproduct is compared between conventionally and ultrasonically mixed samples subjected to the same microwave heating treatments. The results indicated a nearly complete reaction with use of ultrasonics and nearly no reaction with conventional mixing. The concept of using the combination of microwaves and ultrasound to achieve catalyst free transesterification at sub critical temperatures and atmospheric pressure was verified by GC analysis for several samples.

Summary of thesis accomplishments:

In summary, the research goals set forth in this work were met.

1. Determination of the effects of ultrasonic parameters on emulsification.

2. Measurement of the ability of ultrasonics to alter microwave absorption in emulsions
3. Experimental validation of the ability of ultrasound to optimize microwave heating
4. Proof of concept for multi-energy optimized catalyst free biodiesel production
5. A better understanding of how to determine the synergistic effects of ultrasound and microwaves for material processing

7.2 Future Directions for Research:

The work of this thesis represents the first attempt in optimizing the parameters of high intensity ultrasonic sources to improve microwave heating. As a proof of concept study, naturally there remain several avenues for research and practical application that must be addressed before arriving at a commercially viable production technology.

7.2.1 Prototype design

7.2.1.1 Reaction Vessel

The first design consideration recognized in this study involves the reactor vessel. It has been shown that without emulsions stabilizers, destabilization can occur rapidly. In addition, the chemical effect of ultrasound simultaneously with microwaves could not be addressed. Accordingly, the prototype under development will locate the ultrasonic transducers, such that the reaction mixture can be treated with ultrasound while being microwave heated. At a minimum, this will ensure the smallest dispersed droplets at the onset of microwave heating. However, it will also allow

ultrasonic nucleation for rapid quenching of superheated fluids and the investigation of simultaneous treatments. A schematic of the design is in Figure **54**

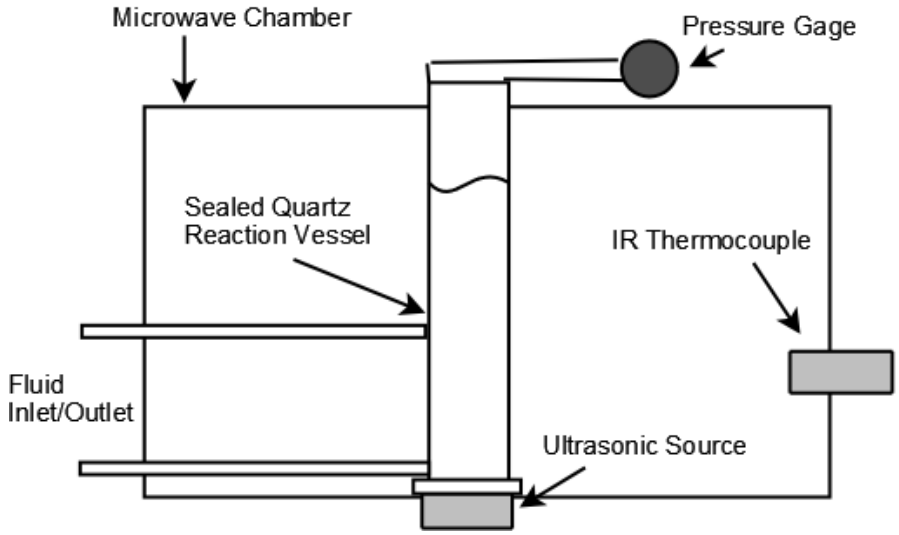

Figure **54**: Schematic diagram of microwave reaction vessel with capabilities for pressure, flow, and ultrasonic treatments.

The reaction vessel should also have the capability to pressurize or run under reflux. In this study, excess amounts of alcohol had to be used to account for the evaporation that occurs during boiling events. This prevented the use of the emulsions identified as the best for superheating. In the new prototype the ability to maintain the methanol percentage needed for conversion can coincide with the best choice for microwave heating, namely the stoichiometric ratio of 3:1.

7.2.1.2 Sensor integration

The next step in research will involve the design and construction of an automated prototype. The automation refers to the incorporation of sensor feedback to the controls of microwave and ultrasonic power. The prototype under development will include a computer controller that will accept temperature, pressure, and flow information from sensors. The controller

can then use the feedback to adjust the power to the magnetron, ultrasonic amplifier, and process pumps. Figure **55**

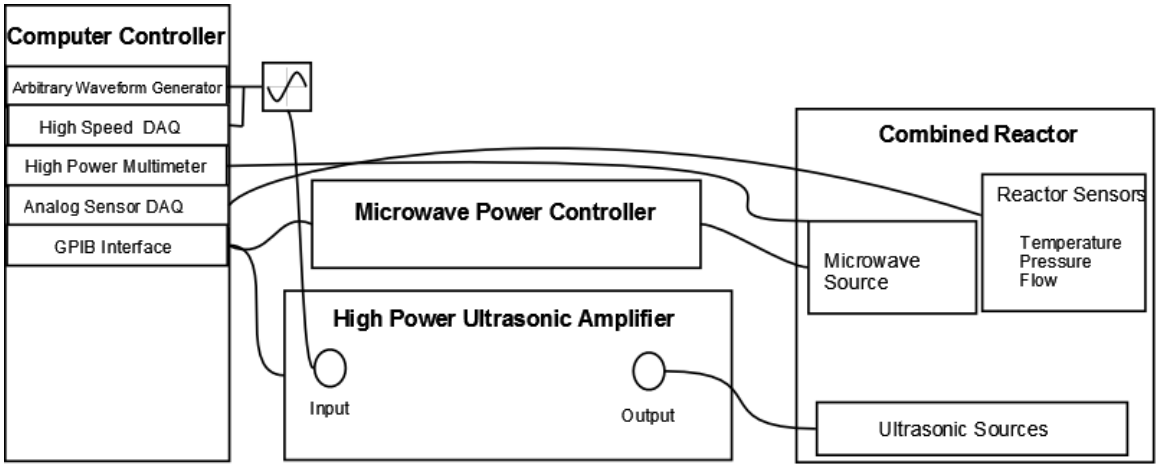

Figure **55**: Schematic diagram of automated multi-energy processor for active control of microwave and ultrasonic treatments from sensor feedback.

The computer will also carry the ability to adjust the ultrasonic frequency and power to maintain performance as the temperature and efficiency change. The automation will allow a series of tests to be conducted and the measurements recorded without user interruption. The controller is also equipped with high speed data acquisition leaving the possibility to incorporate in situ ultrasonic or electromagnetic measurements. Finally, the power needed for each reaction can be monitored to optimize efficiency. This is not possible with the setup used in this study, as there is no monitor of reflected power.

7.2.1.3 Ultrasonic and microwave applicators

One result of this work indicated the need to improve the ultrasonic applicator to obtain more repeatable results. This was evident with the ultrasonic bath, which produced the finest dispersed droplets, but was not as repeatable as the ultrasonic horn. To overcome this obstacle, the reaction vessel must be incorporated into the ultrasonic applicator design. One reason is to

accurately control the volume of fluids that are subjected to the treatment. In addition, the vessel can become a tuned mechanical extension of the transducer. The underlying principle to the design is resonance both in terms of the volume of the container and the mechanical resonance of the container itself.

The microwave applicator should also be considered in terms of resonance. Switching from a multimode chamber to a single mode chamber will increase the electrical efficiency and allow for predictable and repeatable microwave heating zones. The result of the single mode chamber will be a narrow region of intense microwave heating. This type of applicator will prove especially useful for continuous flow application.

7.2.2 Alternative applications

This study focused on the transesterification reaction for biodiesel production. This focus eliminated investigation into other processes involved with biodiesel production and other renewable fuel types. The applicability of the work done here provides a good starting point applying multi energy optimized processing to other fuel related processes.

7.2.2.1 The biodiesel value chain

Besides the transesterification, there are many other processes that could be improved by multi-energy optimized processing. For instance, the oil extraction of soybean oil involves drying, crushing, and ultimately solvent extraction. Once the oil is extracted it is then refined which involves bleaching, deodorizing, and degumming. Each process involves additional chemicals and heating. It is only after these processes that a biodiesel producer receives the oil to react into biodiesel. From an

environmental standpoint these processes are attributed to the total carbon emissions of biodiesel production in a lifecycle assessment. In order for renewable fuels to provide environmental benefit this series of processes should be consolidated. From a business perspective this chain of treatments is called the value chain. Each treatment represents a value added product. For example, the oil extracted from the soybeans can be sold for more than they crop. Likewise, the refined oil can be sold for more than the crude oil and so on. A biodiesel producer should seek to consolidate the processes of the biodiesel value chain to maximize flexibility and profitability.

From either aspect, the importance of eliminating separate, toxic, and energy intensive pretreatments to the feedstock is clear. In the opinion of the other, the drying, crushing, solvent extraction, and biodiesel production could be achieved with a single multi-energy approach. The use of microwaves to dry the grains is a simple and efficient process modification that may already be employed. However, the use of ultrasound and microwaves to simultaneously crush, extract, and react has not been proposed. The solvent properties of methanol are enhanced under microwave heating, which could allow the replacement of hexane. High intensity ultrasonics could ensure the maximum contact between the methanol and feed by emulsification and dispersion. Finally, with superheated methanol, extracted oil, and ultrasonic agitation the conversion to methyl esters could proceed simultaneously.

7.2.2.2 Alternative fuels

It is apparent that renewable fuels will not replace petroleum entirely within the current agricultural capabilities. The expansion into new feedstock sources has already begun with jatropha and algae. As new feedstock becomes available, research should focus on new types of renewable fuels. As mentioned in Chapter two, the properties of biodiesel are determined by the length of the

hydrocarbon chain. In fact, the properties of petroleum fuels also depend on the length of hydrocarbon chains. To change the length of hydrocarbon chains, a process called hydrocarbon cracking is used. The investigation into the use of ultrasonics and microwaves to selectively crack hydrocarbons is an area of research pertinent to both renewable and nonrenewable fuel sources.

Finally, the production of hydrogen from water may prove to be the ultimate renewable fuel source. However, this process is energy intensive partly due to the hydrogen bonding in water. The other aspect in electrochemical production of hydrogen is the anode activity which oxidizes as hydrogen is produced. It is feasible that the hydrogen bond energy could be most efficiently overcome with microwave energy and the oxidation on the surface of electrodes ultrasonically cleaned in situ. The resulting process would improve the rate and possible the efficiency of hydrogen production from water.

Bibliography

1. Tyson, K. S. (2005).DOE analysis of fuels and coproducts from lipids. *Fuel Processing Technology. 86*, 1127-1136.

2. Anastas, P. & Warner, J. (1998). *Green chemistry: Theory and practice*. New York: Oxford University Press.

3. Trost, B. M. (1995).Atom economy-A challenge for organic synthesis : Homogeneous catalysis leads the way. *Angew. Chem. Int. Ed. Engl. 34*, 259-281.

4. Graboski, M. S., & McCormick, R. L. (1998). Combustion of fat and vegetable oil derived fuels in diesel engines. *Prog. Energy Combust. Sci.. 24*, 125-164.

5. Van Gerpen, J. (2005).Biodiesel processing and production. *Fuel Processing Technology. 86*, 1097-1107.

6. Diasakou, M., Louioudi, A., & Papayannakos, N. (1998). Kineticss of the non-catalytic transesterification of soybean oil. *Fuel. 77*, 1297-1302.

7. Dasari, M. A., Goff, M. J., & Suppes, G. J. (2003). Noncatalytic alcoholysis kinetics of soybean oil. *JAOCS. 80*, 189-192.

8. Kusdiana, D., & Saka, S. (2001). Kinetics of transesterification in rapeseed oil to biodiesel fuel as treated in supercritical methanol. *Fuel. 80*, 693-698.

9. Wang, P. S. & Gerpen, J. V. (2005). Catalyst-free biodiesel production at elevated temperatures including supercritical conditions: A review. ASABE Paper No. 056124. St. Joseph, Mich.:ASABE.

10. Kropf, M. (2007). U.S. Provisional Patent No. PST-26718/36. Method for enhancing the rate of a chemical reaction, and apparatus for such method. Washington, DC: U.S. Patent and Trademark Office.

11. Cravotto, G., Boffa, L., Turello, M., Parenti, M., & Barge, A. (2005). Chemical modifications of bile acids under high-intensity ultrasound or microwave irradiation. *Steroids. 70*, 77-83.

12. Chemat, S., Lagha, A., Amar, H. A. , & Chemat, F. (2004). Ultrasound assisted microwave digestion. *Ultrasonics Sonochemistry*, *11*, 5-8.

13. Peng, Y., Song, G., & Dou, R. (2006). Surface cleaning under combined microwave and ultrasound irradiation: flash synthesis of 4H-pyrano{2,3-c}pyrazoles in aqueous media. *Green Chemistry. 8*, 573-575.

14. Cravotto,G. & Cintas, P (2007). The combined use of microwaves and ultrasound: Improved tools in process chemistry and organic synthesis. *Chemistry- A European Journal. 13*, 1902-1909.

15. NIST. Retrieved from NIST Standard Reference Database Number 69, June 2005 Release, Chemistry WebBook Web site: http://webbook.nist.gov/chemistry/

16. Van Gerpen, Jon (2006). Building a Successful Biodiesel Business. Biodiesel Basics.

17. Knothe, G. (2005).Dependence of biodiesel fuel properties on the structure of fatty acid alkyl esters. *Fuel Processing Technology. 86*, 1059-1070.

18. Knothe, G, Matheaus, A.C., & Ryan, T.W. (2002). Cetane numbers of branched and straight-chain fatty. Fuel. 82(2003), 971-975.

19. Knothe, G. (2000).Monitoring a progressing transesterification reaction by fiber-optic near infrared spectroscopy with correlation to 1H nuclear magnetic resonance spectroscopy. *JAOCS. 77*, 489-492.

20. Lide, D (Ed.). (2007). *CRC Handbook of Chemistry and Physics, 88th Edition*. New York, NY: CRC PRESS.

21. Halvorsen, J. D., Mammel, W. C., & Clements, L. D. (1993). Density estimation for fatty acids and vegetable oils based on their fatty acid composition. *JAOCS. 70*, 875-879.

22. Wang, T., & Briggs, J. L. (2002). Rheological and thermal properties of soybean oils with modified FA compositions. *JAOCS. 79*, 831-836.

23. Phillips, J. C., & Mattamal, M. M. (1976). Correlation of liquid heat capacities for carboxylic esters. *Journal of Chemical and Engineering Data. 21*, 228-232.

24. Freedman, B., Pryde, E. H., & Mounts, T. L. (1984). Variables affecting the yields of fatty esters from transesterified vegetable oils. *JAOCS. 61*, 1638-1643.

25. Freedman, B., Butterfield, R. O., & Pryde, E. H. (1986). Transesterification kinetics of soybean oil. *JAOCS. 63*, 1375-1380.

26. Noureddini, H. & Zhu, D (1997). Kinetics of transesterification of soybean oil. *JAOCS. 74*, 1457-1463.

27. Vicente, G., Martinez, M., & Aracil, J. (2007). Optimisation of integrated biodiesel production. Part I. A study of the biodiesel purity and yield. *Bioresource Technology. 98*, 1724-1733.

28. Vicente, G., Martinez, M., & Aracil, J. (2007). Optimisation of integrated biodiesel production. Part II. A study of material balance. *Bioresource Technology. 98*, 1754-1761.

29. Canakci, M., & Van Gerpen, J. (1999). Biodiesel production via acid catalyst. Transactions of the ASAE. 42(5), 1203-1210.

30. Haas, M. J. (2005).Improving the economics of biodiesel production through the use of low value lipids as feedbacks: Vegetable oil soapstock. *Fuel Processing Technology. 86*, 1087-1096.

31. Marchetti, J. M., Miguel, V. U., & Errazu, A. F. (2007). Heterogeneous esterification of oil with high amount of free fatty acids . *Fuel. 86*, 906-910.

32. Marchetti, J. M., Miguel, V. U., & Errazu, A. F. (2007). Possible methods for biodiesel production. *Renewable and Sustainable Energy Reviews. 11*, 1300-1311.

33. Wang, Y., Ou, S., Liu, P., Xue, F., & Tang, S. (2006). Comparison of two different processes to synthesize biodiesel by waste cooking oil. *Journal of Molecular Catalysts A: Chemical. 252*, 107-112.

34. Saka, S. & Kusdiana, D. (2001). Biodiesel fuel from rapeseed oil as prepared in supercritical methanol. *Fuel. 80*, 225-231.

35. Warabi, Y., Kusdiana, D., & Saka, S. (2004). Reactivity of triglycerides and fatty acids of rapeseed oil in supercritical alcohols. *Bioresource Technology. 91*, 283-287.

36. Cao, W., Han, H., & Zhang, J. (2005). Preparation of biodiesel from soybean oil using supercritical methanol and co-solvent. *Fuel. 84*, 347-351.

37. He, H., Sun, S., Wang, T., & Zhu, S. (2007). Transesterification kinetics of soybean oil for production of biodiesel in supercritical methanol. *J Amer Oil Chem Soc*, *84*, 399-404.

38. He, H., Wang, T., & Zhu, S. (2007). Continuous production of biodiesel fuel from vegetable oil using supercritical methanol process. *Fuel. 86*, 442-447.

39. Wang, L., He, H., Xie, Z., Yang, J., & Zhu, S. (2007). Transesterification of the crude oil of rapeseed with NaOH in supercritical and subcritical methanol. *Fuel Processing Technology. 88*, 477-481.

40. Yin, J. Z., Xiao, M., & Song, J. B. (2008). Biodiesel from soybean oil in supercritical methanol with co-solvent. *Energy Conversion and Management. 49*, 908-912.

41. Cheng, J., li, Y., He, S., Shen, W., Liu, Y., & Song, Y. (2008). Reaction kinetics of transesterification between vegetable oil and methanol under supercritical conditions. *30*, 681-688.

42. Imahara, H., Minami, E., Hari, S., & Saka, S. (2008). Thermal stability of biodiesel in supercritical methanol. *Fuel*, *87*, 1-6.

43. D'Ippolito, S. A., Yori, J. C., Iturria, M. E., Pieck, C. L., & Vera, C. R. (2007). Analysis of a two-Step, noncatalytic, supercritical biodiesel production process with heat recovery. *Enery & Fuels. 21*, 339-346.

44. Kiran, E., Debenedetti, P. G. , & Peters, C. J.(Ed.). (2000). *Supercritical fluids: Fundementals and applications*. Dordrecht: Kluwer Academic Publishers.

45. Fermi, Enrico (1956). Thermodynamics. New York: Dover.

46. Clifford, Tony (1999). Fundamentals of supercritical fluids. New York: Oxford Press.

47. Yamaguchi, T, Benmore, C.J., & Soper, A.K. (2000). The structure of subcritical and supercritical methanol. JOURNAL OF CHEMICAL PHYSICS. 112(20), 8976-8987.

48. Becher, P. (2001). *Emulsions: Theory and practice*(3rd Ed.). Oxford: Oxford University Press.

49. Meher, L. C., Sagar, D. V., & Naik, S. N. (2006). Technical aspects of biodiesel production by transesterification- A review. *Renewable and Sustainable Energy Reviews. 10*, 248-268.

50. Griffiths, David (1999). Introduction to electrodynamics. Upper Saddle River, New Jersey: Prentice Hall.

51. Pozar, D. M. (1998). *Microwave Engineering* (2nd ed.). New York: John Wiley and Sons.

52. Metaxas, A. C. (1996). *Foundations of Electroheat: A unified approach*. Chichester, England: John Wiley and Sons.

53. Chemat, F. & Esveld, E. (2001). Microwave super-heated boiling of organic liquids: Origin, effect and application. *Chem. Eng. Technal.. 24*, 735-744.

54. Palacios, J., D' La Mora, F., & Rubio, M. (1996). Microwave heating profiles and property-Structure relationships in a family of alcohols. *Journal of Materials Science Letters. 15*, 1730-1732.

55. Yoshida, H., Kondo, I., & Kajimoto, G. (1992). Participation of free fatty acids in the oxidation of purified soybean oil during microwave heating. *JAOCS. 69*, 1136-1140.

56. Evdokimov, I. N., & Novikov, M. A. (2007). Structural features of industrial water-crude oil emulsions. Microwave studies. *Chemistry and Technology of Fuels and Oils. 43*, 46-50.

57. Abderahman, N. H., Rosli, M. Y., & Zulkifly, J. (2006). Study of demulsification of water-in-oil emulsions via microwave heating technology. *Journal of Applied Sciences. 6*, 2060-2066.

58. Chih-Chieh, C., & Yeong-Ching, C. (2002). Demulsification of W/O Emulsions by microwave radiation. *Separation and Technology. 37*, 3407-3402.

59. Basak, T. (2004).Role of resonances on microwave heating of oil-water emulsions. *AIChE Journal. 50*, 2659-2675.

60. Zhang, H., Datta, A. K., Taub, I. A., & Doona, C. (2001). Elctromagnetics, heat transfer, and thermokinetics in microwave sterilization. *AIChE Journal*, *47*, 1957-1968.

61. Kappe, O. (2004). Controlled microwave heating in modern organic synthesis. *Chem. Int. Ed. 43*, 6250-6284.

62. Strauss, C. R., & Trainor, R. W. (1995). Invited review. Developments in microwave-assisted organic chemistry. *Aust. J. Chem.. 48*, 1665-1692.

63. Zhang, H., Datta, A. K., Taub, I. A., & Doona, C. (2001). Elctromagnetics, heat transfer, and thermokinetics in microwave sterilization. *AIChE Journal*, *47*, 1957-1968.

64. Murthy, G. S., & Prasad, S. (2005). A completely coupled model for microwave heating of foods in microwave oven. *ASAE Paper No. 056062. St Joseph, Mich: ASAE*

65. Lee, M. Z. C., & Marchant, T. R. (2002). Semi-analytical solutions for continuous-flow microwave reactors. *Journal of Engineering Mathematics. 44*, 125-145.

66. Ayappa, K. G., & Sengupta, T. (2002). Microwave heating in multiphase systems: Evaluation of series solutions. *Journal of Engineering Mathematics. 44*, 155-171.

67. Huang, K. M., Lin, Z., & Yang, X. Q. (2004). Numerical simulation of microwave heating on chemical reaction in dilute solution. *Progress In Electromagnetics Research. 49*, 273-289.

68. Drexler, P., Jirku, T., Szabo, Z., & Flala, P. (2006). Model of a reactor chamber with microwave heating. *PIERS*, *2*, 681-684.

69. Chemet , F. , Poux, M., di Martino, J. L., & Berlan, J. (1996). A new continuous-flow recycle microwave reactor for homogeneous and heterogeneous chemical reactions. *Chem. Eng. Technol.*, *19*, 420-424.

70. Bagley, M. C., Jemkins, R. L., Lubinu, M. C., Mason, C., & Wood, R. (2005). A simple continuous flow microwave reactor. *JOCNote. 70*, 7003-7006.

71. Baghurst, D. R. & Mingos, M. P. (1992). A new reaction vessel for accelerated syntheses using microwave dielectric super-heating effects. *Journal of the Chemical Society Dalton Transactions. 7*, 1151-1155.

72. Benali,l.O., & Deal, M. (2005). Continuous flow microwave synthesis; Reaction optimisation and scale-up. *Chem. Soc.. 127*, 8160-8167.

73. Mazzocchia, C., Modica, G., Nannicini, R., & Kaddouri, A. (2002). Fatty acid methyl esters synthesis from triglycerides over heterogeneous catalysts in presence of microwaves. Retrieved March, 2008, from http://www.microwave-rf.org/MWRFApplKaddouri.pdf.

74. Saifuddin, N. & Chua, K. H. (2004). Production of ethyl ester (biodiesel) from used frying oil: Optimization of transesterification process using microwave irradiation. *Malaysian Journal of Chemistry. 6*, 077-082.

75. Leadbeater, N. E. & Stencel, L. M. (2006). Fast, Easy preparation of biodiesel using microwave heating. *Energy & fuels. 20*, 2281-2283.

76. Hernando, J., Leton, P., Matia, M. P., Novella, J. L. , & Alvarez-Builla, J. (2006). Biodiesel and fame synthesis assisted by microwaves. Homogeneous batch and flow processes. *Fuel. 86*, 1641-1644.

77. Chadwick, P. (1976). Continuum mechanics: Consise theory and problems. Toronto,Ontario: General Publishing.

78. Abramov, O. V. (1998). *High-intensity ultrasonics: Theory and industrial applications*. The Netherlands: Gordon and Breach Science Publishers.

79. Davies, J. R., Tapson, J., & Mortimer, B. J. P. (2000). A novel phase locked cavity resonator for B/A measurements in fluid. *Ultrasonics. 38*, 284-291.

80. Henning, B., & Rautenberg, J. (2006). Process monitoring using ultrasonic sensor systems. *Ultrasonics. 44*, 1395-1399.

81. Yi, J., & Tavlarides, L. L. (1990). Model for hold-up measurements in liquid dispersions using an ultrasonic technique. *American Chemical Society. 29*, 475-482.

82. Wang,Y., & Povey, M. J. W. (1999). A simple and rapid method for the determination of particle size in emulsions from ultrasound data. *Colloids and Surfaces B: Biointerfaces. 12*, 417-427.

83. Lorimer, J., & Mason, T. (2002). Applied sonochemistry: Uses of power ultrasound in chemistry and processing. Federal Republic of Germany: Wiley-VCH.

84. Maksimov, A. O. (2000).Symmetry of the rayleigh equation and the analysis of nonlinear gas bubble oscillations in liquid. *Acoustical Physics. 48*, 713-719.

85. Floris, F. M. (2005).Modeling the cavitation free energy. *Journal Phys. Chem.. 109*, 24061-24070.

86. Raman, V., Abbas, A., & Joshi, S. C. (2006). Mapping local cavitation events in high intensity ultrasound fields. *COMSOL Users Conference 2006 Bangalore.*

87. Servant, G., Caltagirone, J. P., Gerard, A., Laborde, J. L., & Hita, A. (2000). Numerical simulation of cavitation bubble dynamics induced by ultrasound waves in a high frequency reactor. *Ultrasonics Sonochemistry. 7*, 217-227.

88. Liauh, C. T. (1998).Fast numerical scheme of computing acoustic pressure fields for planer circular ultrasound transducers. *J. Acoust. Soc. Am.. 105*, 2243-2247.

89. Moholkar, V. S., Rekveld, S., & Warmoeskerken, M. M. C. G. (2000). Modeling of acoustic pressure fields and the distribution of the cavitation phenomena in a duel frequency sonic processor. *Ultrasonics. 38*, 666-670.

90. Bondy, C., & Sollner, K. (1935). On the mechanism of emulsification by ultrasonic waves. *Trans. Faraday Soc.. 31*, 835-843.

91. Binks, B. P. (1998). *Modern aspects of emulsion science*. London: RSC Publishing.

92. Rajagopal, E. S. (1959).Time-variation of particle size distributions during coalescence, dispersion and ultrasonic emulsification. *Colloid and Polymer Science. 167*, 17-23.

93. Rajagopal, E. S. (1960).Phenomenological theory of the kinetics of ultrasonic emulsification. *Colloid and Polymer Science. 175*, 126-129.

94. Rajan, R., & Pandit, A. B. (2001). Correlations to predict droplet size in ultrasonic atomization. *ultrasonics. 39*, 235-255.

95. Behrend, O., Ax, K., & Schubert, H (2000). Influence of continuous phase viscosity on emulsification by ultrasound. *Ultrasonics Sonochemistry. 7*, 77-85.

96. Cucheval,A., & Chow, R. C. Y. (2008). A study on the emulsification of oil by power ultrasound. *Ultrasonics Sonochemistry*. 1-12.

97. Abismail, B., Canselier, J. P., Wilhelm, A. M., Delmas, H., & Gourdon, C. (1999). Emulsification by ultrasound: Drop size distribution and stability. *Ultrasonics Sonochemistry*. *6*, 75-83.

98. Abismail, B., Canselier, J. P., Wilhelm, A. M., Delmas, H., & Gourdon, C. (2000). Emulsification processes: On-line study by multiple light scattering measurements. *Ultrasonics Sonochemistry*. *7*, 187-192.

99. Timko, M., Smith, K., Danheiser, R., Steinfeld, J., & Tester, J. (2005). Reaction Rates in Ultrasonic Emulsions of DenseCarbon Dioxide and Water. AIChE Journal. 52(3), 1127-1141.

100. Richards, W. T., & Loomis, A. L. (1927). The chemical effects of high frequency sound waves: A preliminary survey. *J. Am. Chem. Soc.. 49*, 3086-3100.

101. Suslick, K. S. (1989, February). The chemical effects of ultrasound. *Scientific American*, *260*, 80-86.

102. Thompson, L. H., & Doraiswamy, L. K. (1999). Sonochemistry: Science and engineering. *Ind. Eng. Chem. Res.. 38*, 1215-1249.

103. Hielscher, H. (2005). Ultrasonic production of nano-size Dispersions and emulsions. *European Nano Systems 2005,Paris France.*

104. Lifka, J. & Ondruschka, B. (2004). Influence of mass transfer on the production of biodiesel. *Chem. Eng. Tech.. 27*, 1156-1159.

105. Zhu, N., Tsuchiya, T., Ito, N., & Kato, S. (2005). Study on Synthesizing BDF by Using Ultrasonic Sonochemistry Effect. 3rd Int Enenegy Conversion Eng. Conf. Proceedings, AAIA 2005-5543, 1-7.

106. Singh, A. K. & Fernando, S. D. (2006). Base catalyzed fast-transesterification of soybean oil using ultrasonication. ASABE Paper No. 066220. St. Joseph, Mich.: ASABE.

107. Singh, A. K. , Fernando, S. D. , & Hernandez, R. (2007). Base-catalyzed transesterification of soybean oil using ultrasonication. *Energy & Fuels*. *21*, 1161-1164.

108. Stavarache, C., Vinatoru, M., & Maeda, Y. (2007). Aspects of ultrasonically assisted transesterification of various vegetable oils with methanol. *Ultrasonics Sonochemistry*. *14*, 380-386.

109. Stavarache, C., Vinatoru, M., Maeda, Y., & Bandow, H. (2007). Ultrasonically driven continuous process for vegetable oil transesterification. *Ultrasonics Sonochemistry*, *14*, 413-417.

110. Siatis, N. G., Kimbaris, A. C., Pappas, C. S. , Tarantilis, P. A., & Polissiou, M. G. (2006). Improvement of biodiesel production based on the application of ultrasound: Monitoring of the procedure by FTIR spectroscopy. *JAOCS*. *83*, 53-57.

111. Wu, P., Yang, Y., Colucci, J., & Grulke, E. (2007). Effect of ultrasonification on droplet size in biodiesel mixtures. J Am Oil Soc, 84, 877-884.

112. Lu, Z. (2005). State of water in perfluorosufonic acid membranes studied by microwave dielectric relaxation spectroscopy. (Doctoral dissertation, Pennsylvania State University, University Park, 2005).

113. Plank, C., & Lorbeer, E. (1995). Stimultaneous determination of glycerol, and mono-, di- and triglycerides in vegetable oil methyl esters by capillary gas chromatography. *Journal of Chromatography. 697*, 461-468.

114. Foglia, T. A. , Jones, K. C., Nunez, A., Phillips, J. G., & Mittelbach, M. (2004). Comparison of chromatographic methods for the determination of bound glycerol in biodiesel. *Chromatographia. 60*, 305-311.

115. Von Hippel, Arthur (Ed.). (1954). *Dielectric Materials and Applications*. Cambridge: Technology press of MIT.

116. Inoue, C., Hagura, Y., Ishikawa, M., & Suzuki, K. (2002). The Dielectric Property of Soybean Oil in Deep-Fat Frying and the Effect of Frequency. *Journal of Food Science*, *67(3)*, 1126-1129.

117. Mashimo,lS., & Umehara, T. (1991). Structures of water and primary alcohol studied by microwave dielectric analyses. *J. Chem. Phys.. 95*, 6257-6260.

118. Lane, J. A., & Saxton, J. A. (1952). Dielectric dispersion in pure polar liquids at very high radio frequencies. III. The effect of electrolytes in solution. *Mathematical and Physical Sciences. 214*, 531-545.

119. Kaatze, Udo (1995).MICROWAVE DIELECTRIC PROPERTIES OF LIQUIDS. Radiat. Phys. Chem.. 45(4), 549-566.

120. Von Hippel, Arthur (1988).The dielectric relaxation spectra of water, ice, and aqueous solutions and their interpretations 1. Critical survey of the status quo for water. *IEEE Trans. on Electrical Insulation. 23(5)*, 801-816.

121. Von Hippel, Arthure (1988).The dielectric relaxation spectra of water, ice, and aqueous solutions and their interpretation 2. Tentative interpretation of the relaxation spectrum of water in the time and frequency domain. *IEEE Trans. on Electrical Insulation. 23(5)*, 817-823.

122. Holtze, C., Sivaramakrishnan, R, Antonietti, M., Tsuwi, J., Kremer, F., & Kramer, K. D. (2006). The microwave absorption of emulsions containing aqueous micro-nanodroplets: A means to optimize microwave heating. *Journal of Colloid and Interface Science. 302*, 651-657.

Appendix A

Results Analysis

Debeye Relaxation Calculation:

```
function [erth,eith]=debeye(eh,es,tau)
%eh is permittivy at high frequency limit
%es is DC permittivity
%tau is relaxation time in seconds
%Set frequency range to match point by point with data collected
fo=45*10^6;
ff=5*10^9;
finc=10.31^7;
m=0;
ll=(ff-fo)/finc;
f=zeros([size(ll) 1]);
%Form frequency vector
while m<ll
   a=fo+m*finc;
   m=m+1;
   f(m)=a;
end

L=length(f);
```

```
eth=zeros([L 1]);
n=1;

%Calculation of Debye Relaxation
while n<L+1
   eth(n)=eh+((es-eh)/(1+j*2*pi*f(n)*tau));
   n=n+1;
end

%Convert results into relative permittivity and dielectric loss
erth=real(eth);
eith=-imag(eth);
figure();plot(f,erth,f,eith);
```

Ionic Conductivity Curve Fitting:

(adapted MatLab user example)

```
function [estimates, model] = fitcurvedemo(xdata, ydata)
% Call fminsearch with a random starting point.
start_point = rand(1);
model = @inverse;
estimates = fminsearch(model, start_point);
% invers accepts curve a parameter as an input, and outputs sse,
% the sum of squares error for A./xdata - ydata,and the FittedCurve.
```

```
    function [sse, FittedCurve] = inverse(param)
    A = param;
    FittedCurve = A ./(2*pi*xdata);
    ErrorVector = FittedCurve - ydata;
    sse = sum(ErrorVector .^ 2);
  end
end
```

STANDARD DEVIATION OF EMULSIONS:

3:1,6:1,9:1 full/half

Figure **56**

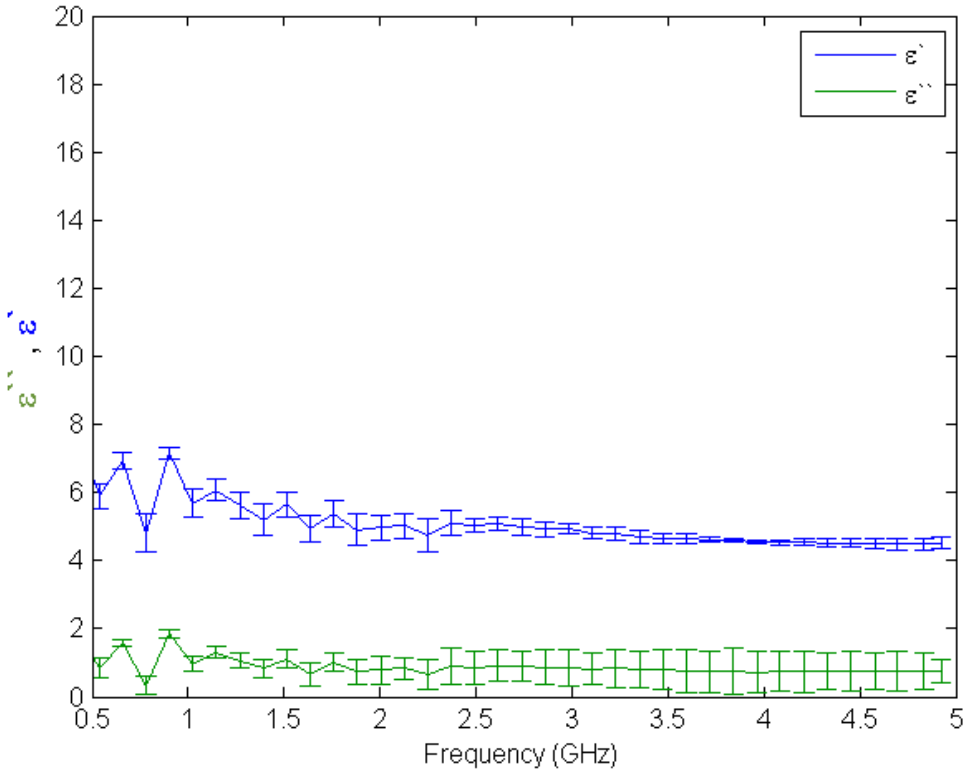

Figure **56**: 3:1 molar ratio emulsion with standard deviation error bars for 22 kHz FULL power case.

Figure 57

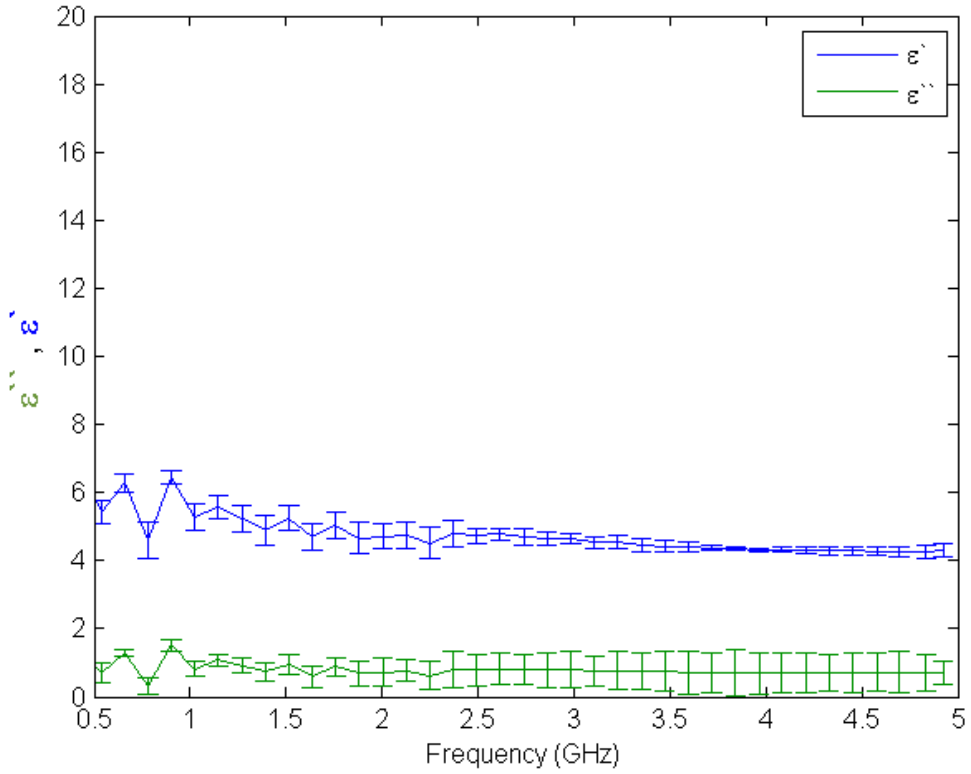

Figure **57**: 3:1 molar ratio emulsion with standard deviation error bars for 22 kHz HALF power case.

Figure 58

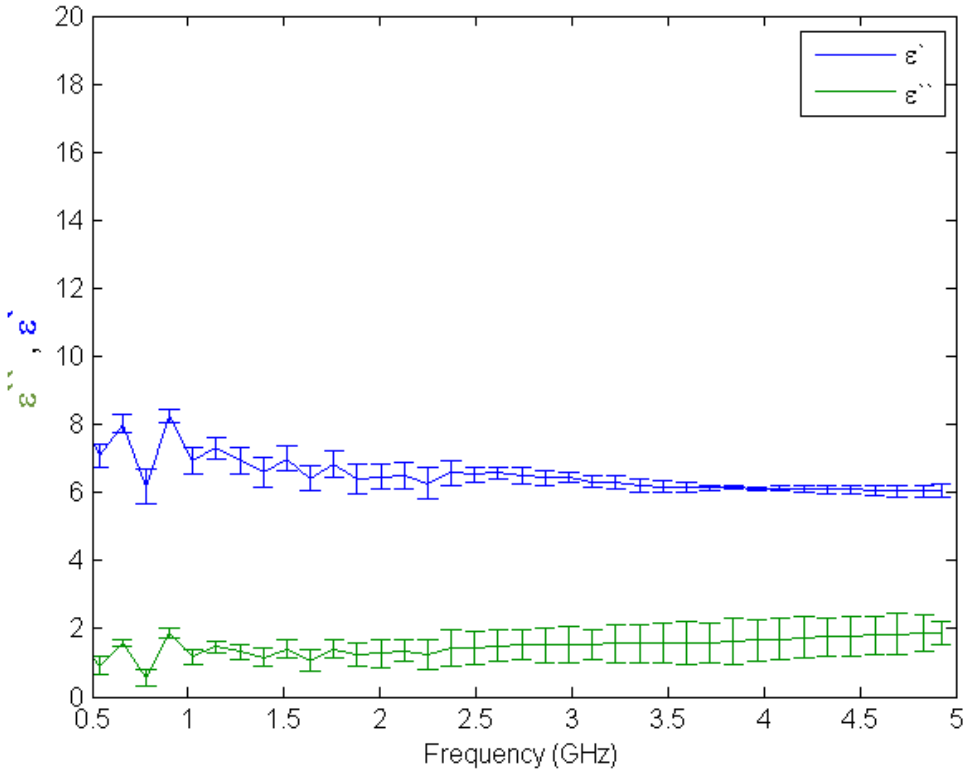

Figure **58**: 6:1 molar ratio emulsion with standard deviation error bars for 22 kHz FULL power case.

Figure 59

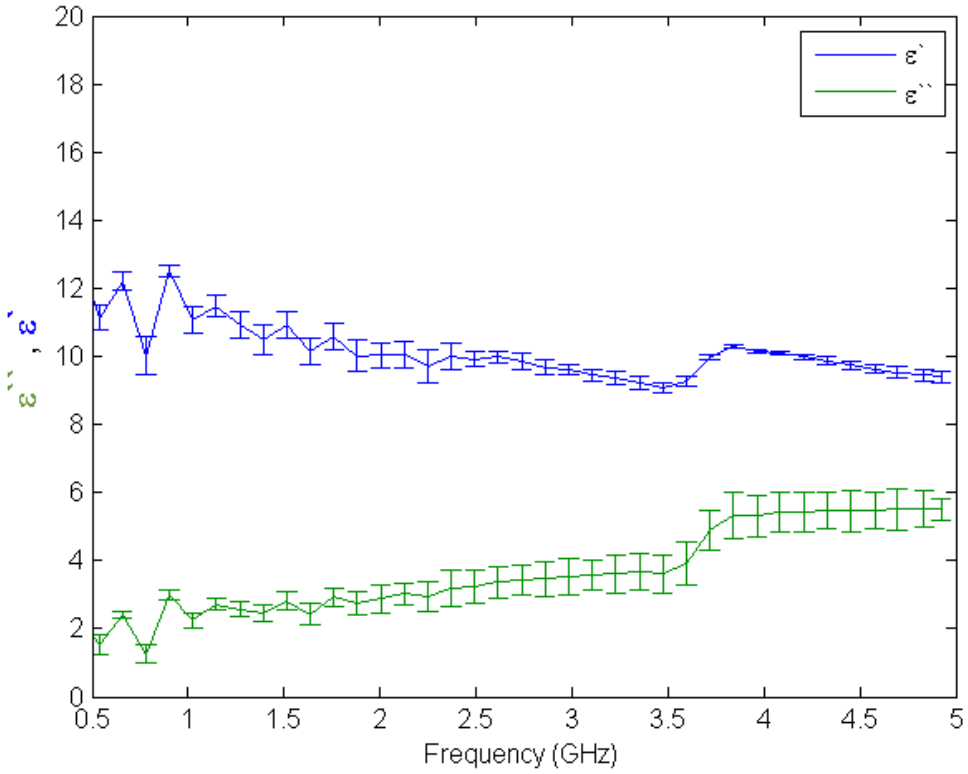

Figure **59**: 6:1 molar ratio emulsion with standard deviation error bars for 22 kHz HALF power case.

Figure 60

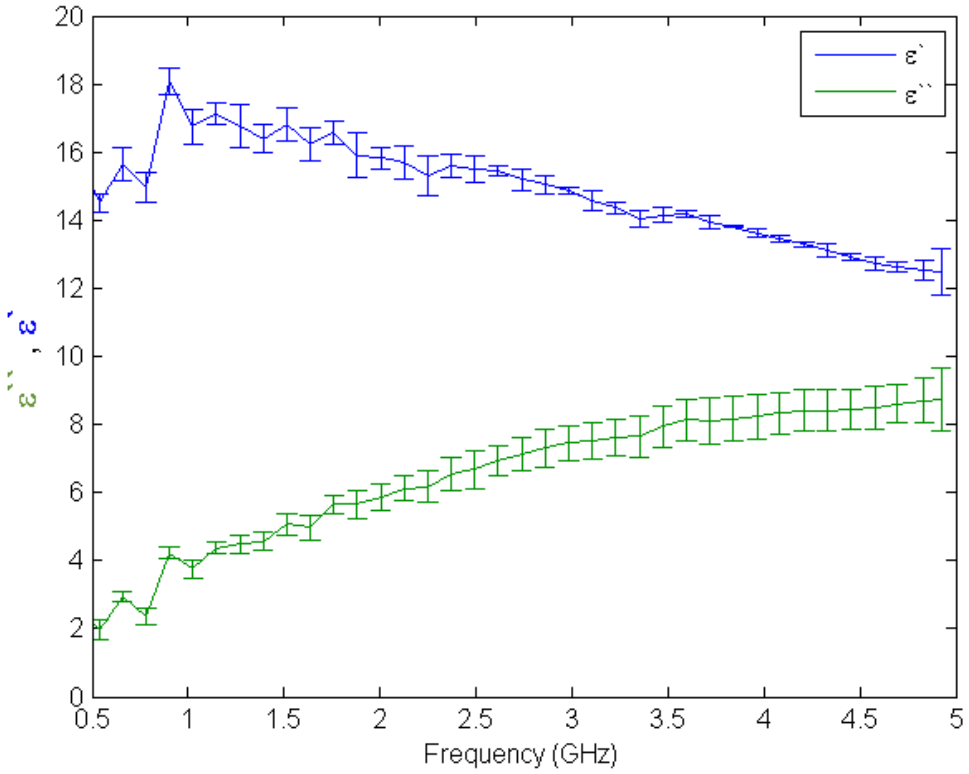

Figure **60**: 9:1 molar ratio emulsion with standard deviation error bars for 22 kHz FULL power case.

Figure 61

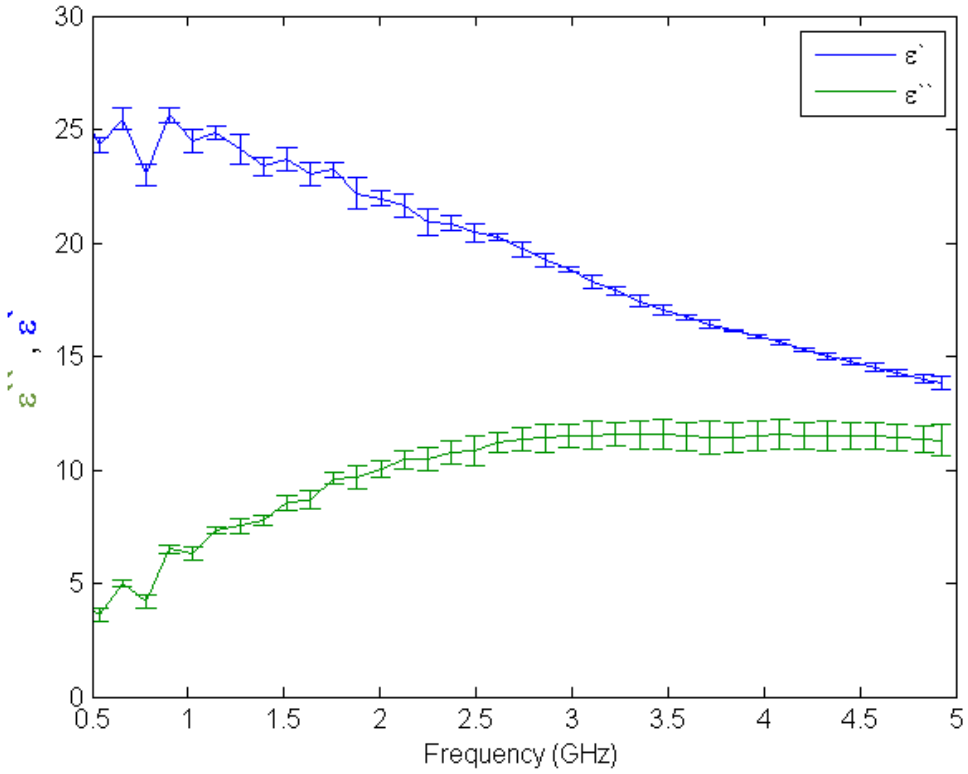

Figure **61**: 9:1 molar ratio emulsion with standard deviation error bars for 22 kHz Half power case.

Heating Rate Calculation:

```
function [Ee R]=dTdt(D)
br=2; %samples/second
L1=length(D);
n=1;
 while n<L1
    t(n)=n*(1/br);
    drs(n)=D(n);
    n=n+1;
```

```
 end

p=polyfit(t,drs,1);

Ee=p(1);

yfit=polyval(p,t);

R=corr2(yfit,drs);
```

GC Analysis of catalyst free transesterification reactions:

Figure 62

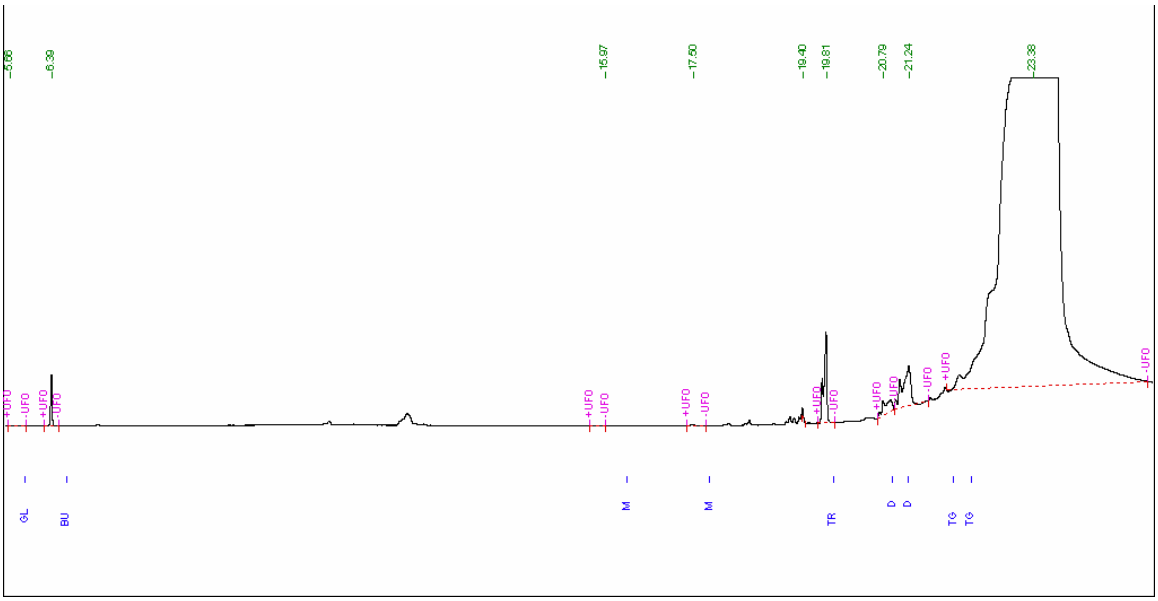

Figure **62**: GC analysis indicating repeat of successful transesterification using 22 kHz ultrasonic emulsification for thirty seconds and microwave superheating to 85 °C for 220 seconds. Sample is of 9:1 molar ratio of methanol to soybean.

Figure 63

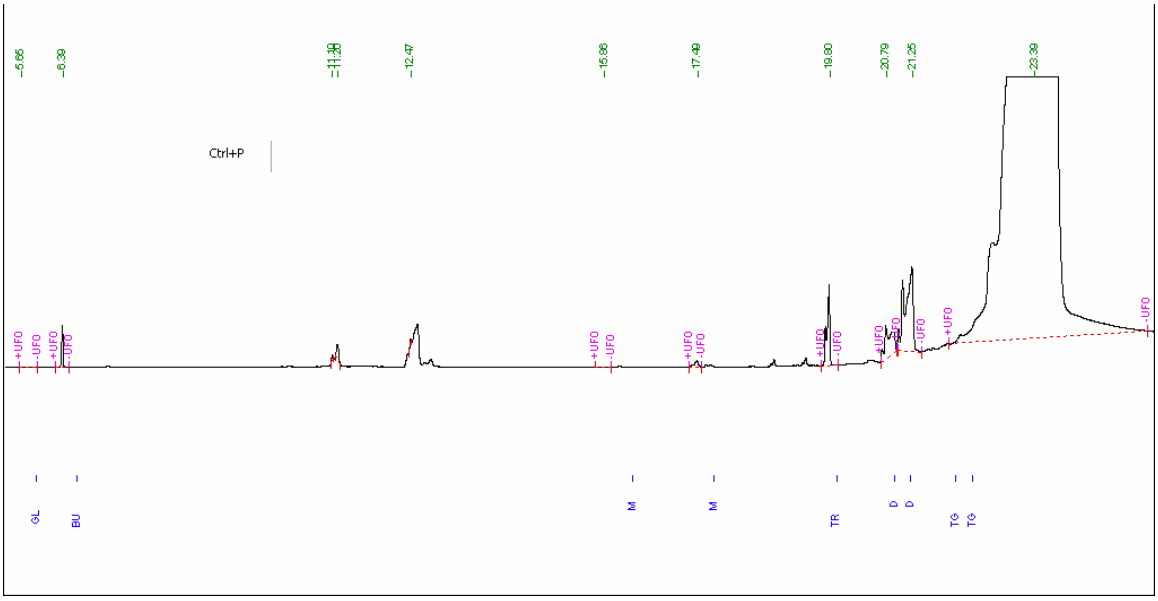

Figure **63**: GC analysis indicating repeat of successful transesterification using 22 kHz ultrasonic emulsification for thirty seconds and microwave superheating to 85 °C for 220 seconds. Sample is of 9:1 molar ratio of methanol to jatropha seed oil.

Figure **64**

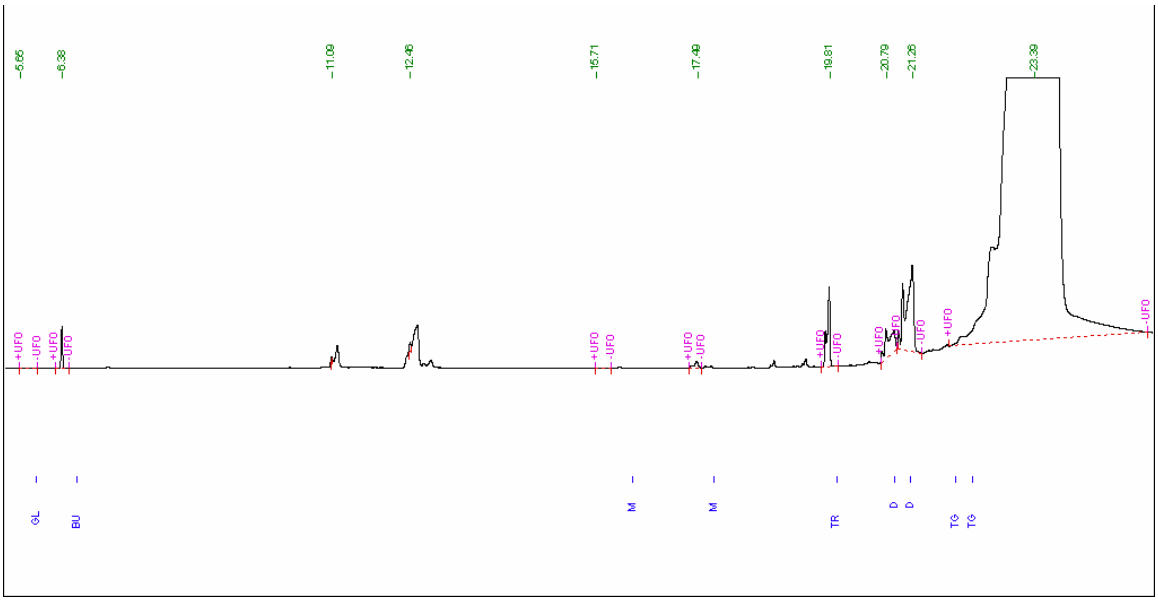

Figure **64**: GC analysis indicating repeat of successful transesterification using 22 kHz ultrasonic emulsification for thirty seconds and microwave superheating to 85 °C for 220 seconds. Sample is of 9:1 molar ratio of methanol to jatropha seed oil.

Appendix B

Non-technical abstract

As the world turns to renewable fuels, chemical processing practices become pivotal to the feasibility of environmental benefits. Green chemistry has become the exemplar for achieving meaningful sustainability with established principles promoting of atom economy, renewable resources, pollution prevention, and energy efficiency. The collective choice to pursue biofuels represents green chemistry principles, as they are chemical products designed from renewable feedstock with the ability lower pollution in use. However, as skeptics warn, this latter attribute may ultimately hinge on aspects of processing the raw materials; namely atom economy, an expression of the amount of chemicals wasted in a process, and energy efficiency, regarding the amount of energy expended to heat, cool, pressurize, mix, and transfer the process chemicals.

In most cases, a chemical product will not have sufficient energy to form from its base chemicals, called stoichiometric reagents. Traditionally, this is overcome using large excess of one reagent and elevating the energy through temperature and pressure. However, the tenants of green chemistry eschew such practice, noting that chemicals used in excess are wasted and the energy to maintain temperatures and pressures can become inhibitory. Instead, green chemists recommend using a small amount of an auxiliary chemical to provide a lower energy route to the product through intermediate reactions. Ideally, this chemical, called catalyst, is not used in the final product and can be conserved. Even still, many chemical reactions will still require mixing and elevated temperatures and pressures. The energy efficiency aspect of green chemical processing is treated as a corollary catalysis, in the form of "process intensification mechanisms", or unconventional methods of heating and mixing chemicals. Such mechanisms include high intensity ultrasonics, microwave heating, and supercritical fluids. Traditionally, however, these mechanisms are considered secondary to the use of

catalyst, for example to accelerate a slow catalytic reaction or to improve the electrical efficiency of heating in a catalytic reaction.

The chemical product biodiesel consists of molecules found in biological oils, soybean oil for example, called fatty acids, and alcohol. However, the fatty acids found in such oil are bonded to glycerin molecules, and alcohol and oil are immiscible, requiring constant vigorous mixing. Following green chemical principles, current industry practice uses a dissolved, or homogenous, catalyst to separate the glycerin and fatty acid, contribute energy to the alcohol replacing the glycerin, and improve reaction rates. However, the catalyst often reacts with the fatty acid forming waste chemicals and trapping product feedstock. In industry this is managed through the use of excess volumes of alcohol and further processing of the biodiesel and glycerin byproduct to remove contamination caused by catalyst and recover lost feedstock. To address this problem, green chemists have attempted sonochemistry, microwave heating, and supercritical reactions. Ultrasonics has shown overcome limitations of mixing and contributes to the chemical activity, improving the reaction rate and reducing catalyst requirements. Similarly, microwave heating has shown to enhance the reaction rate through intense heating, thus reducing catalyst requirements. However, neither area of investigation represents an alterative to the use of catalyst; instead they are incremental improvements in process intensification. Research into supercritical biodiesel production does represent a potentially catalyst free process, however the process requires a large excess of alcohol, co-solvents, and energy to maintain extreme temperatures and pressures.

An innovative combination of the use microwaves and ultrasound is proposed to reduce or eliminate the use of catalyst in biodiesel production. Though the two mechanisms have been used in combination before, but applications have been limited to process intensification and never before considered for biodiesel production. To advance the art and science of ultrasonic and microwave chemical processing and quantify the synergy of combination, experiments spanning several

disciplines of science are conducted. The formation of mixtures, or emulsions, of several volumes of alcohol and oil, using various ultrasonic frequencies and intensities, provide the baseline for experimental analysis. The physical structure resulting from the ultrasonic treatments are measured using microscopy and ultrasonic scattering. Microwave absorption is measured by vector network analysis and microwave heating rates of bulk samples. While the individual measurements are relevant to modern research in surface science, sonochemistry, microwave engineering, food science, chemical engineering, and fuel science. Together, the results elucidate phenomena mysterious to many chemists, particularly the reaction rate enhancements provided by each microwaves and ultrasound that appear to exceed the contributions from of heating and mixing.

The resulting technical innovation leverages fine control over ultrasonic parameters to control microwave heating rates of pure fluid mixtures, enabling previously energetically prohibitive reaction rates with stoichiometric reagents. With economic benefits afforded through catalyst remediation and environmental benefits in approaching perfect atom economy, the technology is a good candidate for widespread adoption in the biofuels processing industry.

VITA

Matthew Mason Kropf

Education:

PhD: Department of Engineering Science and Mechanics
The Pennsylvania State University
Dissertation: Multi-Energy Optimized Processing: The use of high intensity ultrasonic and electromagnetic radiation for biofuel production processes.

Publications:

1. "Ultrasonic magnetostrictive transducers for guided ultrasonic waves in thin wires". Matthew M. Kropf and B. R. Tittmann. SPIE 6532, 65320L (2007)
2. "Investigating a stepped ultrasonic phased array transducer for the evaluation and characterization of defects". M. Bohenick, E. Blickley, B. R. Tittmann, and M. Kropf. SPIE 6532, 653215 (2007)
3. "Transmission Matching for Joining Two Acoustical Waveguides". Xiaowei Wang, Matthew M. Kropf, Manton J. Guers, and Bernhard R. Tittmann. AIP Conf. Proc. 894, 103 (2007)
4. "Investigation of magnetostrictive materials and transducers for the generation of ultrasonic waves". Matthew M. Kropf and B. R. Tittmann. (A) J. Acoust. Soc. Am. 119, 3410 (2006)
5. "Low attenuation waveguide for leaky surface waves". K. Joseph, B. R. Tittmann, M. Pedrick, and M. Kropf. SPIE 6179, 61790E (2006)
6. "Ultrasonic stair case array for NDE". K. Oliver, B. R. Tittmann, and M. Kropf. SPIE 6179, 61790C (2006)
7. "Remote High Temperature Thermometry Using Ultrasonic Guided Waves in Thin Wires". Matthew Kropf, Mike Pedrick, and Bernhard Tittmann. AIP Conf. Proc. 820, 1570 (2006)
8. "Remote Sensing Using Ultrasonic Guided Waves in Thin Wires". Kropf, M., Pedrick, M., Tittmann, B.R. Journal of American Society for Nondestructive Testing. Fall Conference and Quality Testing. (2005).
9. "Advancement of wave generation and signal transmission in wire waveguides for structural health monitoring applications". M. Kropf, M. Pedrick, X. Wang, and B. R. Tittmann. SPIE 5770, 135 (2005)